

Surface Forces Induced by Point Charge in a Multilayered Dielectric System

by

Hasib Ibne Rahman

A thesis submitted in partial fulfillment of the requirements for the degree of

Master of Science

Department of Mechanical Engineering
University of Alberta

© Hasib Ibne Rahman, 2016

ABSTRACT

Local surface force density and total surface force induced by a single point charge embedded in a three-layered homogeneous dielectric system with infinite planar interfaces are calculated using the Maxwell Stress Tensor formulation. The tensor is expressed in terms of the electric field which is first derived from solving the electric potential in all domains. The electric potentials are obtained in closed form using the Hankel transformation. Nondimensionalization of the solutions for electric potential, local surface force density and total surface force reduces the governing parameters into three scalars: a normalized charge location and two dielectric constant ratios. These dimensionless parameters are varied to analyze their influences. The numerical parametric study reveals interesting, coupled influences of these parameters on the distribution of electric potential. It was also found that the two ratios between the dielectric constants of the three layers play a primary role in the forces: they determine the direction of the surface force density and total surface force, as well as the distribution of the surface force density, which can vary monotonically or non-monotonically with the radial position. The position of the point charge, on the other hand, only affects the magnitude of the surface forces. Due to the linear nature of the electrostatic problem, the formulations presented here can be extended to establish a theoretical framework for modeling contact adhesion, where interfacial adhesive forces arise from a distribution of charges. An example to solve this type of problem is presented where a pair of equal and opposite charges are considered in the same model. Comparison between these two systems show that the addition of an extra charge introduces significant changes in the magnitude of surface force density while their directions are found the same in both systems. The results also reveal that the total surface force can be altered both qualitatively and quantitatively by the extra charge. This

additional charge can increase or decrease the net surface forces depending on the charge location and the dielectric constant ratios of the three layers.

DEDICATION

I dedicate this thesis to my parents who had dreamt of this achievement long ago when they chose to give me the best education they could.

ACKNOWLEDGEMENTS

I would first like to express my sincere gratitude to my supervisor, Dr. Tian Tang whose excellent cooperation and valuable guidance provided me all the tools that I needed to finish my thesis successfully. I appreciate her vast knowledge and skill in many areas, and her assistance in writing this thesis and other scientific papers. During the whole period of my research, she provided all the assistance for me, not only in the scientific arena, but also on a personal level.

A very special thanks goes out to the support staffs of the department office for all their administrative and technical support throughout my graduate program. They made it easy for me to stay motivated by making cordial interactions almost every day.

I must also acknowledge my colleagues and group members who relentlessly extended their hands of collaboration at all levels of my graduate studies by exchanging knowledge, thoughts, and transforming my frustration into motivation. I always found them willing to help and encourage me.

Thanks also goes out to my family and friends without whose wise counsel and lifelong sympathetic support, I would not have finished this thesis.

Finally, I would particularly like to thank all the professors in my undergraduate courses who encouraged me to apply for the graduate program and to consider a career in engineering research.

Table of Contents

Chapter 1

INTRODUCTION	1
--------------------	---

Chapter 2

PROBLEM DESCRIPTION AND FORMULATION	7
2.1 Physical description of the problem	7
2.2 Methodology	8
2.3 Formulation.....	9
2.3.1 Governing equation to solve the electric potential	9
2.3.2 Boundary conditions	11

Chapter 3

ELECTRIC POTENTIAL SOLVED WITH HANKEL TRANSFORMATION.....	12
3.1 Hankel Transformation.....	12
3.2 Transformation of boundary value problem (BVP)	14
3.3 Solution of the transformed BVP	18
3.4 Electric potential obtained from inverse Hankel Transform	19
3.5 Solution for the unknowns $\Phi_H(\rho)$ and $\Phi_0(\rho)$	20
3.6 Normalization of electric potential.....	24
3.7 Validation of the electric potential solution.....	25
3.7.1 Case I ($\varepsilon_{21} = \varepsilon_{31} = 1$)	26
3.7.2 Case II ($\varepsilon_{21} \neq 1$; $\varepsilon_{31} = 1$)	27

Chapter 4

INDUCED SURFACE FORCE DENSITY AND TOTAL SURFACE FORCE	29
4.1 Calculation of electric field	29
4.2 Maxwell Stress Tensor (MST).....	32
4.3 Calculation of surface forces	34
4.4 Normalization of electric field	40
4.5 Normalization of total surface force.....	41

Chapter 5

RESULTS AND DISCUSSIONS	42
5.1 Parametric analysis for the electric potential.....	42

5.1.1 Variation of the electric potential with dielectric constant ratios	42
5.1.2 Variation of the electric potential with charge location	46
5.2 Implications of the electric potential	51
5.3 Parametric analysis of the surface force density	51
5.3.1 Variation of the surface force density with dielectric constant ratios	51
5.3.2 Variation of the surface force density with charge location	56
5.4 Parametric analysis of the total surface force	59
5.5 Implications of the total surface force	62
Chapter 6	
EXTENSION OF THE PROBLEM	63
6.1 Extended problem with a distribution of charges	63
6.2 Multilayered dielectrics with a pair of point charges	64
6.3 Calculation of surface forces	65
6.4 Results and comparison	70
6.4.1 Comparison of the surface force density (effect of dielectric constant ratios).....	70
6.4.2 Comparison of the surface force density (effect of charge location).....	77
6.4.3. Comparison of the total surface force	79
Chapter 7	
CONCLUSIONS AND FUTURE WORK	87
BIBLIOGRAPHY.....	90
APPENDIX	97

List of Figures

FIGURE 2.1: Schematic of the electrostatic problem with a single point charge considered in this work.....	8
FIGURE 4.1: Gaussian pillbox used to calculate surface force density on the upper interface from the Maxwell Stress Tensor.	36
FIGURE 5.1: Normalized electric potential of a single point charge in the middle layer of a three-layered dielectric system. The upper and lower interfaces are at the positions of $z/H=1$ and $z/H=0$, and marked by orange and blue lines respectively. (a) $\epsilon_{21}=10$ and $\epsilon_{31}=10$, (b) $\epsilon_{21}=0.1$ and $\epsilon_{31}=10$. For all cases, $\bar{d}=0.5$	44
FIGURE 5.2: Normalized electric potential, plotted against the dielectric constant ratio between the lower and middle regions, at three points $P_1(1,0.5)$, $P_2(0,-0.5)$ and $P_3(0,1.5)$, located in the middle, lower and upper layers respectively. For all cases, $\bar{d}=0.5$ and $\epsilon_{31}=10$	46
FIGURE 5.3: Normalized electric potential, plotted against the normalized location \bar{d} , at three points $P_1(1,0.5)$, $P_2(0,-0.5)$ and $P_3(0,1.5)$ located in the upper, lower and middle layers respectively (see inset in Fig. 5.2). (a) $\epsilon_{21}=10$ and $\epsilon_{31}=10$, (b) $\epsilon_{21}=0.1$ and $\epsilon_{31}=10$	49
FIGURE 5.4: Normalized electric potential at $P_1(1,0.5)$, located in the middle layer, as a function of the normalized location \bar{d} of the point charge. For all cases, $\epsilon_{31}=10$	50
FIGURE 5.5: Normalized surface force density on the interfaces, with red and blue lines corresponding to the upper and lower interfaces respectively. (a) $\epsilon_{21}=0.1$, (b) $\epsilon_{21}=5$. For each subfigure, $\bar{d}=0.5$ and ϵ_{31} varies from 0.1 to 5 (see legend for different line styles used for different ϵ_{31}).	53
FIGURE 5.6: Normalized surface force density on the interfaces for different normalized charge location. (a) Upper interface (b) Lower interface. For all cases, $\epsilon_{21}=5$, $\epsilon_{31}=0.1$ and \bar{d} varies from 0.3 to 0.7 (see legend).	58
FIGURE 5.7: Normalized total surface force on the interfaces, with red and blue lines corresponding to the upper and lower interfaces respectively. (a) $\epsilon_{21}=0.1$, (b) $\epsilon_{21}=5$. For each	

subfigure, ϵ_{31} varies from 0.1 to 5 on the horizontal axis and \bar{d} takes four different values from 0.3 to 0.7 (see legend for different line styles used for different \bar{d}).60

FIGURE 6.1: Schematic of the electrostatic problem with a pair of equal and opposite point charges in the middle layer.65

FIGURE 6.2: Normalized surface force density on the interfaces, with red and blue lines corresponding to the upper and lower interfaces respectively. (a) a single charge, (b) a pair of charges. For each subfigure, $\bar{d} = 0.4$, $\epsilon_{21} = 0.1$ and ϵ_{31} varies from 0.1 to 5 (see legend for different line styles used for different ϵ_{31}).72

FIGURE 6.3: Normalized electric field components on the interfaces with black and red lines correspond to the single and pair of charges respectively. (a) z -component on the lower interface, (b) r -component on the lower interface, (c) z -component on the upper interface, (d) r -component on the upper interface. For each subfigure, $\bar{d} = 0.4$, $\epsilon_{21} = 0.1$ and ϵ_{31} varies from 0.1 to 5 (see legend for different line styles used for different ϵ_{31}).74

FIGURE 6.4: Normalized surface force density on the interfaces, with red and blue lines corresponding to the upper and lower interfaces respectively. (a) a single charge, (b) a pair of charges. For each subfigure, $\bar{d} = 0.4$, $\epsilon_{21} = 5$ and ϵ_{31} varies from 0.1 to 5 (see legend for different line styles used for different ϵ_{31}).76

FIGURE 6.5: Normalized surface force density on the interfaces, with red and blue lines corresponding to the upper and lower interfaces respectively. (a) a single charge, (b) a pair of charges. For each subfigure, $\bar{d} = 0.3$, $\epsilon_{21} = 0.1$ and ϵ_{31} varies from 0.1 to 5 (see legend for different line styles used for different ϵ_{31}).77

FIGURE 6.6: Normalized total surface force due to a single charge and a pair of charges, with red and blue lines corresponding to the upper and lower interfaces respectively. For all cases, $\bar{d} = 0.4$. (a) $\epsilon_{21} = 0.1$, (b) $\epsilon_{21} = 5$ 80

FIGURE 6.7: Normalized total surface force on the upper interface due to a single charge (solid line) and a pair of charges (dashed line). (a) $\bar{d} = 0.1$, (b) $\bar{d} = 0.2$, (c) $\bar{d} = 0.3$. For all cases, $\epsilon_{21} = 0.1$82

FIGURE 6.8: Normalized surface force density on the lower interface. (a) a single charge, (b) a pair of charges. For each subfigure, $\bar{d} = 0.4$, $\varepsilon_{21} = 0.1$ and ε_{31} varies from 0.1 to 5 (see legend for different line styles used for different ε_{31}).83

FIGURE 6.9: Normalized total surface force on the lower interface due to a single charge (solid line) and a pair of charges (dashed line). (a) $\bar{d} = 0.1$, (b) $\bar{d} = 0.2$, (c) $\bar{d} = 0.3$. For all cases, $\varepsilon_{21} = 0.1$85

List of Symbols

Symbol	Description
d	Distance from the point charge to the lower interface
D	Electric displacement
$\mathbf{e}_r, \mathbf{e}_\theta, \mathbf{e}_z$	Unit vectors in cylindrical coordinate system
E	Electric field
f	Surface force density
F	Total surface force
H	Distance between the two interfaces in the layered dielectric system
H_0	Hankel transformation of 0 th order
H_0^{-1}	Inverse Hankel transformation
I	Identity tensor
$J_0(x)$	0 th order Bessel function of the first kind
$J_1(x)$	1 st order Bessel function of the first kind
q	Magnitude of the point charge
r, θ, z	Position within cylindrical coordinate system
T	Maxwell Stress Tensor (MST)
V	Volume
ϵ	Dielectric constant
ϵ_0	Electric permittivity of free space
ϕ	Electric potential
Φ	Transformed electric potential
∇^2	Laplacian operator

Chapter 1

INTRODUCTION

The applications of layered dielectric systems are common in energy storage and electrical insulation devices [1]–[5]. Most of these devices consist of multiple layers of dielectrics between grounded conducting plates or charged conductors. Microwave technologies such as antennas, transmission lines, computers, filters, power dividers etc. are also made of several conductor-dielectric combinations [6]–[8]. The studies on the performance of these electrical devices involve the calculation of electric potential, electric field as well as electrostatic force at the interfaces due to the charge distribution in the system [9]–[12]. As one example, in order to determine the wave-propagation properties of microstrip transmission lines, one must first obtain the electric field for a pair of charged conductors separated by a dielectric sheet [11]. Understanding the electrostatic force induced by a distribution of charges in layered dielectric medium is also important to many problems, especially in electromechanical devices for the semiconductor industry [13]–[16]. Proper handling of dielectrics in these devices is crucial to manufacture contamination free products. Electrostatic chucks are now widely used to replace mechanical holding systems for semiconducting wafers [17], [18]. These chucks normally consist of a planar array of parallel bar electrodes. An attractive electrostatic force is induced with a thinner layer of dielectric between the chuck and the product. For holding purposes, the performance of the electrostatic chucks depends on the magnitude of the generated electrostatic force, which in turn depends on proper selection of the dielectric. Another interesting application is found in the development of wall climbing robot technologies [19], [20]. Many methods have been proposed to introduce adhesive

forces between the wall and the robot, for example, negative air pressure, directional adhesive structures, magnetic force, and electrostatic force [21]–[25]. Liu *et al.* [26] discussed the electrostatic adhesion force while designing a wall climbing robot prototype. Their theoretical model considered a planar array of parallel electrodes, insulation film around the electrode panel and a thin layer of air gap between the electrode panel and the climbing wall. The electrodes acted as the source of the electrostatic field and the air gap corresponded to the wall surface roughness. Maxwell Stress Tensor was used to calculate the electrostatic adhesion force on the wall induced by the potentials applied to the electrodes. A similar work was done by Mao *et al.* [27] where the electrostatic force at the interfaces of a multilayered structure involving concentric ring electrodes was derived and compared with Finite Element simulation data.

Another very common physical phenomenon in layered dielectrics is adhesion (attractive force) between surfaces caused by contact charging [28], [29]. When two surfaces come into contact and then separate, charge transfer can occur between them [30] and this phenomenon is known as contact charging or contact electrification. Contact charging is a very common phenomenon and is important to many long-practiced technologies such as photocopying, electrostatic separation, and laser printing. Due to contact charging, a charge distribution is developed on each surface and this distribution is typically considered as a mosaic with oppositely charged regions on the two surfaces [31]. As a result, the charged surfaces show a tendency to cling to each other, a phenomenon known as contact adhesion. The study on contact charging has a long history, with many theoretical and experimental results including full atomic simulations developed to study the electrostatics of laminated dielectric systems [32], [33]. However, some fundamental issues such as the methods of charge transfer [34], polarity of charged surfaces [35], pattern of charge distribution on the surfaces [31] etc. are still being debated.

Compared with contact charging, the evaluation of adhesion force due to contact charging is much less done. Wan and co-workers [28] calculated the electrostatic attraction between two charged surfaces each having a square checkerboard pattern with domains of linear dimension and finite charge density. The two surfaces were placed in vacuum, and the electrostatic adhesion was calculated for aligned or misorientated boards. Brommann *et al.* [29] performed experiments to evaluate the electrostatic contributions to the work of separation during detachment of micro-structured PDMS samples from glass surface. Theoretical calculation for the adhesion force was also conducted by assuming correlated charge mosaics on the two surfaces and adopting the results of Wan *et al.* [28]. A small adjustment was introduced to account for the difference in the studied systems: in Wan *et al.*, the two surfaces have zero thickness, whereas in Brommann *et al.* the adhesion is between two half-spaces separated by an air gap. This adjustment, however, was empirical and did not result from a rigorous solution of the electrostatic problem. In addition, the different polarizability of the three media (PDMS, glass and air gap) was not taken into consideration in the force evaluation. This class of problems has motivated to conduct the study on electrostatic forces in multi-layered systems, and in this particular thesis, focus has been given on evaluating the forces on dielectric interfaces induced by a nearby point charge. It is evidenced by many other types of research that the calculation of the forces first requires the knowledge of the electric potential in the space induced by the point charge, which is solved in details in the present thesis.

Electrostatic problems for solving the electric potential in multilayered dielectrics have been studied in a number of previous works. Green's function-moment method based on image theory is commonly found in literature to solve such problems [36]–[38]. Pumplin [39] considered the problem of a parallel plate capacitor that consisted of two grounded plates and a point charge

in between. The electric potential was solved using image charge method and presented in terms of Green's function. Specifically, a distribution of point charges was introduced in the upper and lower spaces, with each charge having the same magnitude as the original point charge. The location of the image charges was solved to ensure that the electric potential on the two interfaces (grounded conducting plates) was zero. Pronic *et al.* [40] studied a multilayered dielectric system enclosed by a cylindrical conductor. An analogy was drawn to multistep electrical transmission line which had a current source with its two ends short terminated. Based on the analogy, Green's function satisfying the Poisson's differential equation was obtained for a point charge in the structure and the solution for the electric potential was presented as a double infinite sum. Image charge method was also used in a number of other works to study the potential in a layered dielectric sphere [41], multiconductor transmission lines [9] etc.

Heubrandtner *et al.* [42] presented expressions for the electric field of a point charge in an infinite plane condenser. They mentioned its application in particle detection process through Parallel Plate Chambers (PPC) and Resistive Plate Chambers (RPC), which respectively consisted of one and three homogeneous layers of dielectrics. The condenser was modeled as a single or multilayered dielectrics packed between two grounded conducting plates. Solution for the electric potential in the condenser was given, without detailed derivations, both in terms of infinite series and using an integral representation. The focus of Heubrandtner *et al.*'s study was to examine the convergence performance of the two forms of the solutions. Near the point of divergence, where the point charge is located, the integral representation of the solution gives overall better result than the series solution, due to the faster decay of the integrand and better performance in numerically evaluating the electric field when the electric potential needs to be differentiated.

In another previous work, a simple electrostatic problem was tackled with a three-layered dielectric system to determine the electric potential along with the induced surface density and the total induced charge at the interfaces [43]. The work was done by Barrera *et al.* where they considered a point charge embedded in one of the three homogeneous dielectric layers. They first solved the electric potential using the method of images, a series solution corresponding to an infinite array of image charges, and then converted it into integral form using two-dimensional Fourier transform. The original work contained mistakes, which was pointed out by an erratum published later [44], but without further examination.

It is clear that the method of image charges is the most widely used approach to solve electrostatic problems in layered dielectrics. Even though some works attempted to improve convergence performance using solutions in integral form, series solution obtained from image charges still served as a starting point. Given the apparent axisymmetry in many of those problems, it is surprising that there has been no attempt to tackle them using the Hankel transformation, a technique very useful for axisymmetric problems. In this thesis, a general problem is considered to solve for the electric potential using the Hankel transformation.

In addition, there has not been any work found, after an exhaustive literature search, that tackles the general problem relevant to contact adhesion, that is: what is the force between two dielectric half-spaces with surface charges separated by a dielectric gap? As a step towards solving such a problem, in this work, a simpler problem is tackled, namely the force between two dielectric half-spaces induced by a point charge located in the dielectric gap separating them. The detail description of the specific problem is provided in Chapter 2. At first, the electric potential induced by the single point charge is calculated (Chapter 3). Using the electric potential, distribution of the surface force density along the interfaces is determined and then this result is used to calculate the

total surface force acting on each of the interfaces (formulation in Chapter 4 and results and discussions in Chapter 5). Due to linear nature of the equations governing the electric potential, the methodology and results can be extended easily into broad applications to calculate the electrostatic forces induced by a distribution of charges in layered dielectrics, and hence is useful for quantifying electrostatic-driven interfacial forces in general. An example to solve this type of problem is presented where a pair of equal and opposite charges are considered in the same model (Chapter 6). Conclusion and future work are presented in Chapter 7.

Chapter 2

PROBLEM DESCRIPTION AND FORMULATION

2.1 Physical description of the problem

The schematic of the specific problem with a single point charge being studied in this work is shown in Fig. 2.1. Here, the space is divided into three homogeneous dielectric domains, which are all assumed to be infinitely large in the horizontal direction and can differ in dielectric properties. The middle dielectric (denoted as domain I) has a thickness of H and dielectric constant ε_1 . The lower space (II) extends downward to infinity and has dielectric constant ε_2 . The upper space (III) extends upwards to infinity and has dielectric constant ε_3 . These three domains are separated by hypothetical planar interface. A point charge of magnitude q is located at a distance d above the lower interface ($0 < d < H$). For each interface (between I and II, or between I and III), the polarization caused by the point charge will be different in its two sides due to the difference in dielectric properties. If a small volume is considered at an arbitrary location on the interface, the difference in polarization on the two sides will lead to a net polarization charge within that volume. The interaction between this net polarization charge and the original point charge results in interfacial forces which can be attractive or repulsive depending on the induced electric field and polarization charge. In reality, these forces can cause deformation of the materials on the interface, but solving the deformation field is out of the scope of this work. In addition, the total surface force on each interface is assumed to be balanced by an external force so that the system is in global force balance.

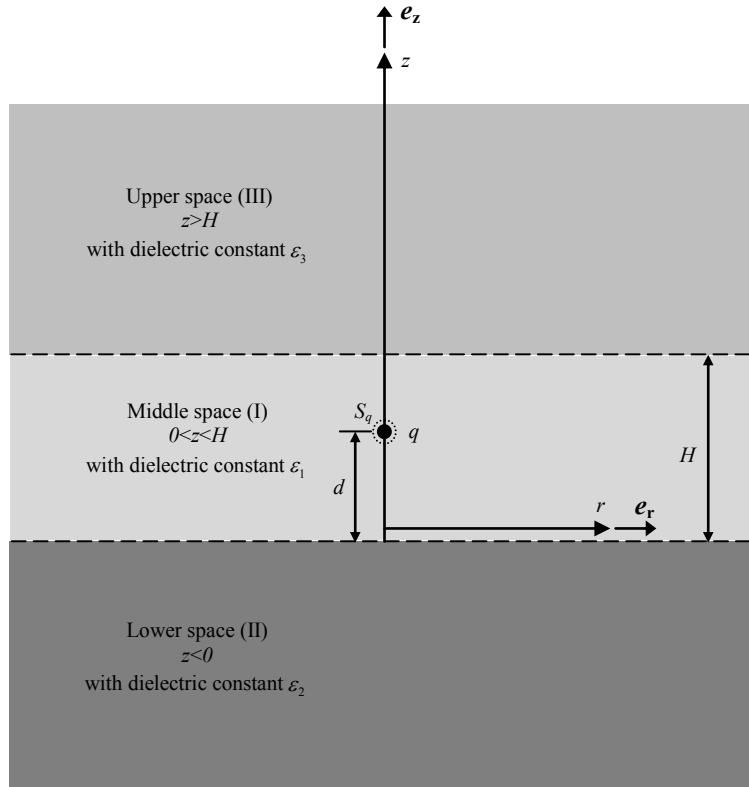


FIGURE 2.1: Schematic of the electrostatic problem with a single point charge considered in this work.

2.2 Methodology

It is clear from Fig. 2.1 that the problem possesses axisymmetry; therefore, it is most appropriate to use the cylindrical coordinate r , θ and z as shown. Without the loss of generality, the z -axis is placed so that the point charge is located directly on it. Due to axisymmetry, the electric potential ϕ is expected to be a function of r and z only. To obtain the axially symmetric $\phi(r, z)$, the following procedure is applied. First, a boundary value problem (BVP) is developed for the electric potential considering the Laplace equation of electrostatics as the governing equation with proper boundary conditions. Then the technique of Hankel transformation is used,

which reduces the dimension of the BVP, to calculate the closed-form solution for ϕ . This solution is used to determine the surface force density \mathbf{f} (local force per unit area acting on the interfaces) and the total surface force \mathbf{F} using the following method. Knowing the electric potential throughout the space, the electric field \mathbf{E} is calculated. Following the calculation of \mathbf{E} , the Maxwell Stress Tensor (MST) \mathbf{T} is computed in terms of the electric field components that is induced by the point charge. The electric forces on a body in an electric field are related to MST by a volume integral which contains the volume of the considered body. This relationship is first used to deduce \mathbf{f} on the interfaces between regions I and II, and regions I and III. Finally, having determined the surface force density, the total force acting on the interfaces is found by taking the surface integral of \mathbf{f} .

2.3 Formulation

2.3.1 Governing equation to solve the electric potential

According to the Maxwell's equation that governs the electrostatic phenomena,

$$\nabla \cdot \mathbf{D} = \rho_v \quad (2.1)$$

where, \mathbf{D} is the electric displacement and ρ_v is the volumetric charge density.

As the specific problem (Fig. 2.1) in this study has no free charges in any region (I, II and III) except at the location of the point charge, Eqn. (2.1) becomes

$$\nabla \cdot \mathbf{D} = 0 \quad (2.2)$$

where the presence of the point charge will be considered later as a boundary condition (BC). Following the general relationship between the electric displacement, \mathbf{D} and the electrostatic field, \mathbf{E} ($\mathbf{D} = \varepsilon_0 \varepsilon_i \mathbf{E}$; ε_0 is the electric permittivity of free space and ε_i is the dielectric constant of the corresponding region ($i = 1, 2$ and 3)), and because ε_i is spatially invariant in each region, Eqn. (2.2) becomes

$$\nabla \cdot \mathbf{E} = 0. \quad (2.3)$$

The electric field also satisfies the following Maxwell equation

$$\nabla \times \mathbf{E} = 0 \quad (2.4)$$

which implies that \mathbf{E} can be expressed as the gradient of a scalar function, specifically the electric potential ϕ :

$$\mathbf{E} = -\nabla \phi(r, z). \quad (2.5)$$

Eqs. (2.3), (2.4) and (2.5) can be combined into one partial differential equation for the electric potential ϕ :

$$\nabla^2 \phi(r, z) = 0. \quad (2.6)$$

This Laplace equation is the governing equation in a homogeneous charge-free dielectric system. Eqn. (2.6) is solved using the Hankel transformation to determine the electric potential $\phi(r, z)$ in each region individually. Eqn. (2.6) applies to all the spatial points in region I except for the location where the point charge q is embedded.

2.3.2 Boundary conditions

To find the appropriate solution to the Laplace equation, we must consider the effect of point charge that will be represented by a BC given below. In addition, the governing equation (Eqn. (2.6)) is subject to the BCs on the interfaces ($z = 0$ and $z = H$) as well as at $r, z \rightarrow \infty$:

$$\lim_{S_q \rightarrow 0} \oint_{S_q} (-\varepsilon_0 \varepsilon_1 \nabla \phi) \cdot \mathbf{n} dA = q, \quad (2.7)$$

$$\lim_{z \rightarrow 0^+} \phi = \lim_{z \rightarrow 0^-} \phi, \quad (2.8)$$

$$\lim_{z \rightarrow 0^+} \varepsilon_1 \frac{\partial \phi}{\partial z} = \lim_{z \rightarrow 0^-} \varepsilon_2 \frac{\partial \phi}{\partial z}, \quad (2.9)$$

$$\lim_{z \rightarrow H^+} \phi = \lim_{z \rightarrow H^-} \phi, \quad (2.10)$$

$$\lim_{z \rightarrow H^+} \varepsilon_3 \frac{\partial \phi}{\partial z} = \lim_{z \rightarrow H^-} \varepsilon_1 \frac{\partial \phi}{\partial z}, \quad (2.11)$$

$$\phi(r, z \rightarrow \infty) \rightarrow 0, \quad (2.12)$$

$$\phi(r, z \rightarrow -\infty) \rightarrow 0. \quad (2.13)$$

Eqn. (2.7) is the BC for the point charge, where S_q is a closed surface enclosing q and \mathbf{n} is the outward normal of S_q . Eqs. (2.8) and (2.10) are the continuity conditions for the electric potential across the two interfaces; and Eqs. (2.9) and (2.11) describe the continuity for the normal electric displacement across the interfaces [46]. Eqs. (2.12) and (2.13) are the far field boundary conditions, i.e., vanishing potential at infinity.

Chapter 3

ELECTRIC POTENTIAL SOLVED WITH HANKEL TRANSFORMATION

3.1 Hankel Transformation

There are different methods exist to solve the BVPs in electrostatics. In this work. The governing equation is solved by using the Hankel transforms which are integral transformations that consist of Bessel functions as kernels. While dealing with the problem that shows cylindrical symmetry like the current one, the Hankel transformations are found very useful. Specifically, the Laplace's partial differential equation in cylindrical coordinates can be transformed into an ordinary differential equation by using the Hankel transformation which motivates applying this method to solve the present problem.

For a function $\phi(r)$; $r = 0$ to ∞ , its Hankel transformation of the 0th order is defined by [47]

$$\Phi(\rho) = H_0[\phi(r); \rho] \equiv \int_0^{\infty} r\phi(r)J_0(\rho r)dr \quad (3.1)$$

where, H_0 is the Hankel transform of 0th order and $J_0(x)$ is the 0th order Bessel function of the first kind. The inverse Hankel transform of order zero is defined by [47]

$$\phi(r) = H_0^{-1}[\Phi(\rho); r] \equiv \int_0^{\infty} \rho\Phi(\rho)J_0(\rho r)d\rho. \quad (3.2)$$

Among the few elementary properties of the Hankel transforms, the following property is considered the principal one for its applications to solving differential equations [47]:

$$H_0 \left[\frac{1}{r} \frac{\partial}{\partial r} \left(r \frac{\partial \phi}{\partial r} \right); \rho \right] = -\rho^2 H_0 [\phi(r); \rho]. \quad (3.3)$$

The Laplacian operator under cylindrical coordinates is in the following form:

$$\nabla^2 = \frac{\partial^2}{\partial r^2} + \frac{1}{r} \frac{\partial}{\partial r} + \frac{1}{r^2} \frac{\partial^2}{\partial \theta^2} + \frac{\partial^2}{\partial z^2} \equiv \frac{1}{r} \frac{\partial}{\partial r} \left(r \frac{\partial}{\partial r} \right) + \frac{1}{r^2} \frac{\partial^2}{\partial \theta^2} + \frac{\partial^2}{\partial z^2}. \quad (3.4)$$

For a problem with cylindrical symmetry, Eqn. (3.4) reduces to:

$$\nabla^2 = \frac{1}{r} \frac{\partial}{\partial r} \left(r \frac{\partial}{\partial r} \right) + \frac{\partial^2}{\partial z^2}. \quad (3.5)$$

Using the property of the Hankel transform (Eqn. (3.3)), it is clear from Eqn. (3.5) that a partial differential equation involving the Laplacian operator can be transformed into an ordinary differential equation, which can simplify the solution of the BVP.

There are some functions whose 0th order Hankel transformation can be evaluated in closed form. The following transformed entities are presented as examples which are applied while solving for the electric potential in this work [48]

$$\int_0^{\infty} r (a^2 + r^2)^{-\frac{1}{2}} J_0(\rho r) dr = \frac{e^{-a\rho}}{\rho}, \quad (3.6)$$

$$\int_0^{\infty} a (a^2 + r^2)^{-\frac{3}{2}} J_0(\rho r) dr = \frac{e^{-a\rho}}{a}, \quad (3.7)$$

$$\int_0^{\infty} e^{-a\rho} J_0(\rho r) d\rho = (a^2 + r^2)^{-\frac{1}{2}}. \quad (3.8)$$

where, these equations are valid for $a > 0$.

3.2 Transformation of boundary value problem (BVP)

To solve Eqs. (2.6) to (2.11) for the problem model (Fig. 2.1), first the electric potentials on the interfaces $z = 0$ and $z = H$ are denoted by two unknown functions $\phi_0(r)$ and $\phi_H(r)$ respectively. This is warranted by the continuity conditions (2.8) and (2.10) and facilitates the construction of separate Dirichlet BVPs in all three domains. Let the electric potential of the middle, lower and upper regions satisfy the following Dirichlet BVP:

Region I ($0 < z < H$):

$$\nabla^2 \phi_I(r, 0 < z < H) = 0, \quad (3.9)$$

$$\phi_I(r, H) = \phi_H(r), \quad (3.10)$$

$$\phi_I(r, 0) = \phi_0(r). \quad (3.11)$$

Region II ($z < 0$):

$$\nabla^2 \phi_{II}(r, z < 0) = 0, \quad (3.12)$$

$$\phi_{II}(r, z \rightarrow -\infty) \rightarrow 0, \quad (3.13)$$

$$\phi_{II}(r, 0) = \phi_0(r). \quad (3.14)$$

Region III ($z > H$):

$$\nabla^2 \phi_{III}(r, z > H) = 0, \quad (3.15)$$

$$\phi_{III}(r, z \rightarrow \infty) \rightarrow 0, \quad (3.16)$$

$$\phi_{III}(r, H) = \phi_H(r). \quad (3.17)$$

Taking the Hankel transform of order zero according to Eqn. (3.1) and making the use of its property from Eqn. (3.3), the BVPs in regions II and III for the transformed electric potential $\Phi(\rho, z)$ now read

Region II ($z < 0$):

$$\frac{\partial^2 \Phi_{II}(\rho, z < 0)}{\partial^2 z} - \rho^2 \Phi_{II}(\rho, z < 0) = 0, \quad (3.18)$$

$$\Phi_{II}(\rho, z \rightarrow -\infty) \rightarrow 0, \quad (3.19)$$

$$\Phi_{II}(\rho, 0) = \Phi_0(\rho). \quad (3.20)$$

Region III ($z > H$):

$$\frac{\partial^2 \Phi_{III}(\rho, z > H)}{\partial^2 z} - \rho^2 \Phi_{III}(\rho, z > H) = 0, \quad (3.21)$$

$$\Phi_{III}(\rho, z \rightarrow \infty) \rightarrow 0, \quad (3.22)$$

$$\Phi_{III}(\rho, H) = \Phi_H(\rho). \quad (3.23)$$

where $\Phi_0(\rho)$ and $\Phi_H(\rho)$ are the Hankel transformation of the functions $\phi_0(r)$ and $\phi_H(r)$ respectively. Eqs. (3.19) and (3.20) are the corresponding Hankel transformed BCs to Eqn. (3.18) while Eqs. (3.22) and (3.23) correspond to Eqn. (3.21) as the transformed BCs.

For region I ($0 < z < H$), since it contains a singularity (point charge q), the singular part of the electric potential is first separated out which is denoted by ϕ_A and is expressed as

$$\phi_A(r, 0 < z < H) = \frac{q}{4\pi\epsilon_0\epsilon_1\sqrt{r^2 + (z-d)^2}}. \quad (3.24)$$

Here, ϕ_A is the potential due to q in absence of the interfaces, i.e., if the upper and lower regions had the same dielectric property as the middle region. This gives the correct singularity at the location of the point charge and allows the BC (2.7) to be satisfied. It can be easily seen that ϕ_A is a function of the distance $\sqrt{r^2 + (z-d)^2}$ from the point charge and its values on the interfaces are obtained by setting $z = 0$ and $z = H$ in Eqn. (3.24). ϕ_A on the lower interface is denoted by ϕ_{A0} and is

$$\phi_{A0}(r) \equiv \phi_{A0}(r, 0) = \frac{q}{4\pi\epsilon_0\epsilon_1\sqrt{r^2 + d^2}}. \quad (3.25)$$

Similarly, ϕ_{AH} is the electric potential on the upper interface which reads

$$\phi_{AH}(r) \equiv \phi_{AH}(r, H) = \frac{q}{4\pi\epsilon_0\epsilon_1\sqrt{r^2 + (H-d)^2}}. \quad (3.26)$$

The second part of the electric potential in region I, denoted as ϕ_B , is non-singular everywhere, and is the difference between ϕ_A and the total electric potential in the middle region. ϕ_B satisfies the following BVP:

$$\nabla^2 \phi_B(r, 0 < z < H) = 0, \quad (3.27)$$

$$\phi_B(r, z = 0) = \phi_0(r) - \phi_{A0}(r), \quad (3.28)$$

$$\phi_B(r, z = H) = \phi_H(r) - \phi_{AH}(r). \quad (3.29)$$

Applying the Hankel transformation to ϕ_B and using its property gives the following transformed BVP:

$$\frac{\partial^2 \Phi_B(\rho, 0 < z < H)}{\partial^2 z} - \rho^2 \Phi_B(\rho, 0 < z < H) = 0, \quad (3.30)$$

$$\Phi_B(\rho, 0) = \Phi_0(\rho) - \Phi_{A0}(\rho), \quad (3.31)$$

$$\Phi_B(\rho, H) = \Phi_H(\rho) - \Phi_{AH}(\rho). \quad (3.32)$$

Here, $\Phi_{A0}(\rho)$ is the Hankel transform of $\phi_{A0}(r)$, which can be analytically evaluated from Eqn.

(3.25) following Eqn. (3.6):

$$\Phi_{A0}(\rho) = \int_0^\infty r \frac{q}{4\pi\epsilon_0\epsilon_1\sqrt{r^2+d^2}} J_0(\rho r) dr = \frac{qe^{-d\rho}}{4\pi\epsilon_0\epsilon_1\rho}, \quad d > 0. \quad (3.33)$$

Similarly, $\Phi_{AH}(\rho)$ is the Hankel transform of $\phi_{AH}(r)$ where applying the property of Eqn. (3.6)

again yields:

$$\Phi_{AH}(\rho) = \int_0^{\infty} r \frac{q}{4\pi\epsilon_0\epsilon_1\sqrt{r^2 + (H-d)^2}} J_0(\rho r) dr = \frac{qe^{-(H-d)\rho}}{4\pi\epsilon_0\epsilon_1\rho}, \quad d < H. \quad (3.34)$$

3.3 Solution of the transformed BVP

So far, we have constructed separate Dirichlet BVP for each domain, and each BVP can be solved individually to obtain $\Phi(\rho, z)$ in terms of the unknown functions $\Phi_H(\rho)$ and $\Phi_0(\rho)$. All the BCs have been used except Eqs. (2.9) and (2.11), which will be used later to determine these two unknown functions.

It is straightforward to solve Eqs. (3.18)-(3.20) and (3.21)-(3.23) to obtain the transformed electric potential in regions II and III. First, solving the differential equation in Eqn. (3.18) gives:

$$\Phi_{II}(\rho, z < 0) = C_1 e^{\rho z} + C_2 e^{-\rho z} \quad (3.35)$$

where, $C_1 = \Phi_0(\rho)$ and $C_2 = 0$ are unknown constants which are determined by using the BCs (3.19) and (3.20). Substituting the values of C_1 and C_2 in Eqn. (3.35):

$$\Phi_{II}(\rho, z < 0) = \Phi_0(\rho) e^{\rho z}. \quad (3.36)$$

Similarly, the transformed electric potential in region III is found:

$$\Phi_{III}(\rho, z > H) = \Phi_H(\rho) e^{\rho(H-z)}. \quad (3.37)$$

The same method is applied to solve Eqn. (3.30) by using the BCs (3.31) and (3.32) that yields

$$\begin{aligned}\Phi_B(\rho, 0 < z < H) = & \frac{(\Phi_H(\rho) - \Phi_{AH}(\rho)) \sinh(\rho z)}{\sinh(\rho H)} \\ & + \frac{(\Phi_0(\rho) - \Phi_{A0}(\rho)) \sinh[\rho(H-z)]}{\sinh(\rho H)}.\end{aligned}\quad (3.38)$$

3.4 Electric potential obtained from inverse Hankel Transform

According to Eqn. (3.2) the inverse Hankel transformation of Eqs. (3.36) and (3.37) immediately transforms back the original electric potential in region II and III respectively in following forms:

$$\phi_{II}(r, z < 0) = \int_0^{\infty} \rho \Phi_0(\rho) e^{\rho z} J_0(\rho r) d\rho \quad (3.39)$$

and,

$$\phi_{III}(r, z > H) = \int_0^{\infty} \rho \Phi_H(\rho) e^{\rho(H-z)} J_0(\rho r) d\rho. \quad (3.40)$$

The inverse Hankel transformation is also applied to Eqn. (3.38) which corresponds to

$$\begin{aligned}\phi_B(r, 0 < z < H) = & \int_0^{\infty} \rho \frac{\Phi_H(\rho) \sinh(\rho z) + \Phi_0(\rho) \sinh[\rho(H-z)]}{\sinh(\rho H)} J_0(\rho r) d\rho \\ & + \frac{q}{4\pi\epsilon_0\epsilon_1} \int_0^{\infty} \frac{e^{-\rho(H-d)} \sinh(\rho z) - e^{-\rho d} \sinh[\rho(H-z)]}{\sinh(\rho H)} J_0(\rho r) d\rho.\end{aligned}\quad (3.41)$$

Thus, the total electric potential in the region I is the sum of $\phi_A(r, 0 < z < H)$ and $\phi_B(r, 0 < z < H)$:

$$\phi(r, 0 < z < H) = \frac{q}{4\pi\epsilon_0\epsilon_1 \sqrt{r^2 + (z-d)^2}} + \phi_B(r, 0 < z < H). \quad (3.42)$$

3.5 Solution for the unknowns $\Phi_H(\rho)$ and $\Phi_0(\rho)$

It can be seen from Eqs. (3.39), (3.40) and (3.42) that the solutions for all three regions are in terms of $\Phi_H(\rho)$ and $\Phi_0(\rho)$. To determine these two functions, the BCs (2.9) and (2.11) are applied, using the expressions for the potentials. Eqs. (3.39) and (3.42) are used in Eqn. (2.9) where the terms of the Left Hand Side (LHS) of Eqn. (2.9) can be presented as follows:

$$\lim_{z \rightarrow 0^+} \varepsilon_1 \frac{\partial}{\partial z} \left[\frac{q}{4\pi\varepsilon_0\varepsilon_1 \sqrt{r^2 + (z-d)^2}} \right] = \frac{qd}{4\pi\varepsilon_0 (r^2 + d^2)^{\frac{3}{2}}},$$

$$\lim_{z \rightarrow 0^+} \varepsilon_1 \frac{\partial}{\partial z} \left[\int_0^\infty \frac{\rho\Phi_H \sinh(\rho z)}{\sinh(\rho H)} J_0(\rho r) d\rho \right] = \int_0^\infty \frac{\varepsilon_1 \rho^2 \Phi_H}{\sinh(\rho H)} J_0(\rho r) d\rho,$$

$$\lim_{z \rightarrow 0^+} \varepsilon_1 \frac{\partial}{\partial z} \left[\int_0^\infty \frac{\rho\Phi_0 \sinh[\rho(H-z)]}{\sinh(\rho H)} J_0(\rho r) d\rho \right] = - \int_0^\infty \frac{\varepsilon_1 \rho^2 \Phi_0 \cosh(\rho H)}{\sinh(\rho H)} J_0(\rho r) d\rho,$$

$$\lim_{z \rightarrow 0^+} \varepsilon_1 \frac{\partial}{\partial z} \left[\frac{q}{4\pi\varepsilon_0\varepsilon_1} \int_0^\infty \frac{e^{-\rho(H-d)} \sinh(\rho z)}{\sinh(\rho H)} J_0(\rho r) d\rho \right] = \frac{q}{4\pi\varepsilon_0} \int_0^\infty \frac{\rho e^{-\rho(H-d)}}{\sinh(\rho H)} J_0(\rho r) d\rho,$$

$$\lim_{z \rightarrow 0^+} \varepsilon_1 \frac{\partial}{\partial z} \left[\frac{q}{4\pi\varepsilon_0\varepsilon_1} \int_0^\infty \frac{e^{-\rho d} \sinh[\rho(H-z)]}{\sinh(\rho H)} J_0(\rho r) d\rho \right] = - \frac{q}{4\pi\varepsilon_0} \int_0^\infty \frac{\rho e^{-\rho d} \cosh(\rho H)}{\sinh(\rho H)} J_0(\rho r) d\rho.$$

The Right Hand Side (RHS) of Eqn. (2.9) can be expressed as

$$\lim_{z \rightarrow 0^-} \varepsilon_2 \frac{\partial}{\partial z} \left[\int_0^\infty \rho\Phi_0(\rho) e^{\rho z} J_0(\rho r) d\rho \right] = \int_0^\infty \varepsilon_2 \rho^2 \Phi_0(\rho) J_0(\rho r) d\rho.$$

Finally, Eqn. (2.9) stands in following form:

$$\begin{aligned}
& \frac{qd}{4\pi\varepsilon_0(r^2+d^2)^{\frac{3}{2}}} + \int_0^\infty \frac{\varepsilon_1\rho^2[\Phi_H(\rho)-\Phi_0(\rho)\cosh(\rho H)]}{\sinh(\rho H)} J_0(\rho r) d\rho \\
& - \frac{q}{4\pi\varepsilon_0} \int_0^\infty \frac{\rho[e^{-\rho(H-d)}-e^{-\rho d}\cosh(\rho H)]}{\sinh(\rho H)} J_0(\rho r) d\rho = \int_0^\infty \varepsilon_2\rho^2\Phi_0(\rho)J_0(\rho r) d\rho.
\end{aligned} \tag{3.43}$$

Similarly, substituting Eqs. (3.40) and (3.42) in BC (2.11) gives another expression that includes both the unknowns $\Phi_H(\rho)$ and $\Phi_0(\rho)$ where the LHS of Eqn. (2.11) corresponds to

$$\lim_{z \rightarrow H^+} \varepsilon_3 \frac{\partial}{\partial z} \left[\int_0^\infty \rho \Phi_H(\rho) e^{\rho(H-z)} J_0(\rho r) d\rho \right] = - \int_0^\infty \varepsilon_3 \rho^2 \Phi_H(\rho) J_0(\rho r) d\rho$$

and the RHS terms are evaluated as

$$\lim_{z \rightarrow H^-} \varepsilon_1 \frac{\partial}{\partial z} \left[\frac{q}{4\pi\varepsilon_0\varepsilon_1 \sqrt{r^2+(z-d)^2}} \right] = - \frac{q(H-d)}{4\pi\varepsilon_0 [r^2+(H-d)^2]^{\frac{3}{2}}},$$

$$\lim_{z \rightarrow H^-} \varepsilon_1 \frac{\partial}{\partial z} \left[\int_0^\infty \frac{\rho \Phi_H \sinh(\rho z)}{\sinh(\rho H)} J_0(\rho r) d\rho \right] = \int_0^\infty \frac{\varepsilon_1 \rho^2 \Phi_H(\rho) \cosh(\rho H)}{\sinh(\rho H)} J_0(\rho r) d\rho,$$

$$\lim_{z \rightarrow H^-} \varepsilon_1 \frac{\partial}{\partial z} \left[\int_0^\infty \frac{\rho \Phi_0 \sinh[\rho(H-z)]}{\sinh(\rho H)} J_0(\rho r) d\rho \right] = - \int_0^\infty \frac{\varepsilon_1 \rho^2 \Phi_0(\rho)}{\sinh(\rho H)} J_0(\rho r) d\rho,$$

$$\lim_{z \rightarrow H^-} \varepsilon_1 \frac{\partial}{\partial z} \left[\frac{q}{4\pi\varepsilon_0\varepsilon_1} \int_0^\infty \frac{e^{-\rho(H-d)} \sinh(\rho z)}{\sinh(\rho H)} J_0(\rho r) d\rho \right] = \frac{q}{4\pi\varepsilon_0} \int_0^\infty \frac{\rho e^{-\rho(H-d)} \cosh(\rho H)}{\sinh(\rho H)} J_0(\rho r) d\rho,$$

$$\lim_{z \rightarrow H^-} \varepsilon_1 \frac{\partial}{\partial z} \left[\frac{q}{4\pi\varepsilon_0\varepsilon_1} \int_0^\infty \frac{e^{-\rho d} \sinh[\rho(H-z)]}{\sinh(\rho H)} J_0(\rho r) d\rho \right] = - \frac{q}{4\pi\varepsilon_0} \int_0^\infty \frac{\rho e^{-\rho d}}{\sinh(\rho H)} J_0(\rho r) d\rho.$$

Finally, the new form of Eqn. (2.11) yields

$$\begin{aligned}
-\int_0^{\infty} \varepsilon_3 \rho^2 \Phi_H(\rho) J_0(\rho r) d\rho &= -\frac{q(H-d)}{4\pi\varepsilon_0 \left[r^2 + (H-d)^2 \right]^{\frac{3}{2}}} \\
&+ \int_0^{\infty} \frac{\varepsilon_1 \rho^2 \left[\Phi_H(\rho) \cosh(\rho H) - \Phi_0(\rho) \right]}{\sinh(\rho H)} J_0(\rho r) d\rho \\
&- \frac{q}{4\pi\varepsilon_0} \int_0^{\infty} \frac{\rho \left[e^{-\rho(H-d)} \cosh(\rho H) - e^{-\rho d} \right]}{\sinh(\rho H)} J_0(\rho r) d\rho.
\end{aligned} \tag{3.44}$$

After applying the Hankel transformation on both sides of Eqs. (3.43) and (3.44) and considering the transformed quantities of Eqn. (3.7), the following equations are formed:

$$\begin{aligned}
\frac{\varepsilon_1 \Phi_H(\rho)}{\sinh(\rho H)} - \Phi_0(\rho) \left[\varepsilon_1 \coth(\rho H) + \varepsilon_2 \right] &= \frac{q}{4\pi\varepsilon_0 \rho} \\
&\times \left[\frac{e^{-\rho(H-d)}}{\sinh(\rho H)} - e^{-\rho d} \coth(\rho H) - e^{-\rho d} \right],
\end{aligned} \tag{3.45}$$

$$\begin{aligned}
\Phi_H(\rho) \left[-\varepsilon_3 - \varepsilon_1 \coth(\rho H) \right] + \frac{\varepsilon_1 \Phi_0(\rho)}{\sinh(\rho H)} &= \frac{q}{4\pi\varepsilon_0 \rho} \\
&\times \left[-e^{-\rho(H-d)} - e^{-\rho(H-d)} \coth(\rho H) + \frac{e^{-\rho d}}{\sinh(\rho H)} \right].
\end{aligned} \tag{3.46}$$

Solving Eqs. (3.45) and (3.46) as well as after some algebra, $\Phi_H(\rho)$ and $\Phi_0(\rho)$ are found to be

$$\Phi_H(\rho) = \frac{q}{4\pi\varepsilon_0 \rho} \left[\frac{2 \sinh[\rho(H-d)] + 2 \sinh(\rho d) \left[\cosh(\rho H) + \frac{\varepsilon_2}{\varepsilon_1} \sinh(\rho H) \right] e^{-\rho d}}{\sinh^2(\rho H) \left[(\varepsilon_2 + \varepsilon_3) \coth(\rho H) + \left(\frac{\varepsilon_2 \varepsilon_3}{\varepsilon_1} + \varepsilon_1 \right) \right]} \right], \tag{3.47}$$

$$\Phi_0(\rho) = \frac{q}{4\pi\epsilon_0\rho} \left[\frac{2 \sinh(\rho d) + 2 \sinh[\rho(H-d)] \left[\cosh(\rho H) + \frac{\epsilon_3}{\epsilon_1} \sinh(\rho H) \right]}{\sinh^2(\rho H) \left[(\epsilon_2 + \epsilon_3) \coth(\rho H) + \left(\frac{\epsilon_2 \epsilon_3}{\epsilon_1} + \epsilon_1 \right) \right]} \right]. \quad (3.48)$$

The solutions for $\Phi_H(\rho)$ and $\Phi_0(\rho)$ are used in Eqs. (3.39), (3.40) and (3.42) which give

Region I:

$$\begin{aligned} \phi_I(r, 0 < z < H) = & \frac{q}{4\pi\epsilon_0\epsilon_1\sqrt{r^2 + (z-d)^2}} \\ & + \frac{q}{4\pi\epsilon_0} \int_0^\infty \left[\frac{2 \sinh[\rho(H-d)] + 2 \sinh(\rho d) \left[\cosh(\rho H) + \frac{\epsilon_2}{\epsilon_1} \sinh(\rho H) \right]}{\sinh^3(\rho H) \left[(\epsilon_2 + \epsilon_3) \coth(\rho H) + \left(\frac{\epsilon_2 \epsilon_3}{\epsilon_1} + \epsilon_1 \right) \right]} \right] \\ & \quad \times \sinh(\rho z) J_0(\rho r) d\rho \\ & + \frac{q}{4\pi\epsilon_0} \int_0^\infty \left[\frac{2 \sinh(\rho d) + 2 \sinh[\rho(H-d)] \left[\cosh(\rho H) + \frac{\epsilon_3}{\epsilon_1} \sinh(\rho H) \right]}{\sinh^3(\rho H) \left[(\epsilon_2 + \epsilon_3) \coth(\rho H) + \left(\frac{\epsilon_2 \epsilon_3}{\epsilon_1} + \epsilon_1 \right) \right]} \right] \\ & \quad \times \sinh[\rho(H-z)] J_0(\rho r) d\rho \\ & - \frac{q}{4\pi\epsilon_0\epsilon_1} \int_0^\infty \frac{e^{-\rho(H-d)} \sinh(\rho z) + e^{-\rho d} \sinh[\rho(H-z)]}{\sinh(\rho H)} J_0(\rho r) d\rho, \end{aligned} \quad (3.49)$$

Region II:

$$\begin{aligned} \phi_{II}(r, z < 0) = & \frac{q}{4\pi\epsilon_0} \\ & \times \int_0^\infty \left[\frac{2 \sinh(\rho d) + 2 \sinh[\rho(H-d)] \left[\cosh(\rho H) + \frac{\epsilon_3}{\epsilon_1} \sinh(\rho H) \right]}{\sinh^2(\rho H) \left[(\epsilon_2 + \epsilon_3) \coth(\rho H) + \left(\frac{\epsilon_2 \epsilon_3}{\epsilon_1} + \epsilon_1 \right) \right]} \right] e^{\rho z} J_0(\rho r) d\rho, \end{aligned} \quad (3.50)$$

Region III:

$$\phi_{III}(r, z > H) = \frac{q}{4\pi\epsilon_0} \times \int_0^\infty \left[\frac{2 \sinh[\rho(H-d)] + 2 \sinh(\rho d) \left[\cosh(\rho H) + \frac{\epsilon_2}{\epsilon_1} \sinh(\rho H) \right]}{\sinh^2(\rho H) \left[(\epsilon_2 + \epsilon_3) \coth(\rho H) + \left(\frac{\epsilon_2 \epsilon_3}{\epsilon_1} + \epsilon_1 \right) \right]} \right] e^{\rho(H-z)} J_0(\rho r) d\rho. \quad (3.51)$$

Eqs. (3.49)-(3.51) are the complete solutions to the electric potential in all three domains, as these satisfy the governing equation and all BCs in the system.

3.6 Normalization of electric potential

To reduce the number of independent variables and allow broader application of the results, the following normalization is introduced:

$$\bar{\phi} = \frac{4\pi\epsilon_0\epsilon_1 H}{q} \phi, \quad \bar{r} = \frac{r}{H}, \quad \bar{z} = \frac{z}{H}, \quad \bar{\rho} = \rho H, \quad \bar{d} = \frac{d}{H}, \quad \epsilon_{21} = \frac{\epsilon_2}{\epsilon_1}, \quad \epsilon_{31} = \frac{\epsilon_3}{\epsilon_1}. \quad (3.52)$$

The normalized electric potential for upper, lower and middle regions are respectively given by

Region I ($0 < \bar{z} < 1$):

$$\begin{aligned}
\bar{\phi}_I(\bar{r}, 0 < \bar{z} < 1) = & \frac{1}{\sqrt{\bar{r}^2 + (\bar{z} - \bar{d})^2}} \\
& + 2 \int_0^\infty \frac{\sinh[\bar{\rho}(1 - \bar{d})] + [\cosh(\bar{\rho}) + \varepsilon_{21} \sinh(\bar{\rho})] \sinh(\bar{\rho}\bar{d})}{\sinh^3(\bar{\rho}) [(\varepsilon_{21} + \varepsilon_{31}) \coth(\bar{\rho}) + (\varepsilon_{21}\varepsilon_{31} + 1)]} \sinh(\bar{\rho}\bar{z}) J_0(\bar{\rho}\bar{r}) d\bar{\rho} \\
& + 2 \int_0^\infty \frac{\sinh(\bar{\rho}\bar{d}) + [\cosh(\bar{\rho}) + \varepsilon_{31} \sinh(\bar{\rho})] \sinh[\bar{\rho}(1 - \bar{d})]}{\sinh^3(\bar{\rho}) [(\varepsilon_{21} + \varepsilon_{31}) \coth(\bar{\rho}) + (\varepsilon_{21}\varepsilon_{31} + 1)]} \sinh[\bar{\rho}(1 - \bar{z})] J_0(\bar{\rho}\bar{r}) d\bar{\rho} \\
& - \int_0^\infty \frac{e^{-\bar{\rho}(1 - \bar{d})} \sinh(\bar{\rho}\bar{z}) + e^{-\bar{\rho}\bar{d}} \sinh[\bar{\rho}(1 - \bar{z})]}{\sinh(\bar{\rho})} J_0(\bar{\rho}\bar{r}) d\bar{\rho},
\end{aligned} \tag{3.53}$$

Region II ($\bar{z} < 0$):

$$\bar{\phi}_{II}(\bar{r}, \bar{z} < 0) = 2 \int_0^\infty \frac{\sinh(\bar{\rho}\bar{d}) + [\cosh(\bar{\rho}) + \varepsilon_{31} \sinh(\bar{\rho})] \sinh[\bar{\rho}(1 - \bar{d})]}{\sinh^2(\bar{\rho}) [(\varepsilon_{21} + \varepsilon_{31}) \coth(\bar{\rho}) + (\varepsilon_{21}\varepsilon_{31} + 1)]} e^{\bar{\rho}\bar{z}} J_0(\bar{\rho}\bar{r}) d\bar{\rho}, \tag{3.54}$$

Region III ($\bar{z} > 1$):

$$\bar{\phi}_{III}(\bar{r}, \bar{z} > 1) = 2 \int_0^\infty \frac{\sinh[\bar{\rho}(1 - \bar{d})] + [\cosh(\bar{\rho}) + \varepsilon_{21} \sinh(\bar{\rho})] \sinh(\bar{\rho}\bar{d})}{\sinh^2(\bar{\rho}) [(\varepsilon_{21} + \varepsilon_{31}) \coth(\bar{\rho}) + (\varepsilon_{21}\varepsilon_{31} + 1)]} e^{\bar{\rho}(1 - \bar{z})} J_0(\bar{\rho}\bar{r}) d\bar{\rho}. \tag{3.55}$$

where ε_{21} and ε_{31} , the ratios between dielectric constants that describe the relative permittivity of the three regions, and \bar{d} , the normalized location of the point charge, are the only three independent parameters.

3.7 Validation of the electric potential solution

The normalized results for the electric potential of a single point charge can be validated by considering following two special cases where the general solutions given by Eqs. (3.53)-(3.55) can be reduced into analytical form.

3.7.1 Case I ($\epsilon_{21} = \epsilon_{31} = 1$)

In the first special case, two dielectric constant ratios ϵ_{21} and ϵ_{31} are considered same, i.e., the three regions contain exactly the same dielectric material. It is expected that the electric potential in this case should simply be that of a point charge in a uniform dielectric, i.e.,

$$\bar{\phi}(\bar{r}, \bar{z}) = \frac{1}{\sqrt{\bar{r}^2 + (\bar{z} - \bar{d})^2}}. \quad (3.56)$$

Now, substituting $\epsilon_{21} = \epsilon_{31} = 1$ into Eqn. (3.53) and expanding the hyperbolic functions into exponentials gives

$$\bar{\phi}(\bar{r}, \bar{z} > 1) = \int_0^{\infty} e^{-\bar{\rho}(\bar{z} - \bar{d})} J_0(\bar{\rho}\bar{r}) d\bar{\rho} \quad (3.57)$$

with $\bar{z} - \bar{d} > 0$. Similarly, for the lower region, the electric potential from Eqn. (3.54) is simplified to:

$$\bar{\phi}(\bar{r}, \bar{z} < 0) = \int_0^{\infty} e^{-\bar{\rho}(\bar{d} - \bar{z})} J_0(\bar{\rho}\bar{r}) d\bar{\rho} \quad (3.58)$$

with $\bar{d} - \bar{z} > 0$. Both integrals above in Eqs. (3.57) and (3.58) can be analytically evaluated (Eqn. (3.8)) to

$$\bar{\phi}(\bar{r}, \bar{z}) = \int_0^{\infty} e^{-\bar{\rho}|\bar{z} - \bar{d}|} J_0(\bar{\rho}\bar{r}) d\bar{\rho} = \frac{1}{\sqrt{\bar{r}^2 + (\bar{z} - \bar{d})^2}}. \quad (3.59)$$

For the middle region, considering the same expansion of the hyperbolic functions, all the terms in Eqn. (3.55) cancel each other except the first one which is $1/\sqrt{\bar{r}^2 + (\bar{z} - \bar{d})^2}$. Clearly, these results are the same as Eqn. (3.56), the potential of a point charge in a uniform dielectric.

3.7.2 Case II ($\epsilon_{21} \neq 1$; $\epsilon_{31} = 1$)

The second special case to be considered is where the dielectric constant ratios ϵ_{21} and ϵ_{31} are different and one of the ratios ϵ_{31} has a value of unity. This corresponds to a system where the space is separated by one interface into two dielectric domains with the point charge located in the upper domain. Analytical solution for the electric potential in this case is also available using the method of image charges [49], which in the normalized form is

$$\bar{\phi}(\bar{r}, \bar{z} > 0) = \frac{1}{\sqrt{\bar{r}^2 + (\bar{z} - \bar{d})^2}} - \left(\frac{\epsilon_{21} - 1}{\epsilon_{21} + 1} \right) \frac{1}{\sqrt{\bar{r}^2 + (\bar{z} + \bar{d})^2}} \quad (3.60)$$

applicable to regions I and III, and

$$\bar{\phi}(\bar{r}, \bar{z} < 0) = \left(\frac{2}{\epsilon_{21} + 1} \right) \frac{1}{\sqrt{\bar{r}^2 + (\bar{z} - \bar{d})^2}} \quad (3.61)$$

applicable to region II. Considering $\epsilon_{31} = 1$ and simplifying Eqs. (3.53) and (3.54) results in the following two expressions for regions III and I respectively:

$$\bar{\phi}(\bar{r}, \bar{z} > 1) = \int_0^\infty e^{-\bar{\rho}(\bar{z} - \bar{d})} J_0(\bar{\rho}\bar{r}) d\bar{\rho} - \left(\frac{\epsilon_{21} - 1}{\epsilon_{21} + 1} \right) \int_0^\infty e^{-\bar{\rho}(\bar{z} + \bar{d})} J_0(\bar{\rho}\bar{r}) d\bar{\rho}, \quad (3.62)$$

$$\bar{\phi}(\bar{r}, 0 < \bar{z} < 1) = \frac{1}{\sqrt{\bar{r}^2 + (\bar{z} - \bar{d})^2}} - \left(\frac{\epsilon_{21} - 1}{\epsilon_{21} + 1} \right) \int_0^\infty e^{-\bar{\rho}(\bar{z} + \bar{d})} J_0(\bar{\rho}\bar{r}) d\bar{\rho}. \quad (3.63)$$

Similar to Eqn. (3.59), the integrals in Eqs. (3.62) and (3.63) can be analytically evaluated to [48]

$$\text{(Eqn. (3.8)) } \int_0^\infty e^{-\bar{\rho}(\bar{z} - \bar{d})} J_0(\bar{\rho}\bar{r}) d\bar{\rho} = [\bar{r}^2 + (\bar{z} - \bar{d})^2]^{-1/2} \quad \text{and} \quad \int_0^\infty e^{-\bar{\rho}(\bar{z} + \bar{d})} J_0(\bar{\rho}\bar{r}) d\bar{\rho} = [\bar{r}^2 + (\bar{z} + \bar{d})^2]^{-1/2}$$

which reduce both Eqs. (3.62) and (3.63) to

$$\bar{\phi}(\bar{r}, \bar{z} > 1) = \bar{\phi}(\bar{r}, 0 < \bar{z} < 1) = \frac{1}{\sqrt{\bar{r}^2 + (\bar{z} - \bar{d})^2}} - \left(\frac{\varepsilon_{21} - 1}{\varepsilon_{21} + 1} \right) \frac{1}{\sqrt{\bar{r}^2 + (\bar{z} + \bar{d})^2}}. \quad (3.64)$$

Eqn. (3.64) is exactly the same as Eqn. (3.60). Thus our solutions for region I and III comply with the established results under the condition of $\varepsilon_{21} \neq 1$ and $\varepsilon_{31} = 1$. Now, the simplified form of Eqn. (3.54) yields, for the normalized potential in region II:

$$\bar{\phi}(\bar{r}, \bar{z} < 0) = \left(\frac{2}{\varepsilon_{21} + 1} \right) \int_0^\infty e^{-\bar{\rho}(\bar{d} - \bar{z})} J_0(\bar{\rho}\bar{r}) d\bar{\rho}. \quad (3.65)$$

Evaluating the integral analytically as Eqn. (3.59), Eqn. (3.65) instantly reduces to Eqn. (3.61). Thus the solution in region II is also verified by comparing it to the established solution.

Chapter 4

INDUCED SURFACE FORCE DENSITY AND TOTAL SURFACE FORCE

In this section, the detail formulation of the induced surface force density and the total surface force is described. The main interest is to determine the forces acting on the upper and lower interfaces caused by the point charge, in terms of the physical parameters q , d , H , ε_1 , ε_2 and ε_3 .

4.1 Calculation of electric field

To determine the surface forces, first the electric field \mathbf{E} in all three regions is evaluated from the electric potential $\phi(r, z)$ which is calculated in Chapter 3. Knowing the electric potential throughout the space, the electric field \mathbf{E} can be calculated from the relation in Eqn. (2.5) which reads,

$$\mathbf{E} = -\mathbf{e}_r \frac{\partial \phi(r, z)}{\partial r} - \mathbf{e}_\theta \frac{1}{r} \frac{\partial \phi(r, z)}{\partial \theta} - \mathbf{e}_z \frac{\partial \phi(r, z)}{\partial z} \quad (4.1)$$

where \mathbf{e}_r , \mathbf{e}_θ and \mathbf{e}_z are the unit vectors in r , θ and z directions respectively. Due to cylindrical symmetry as shown in Fig. 2.1, the electric field along the angular coordinate θ is zero and hence Eqn. (4.1) yields

$$\mathbf{E} = -\mathbf{e}_r \frac{\partial \phi(r, z)}{\partial r} - \mathbf{e}_z \frac{\partial \phi(r, z)}{\partial z}. \quad (4.2)$$

For convenience, the electric field components are denoted as $E_r = -\partial \phi / \partial r$ and $E_z = -\partial \phi / \partial z$.

To calculate these components in each region, the corresponding electric potentials are used.

Differentiating Eqn. (3.49) with respect to r and z gives the electric field components in region

I:

$$\begin{aligned} E_{r,1} = -\frac{\partial \phi_I}{\partial r} = & \frac{qr}{4\pi\epsilon_0\epsilon_1 \left[r^2 + (z-d)^2 \right]^{\frac{3}{2}}} \\ & + \frac{q}{2\pi\epsilon_0} \int_0^\infty \left[\frac{\sinh[\rho(H-d)] + \sinh(\rho d) \left[\cosh(\rho H) + \frac{\epsilon_2}{\epsilon_1} \sinh(\rho H) \right]}{\sinh^3(\rho H) \left[(\epsilon_2 + \epsilon_3) \coth(\rho H) + \left(\frac{\epsilon_2 \epsilon_3}{\epsilon_1} + \epsilon_1 \right) \right]} \right] \\ & \quad \times \sinh(\rho z) J_1(\rho r) \rho d \rho \\ & + \frac{q}{2\pi\epsilon_0} \int_0^\infty \left[\frac{\sinh(\rho d) + \sinh[\rho(H-d)] \left[\cosh(\rho H) + \frac{\epsilon_3}{\epsilon_1} \sinh(\rho H) \right]}{\sinh^3(\rho H) \left[(\epsilon_2 + \epsilon_3) \coth(\rho H) + \left(\frac{\epsilon_2 \epsilon_3}{\epsilon_1} + \epsilon_1 \right) \right]} \right] \\ & \quad \times \sinh[\rho(H-z)] J_1(\rho r) \rho d \rho \\ & - \frac{q}{4\pi\epsilon_0\epsilon_1} \int_0^\infty \frac{e^{-\rho(H-d)} \sinh(\rho z) + e^{-\rho d} \sinh[\rho(H-z)]}{\sinh(\rho H)} J_1(\rho r) \rho d \rho \end{aligned} \quad (4.3)$$

and

$$\begin{aligned}
E_{z1} = -\frac{\partial \phi_I}{\partial z} = & \frac{q(z-d)}{4\pi\epsilon_0\epsilon_1 \left[r^2 + (z-d)^2 \right]^{\frac{3}{2}}} \\
& - \frac{q}{2\pi\epsilon_0} \int_0^\infty \frac{\left[\sinh[\rho(H-d)] + \sinh(\rho d) \right] \left[\cosh(\rho H) + \frac{\epsilon_2}{\epsilon_1} \sinh(\rho H) \right]}{\sinh^3(\rho H) \left[(\epsilon_2 + \epsilon_3) \coth(\rho H) + \left(\frac{\epsilon_2\epsilon_3}{\epsilon_1} + \epsilon_1 \right) \right]} \\
& \quad \times \cosh(\rho z) J_0(\rho r) \rho d \rho \\
& + \frac{q}{2\pi\epsilon_0} \int_0^\infty \frac{\left[\sinh(\rho d) + \sinh[\rho(H-d)] \right] \left[\cosh(\rho H) + \frac{\epsilon_3}{\epsilon_1} \sinh(\rho H) \right]}{\sinh^3(\rho H) \left[(\epsilon_2 + \epsilon_3) \coth(\rho H) + \left(\frac{\epsilon_2\epsilon_3}{\epsilon_1} + \epsilon_1 \right) \right]} \\
& \quad \times \cosh[\rho(H-z)] J_0(\rho r) \rho d \rho \\
& + \frac{q}{4\pi\epsilon_0\epsilon_1} \int_0^\infty \frac{e^{-\rho(H-d)} \cosh(\rho z) - e^{-\rho d} \cosh[\rho(H-z)]}{\sinh(\rho H)} J_0(\rho r) \rho d \rho \quad (4.4)
\end{aligned}$$

where, J_1 is the 1st order Bessel function of the first kind.

Similarly, E_r and E_z in region II are calculated by differentiating Eqn. (3.50):

$$\begin{aligned}
E_{r \text{ II}} = -\frac{\partial \phi_{II}}{\partial r} \\
= \frac{q}{2\pi\epsilon_0} \int_0^\infty \frac{\left[\sinh(\rho d) + \sinh[\rho(H-d)] \right] \left[\cosh(\rho H) + \frac{\epsilon_3}{\epsilon_1} \sinh(\rho H) \right]}{\sinh^2(\rho H) \left[(\epsilon_2 + \epsilon_3) \coth(\rho H) + \left(\frac{\epsilon_2\epsilon_3}{\epsilon_1} + \epsilon_1 \right) \right]} e^{\rho z} J_1(\rho r) \rho d \rho \quad (4.5)
\end{aligned}$$

and

$$\begin{aligned}
E_{z\text{II}} &= -\frac{\partial\phi_{\text{II}}}{\partial z} \\
&= -\frac{q}{2\pi\epsilon_0} \int_0^\infty \left[\frac{\sinh(\rho d) + \sinh[\rho(H-d)] \left[\cosh(\rho H) + \frac{\epsilon_3}{\epsilon_1} \sinh(\rho H) \right]}{\sinh^2(\rho H) \left[(\epsilon_2 + \epsilon_3) \coth(\rho H) + \left(\frac{\epsilon_2 \epsilon_3}{\epsilon_1} + \epsilon_1 \right) \right]} \right] e^{\rho z} J_0(\rho r) \rho d \rho.
\end{aligned} \tag{4.6}$$

In region III, the electric field components are found from Eqn. (3.51) which read

$$\begin{aligned}
E_{r\text{III}} &= -\frac{\partial\phi_{\text{III}}}{\partial r} \\
&= \frac{q}{2\pi\epsilon_0} \int_0^\infty \left[\frac{\sinh[\rho(H-d)] + \sinh(\rho d) \left[\cosh(\rho H) + \frac{\epsilon_2}{\epsilon_1} \sinh(\rho H) \right]}{\sinh^2(\rho H) \left[(\epsilon_2 + \epsilon_3) \coth(\rho H) + \left(\frac{\epsilon_2 \epsilon_3}{\epsilon_1} + \epsilon_1 \right) \right]} \right] e^{\rho(H-z)} J_1(\rho r) \rho d \rho
\end{aligned} \tag{4.7}$$

and

$$\begin{aligned}
E_{z\text{III}} &= -\frac{\partial\phi_{\text{III}}}{\partial z} \\
&= \frac{q}{2\pi\epsilon_0} \int_0^\infty \left[\frac{\sinh[\rho(H-d)] + \sinh(\rho d) \left[\cosh(\rho H) + \frac{\epsilon_2}{\epsilon_1} \sinh(\rho H) \right]}{\sinh^2(\rho H) \left[(\epsilon_2 + \epsilon_3) \coth(\rho H) + \left(\frac{\epsilon_2 \epsilon_3}{\epsilon_1} + \epsilon_1 \right) \right]} \right] e^{\rho(H-z)} J_0(\rho r) \rho d \rho.
\end{aligned} \tag{4.8}$$

4.2 Maxwell Stress Tensor (MST)

Following the calculation of \mathbf{E} in all regions, the MST \mathbf{T} is computed. MST was introduced as a consequence of linear momentum balance, where the total force acting on a volume in a body can be expressed as the sum of tractions (MST) applied to the surface enclosing that volume [46]. MST in absence of magnetic field is given by [50]

$$\mathbf{T} = \mathbf{E} \otimes \mathbf{D} - \frac{(\mathbf{E} \cdot \mathbf{D})}{2} \mathbf{I}. \quad (4.9)$$

Here, \mathbf{D} is the electric displacement which is related to the electric field by $\mathbf{D} = \varepsilon_0 \varepsilon_i \mathbf{E}$ where ε_0 is the electric permittivity of free space and ε_i is the dielectric constant of the corresponding region ($i = 1, 2, 3$) and \mathbf{I} corresponds to the identity tensor. Eqn. (4.9) can be re-written as

$$\mathbf{T} = \varepsilon_0 \varepsilon_i (\mathbf{E} \otimes \mathbf{E}) - \varepsilon_0 \varepsilon_i (\mathbf{E} \cdot \mathbf{E}) \begin{pmatrix} 1 & 0 & 0 \\ 0 & 1 & 0 \\ 0 & 0 & 1 \end{pmatrix}. \quad (4.10)$$

In the cylindrical coordinate with the electric field components

$$E = \begin{Bmatrix} E_r \\ E_\theta (= 0) \\ E_z \end{Bmatrix}, \quad (4.11)$$

the elements of the MST can be computed as follows

$$T_{rr} = \frac{1}{2} \varepsilon_0 \varepsilon_i (E_r^2 - E_z^2),$$

$$T_{r\theta} = \varepsilon_0 \varepsilon_i E_r E_\theta = 0,$$

$$T_{rz} = \varepsilon_0 \varepsilon_i E_r E_z,$$

$$T_{\theta r} = \varepsilon_0 \varepsilon_i E_r E_\theta = 0,$$

$$T_{\theta\theta} = \frac{1}{2} \varepsilon_0 \varepsilon_i (-E_r^2 - E_z^2),$$

$$T_{\theta z} = \varepsilon_0 \varepsilon_i E_\theta E_z = 0,$$

$$T_{zr} = \varepsilon_0 \varepsilon_i E_r E_z,$$

$$T_{z\theta} = \varepsilon_0 \varepsilon_i E_\theta E_z = 0,$$

$$T_{zz} = \frac{1}{2} \varepsilon_0 \varepsilon_i (E_z^2 - E_r^2).$$

That is,

$$T = \varepsilon_0 \varepsilon_i \begin{pmatrix} \frac{E_r^2 - E_z^2}{2} & 0 & E_r E_z \\ 0 & \frac{-E_r^2 - E_z^2}{2} & 0 \\ E_r E_z & 0 & \frac{E_z^2 - E_r^2}{2} \end{pmatrix}. \quad (4.12)$$

4.3 Calculation of surface forces

The electric force acting on a body in an electric field is related to the MST by $\mathbf{F} = \int_V \nabla \cdot \mathbf{T} dV$, where the volume V contains the considered body. Using the divergence theorem,

this volume integral can be converted into a surface integral $\mathbf{F} = \oint_S \mathbf{T} \cdot \mathbf{n} dS$, where S is the closed

surface enclosing the volume V and \mathbf{n} is the outward normal to the surface which can be expressed

as $\mathbf{n} = n_r \mathbf{e}_r + n_\theta \mathbf{e}_\theta + n_z \mathbf{e}_z$. This relationship can be used to deduce the force on an interface between

two different media. Taking the upper interface as an example, in Fig. 4.1, a Gaussian pillbox is

constructed for an infinitesimal volume at an arbitrary location $(r, z = H)$, with width dr , out-of-plane depth $r d\theta$ and thickness Δ , which encloses an infinitesimal portion of the interface

between regions I and III. The closed surface bounding the pillbox can be written as $S = S_1 + S_2 +$

S_3 , where S_1 is the surface on the top (in region III), S_2 is the surface at the bottom (in region I), and S_3 is the surface on the side (proportional to Δ). Taking $\Delta \rightarrow 0$ the contribution to the surface integral along S_3 becomes vanishingly small and the only contributions come from the integrals along S_1 and S_2 . That is, the surface force density $\mathbf{f}_{I,III}$ (local force per unit area acting on the upper interface) is related to the MST by $\mathbf{f}_{I,III} r dr d\theta = \int_{S_1} \mathbf{T} \cdot \mathbf{n} dS + \int_{S_2} \mathbf{T} \cdot \mathbf{n} dS$. As \mathbf{n} is the outward normal, it is equal to \mathbf{e}_z on S_1 as $n_r = n_\theta = 0$ and $n_z = 1$ in this case. Similarly, $n_r = n_\theta = 0$ and $n_z = -1$ on S_2 and therefore \mathbf{n} is equal to $-\mathbf{e}_z$ for this surface element. The two surface elements S_1 and S_2 both have an area of $r dr d\theta$. Using these relations with Eqs. (4.2) and (4.12), the surface force density on the upper interface is found to be

$$\mathbf{f}_{I,III}(r, H) = f_{r, I,III} \mathbf{e}_r + f_{z, I,III} \mathbf{e}_z \quad (4.13)$$

where,

$$f_{r, I,III} = \varepsilon_0 [E_{z,III} E_{r,III} \varepsilon_3 - E_{z,I} E_{r,I} \varepsilon_1]_{z=H}, \quad (4.14)$$

$$f_{z, I,III} = \frac{\varepsilon_0}{2} [(E_{z,III}^2 - E_{r,III}^2) \varepsilon_3 - (E_{z,I}^2 - E_{r,I}^2) \varepsilon_1]_{z=H} \quad (4.15)$$

are the r - and z -components of the surface force density respectively.

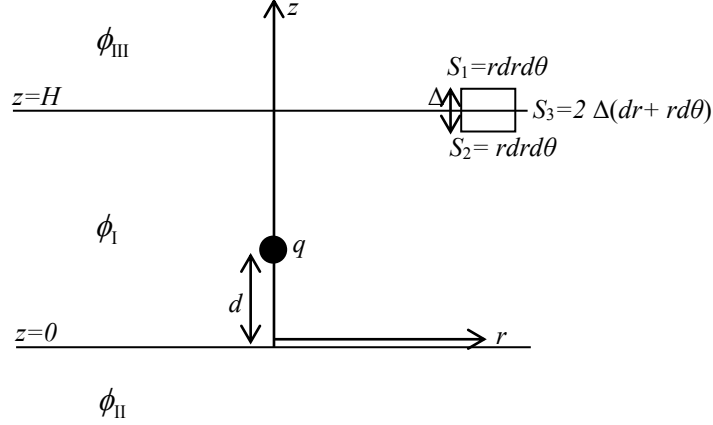


FIGURE 4.1: Gaussian pillbox used to calculate surface force density on the upper interface from the Maxwell Stress Tensor.

The electric field components on the interfaces in Eqs. (4.14) and (4.15) can be easily obtained from the solutions of \mathbf{E} that is calculated for all regions in the system. Using $z = H$ in Eqs. (4.3), (4.4), (4.7) and (4.8), r - and z -components of the electric field on the upper interface yield

$$\begin{aligned}
 E_{r1}|_{z=H} = & \frac{qr}{4\pi\epsilon_0\epsilon_1 \left[r^2 + (H-d)^2 \right]^{\frac{3}{2}}} \\
 & + \frac{q}{2\pi\epsilon_0} \int_0^\infty \frac{\sinh[\rho(H-d)] + \sinh(\rho d) \left[\cosh(\rho H) + \frac{\epsilon_2}{\epsilon_1} \sinh(\rho H) \right]}{\sinh^3(\rho H) \left[(\epsilon_2 + \epsilon_3) \coth(\rho H) + \left(\frac{\epsilon_2 \epsilon_3}{\epsilon_1} + \epsilon_1 \right) \right]} \\
 & \quad \times \sinh(\rho H) J_1(\rho r) \rho d \rho \\
 & - \frac{q}{4\pi\epsilon_0\epsilon_1} \int_0^\infty e^{-\rho(H-d)} J_1(\rho r) \rho d \rho,
 \end{aligned} \tag{4.16}$$

$$\begin{aligned}
E_{z\text{I}}|_{z=H} &= \frac{q(H-d)}{4\pi\epsilon_0\epsilon_1 \left[r^2 + (H-d)^2 \right]^{\frac{3}{2}}} \\
&- \frac{q}{2\pi\epsilon_0} \int_0^\infty \frac{\left[\frac{\sinh[\rho(H-d)] + \sinh(\rho d) \left[\cosh(\rho H) + \frac{\epsilon_2}{\epsilon_1} \sinh(\rho H) \right]}{\sinh^3(\rho H) \left[(\epsilon_2 + \epsilon_3) \coth(\rho H) + \left(\frac{\epsilon_2\epsilon_3}{\epsilon_1} + \epsilon_1 \right) \right]} \right]}{\times \cosh(\rho H) J_0(\rho r) \rho d \rho} \\
&+ \frac{q}{2\pi\epsilon_0} \int_0^\infty \frac{\left[\frac{\sinh(\rho d) + \sinh[\rho(H-d)] \left[\cosh(\rho H) + \frac{\epsilon_3}{\epsilon_1} \sinh(\rho H) \right]}{\sinh^3(\rho H) \left[(\epsilon_2 + \epsilon_3) \coth(\rho H) + \left(\frac{\epsilon_2\epsilon_3}{\epsilon_1} + \epsilon_1 \right) \right]} \right]}{J_0(\rho r) \rho d \rho} \\
&+ \frac{q}{4\pi\epsilon_0\epsilon_1} \int_0^\infty \frac{e^{-\rho(H-d)} \cosh(\rho H) - e^{-\rho d}}{\sinh(\rho H)} J_0(\rho r) \rho d \rho,
\end{aligned} \tag{4.17}$$

$$\begin{aligned}
E_{r\text{III}}|_{z=H} &= \frac{q}{2\pi\epsilon_0} \\
&\times \int_0^\infty \frac{\left[\frac{\sinh[\rho(H-d)] + \sinh(\rho d) \left[\cosh(\rho H) + \frac{\epsilon_2}{\epsilon_1} \sinh(\rho H) \right]}{\sinh^2(\rho H) \left[(\epsilon_2 + \epsilon_3) \coth(\rho H) + \left(\frac{\epsilon_2\epsilon_3}{\epsilon_1} + \epsilon_1 \right) \right]} \right]}{J_1(\rho r) \rho d \rho}
\end{aligned} \tag{4.18}$$

and

$$\begin{aligned}
E_{z\text{III}}|_{z=H} &= \frac{q}{2\pi\epsilon_0} \\
&\times \int_0^\infty \frac{\left[\frac{\sinh[\rho(H-d)] + \sinh(\rho d) \left[\cosh(\rho H) + \frac{\epsilon_2}{\epsilon_1} \sinh(\rho H) \right]}{\sinh^2(\rho H) \left[(\epsilon_2 + \epsilon_3) \coth(\rho H) + \left(\frac{\epsilon_2\epsilon_3}{\epsilon_1} + \epsilon_1 \right) \right]} \right]}{J_0(\rho r) \rho d \rho.}
\end{aligned} \tag{4.19}$$

It can be shown that $f_{r, \text{I,III}}$ vanishes everywhere on the upper interface. Briefly, the electric potential must be continuous across the interface for all r : $\lim_{z \rightarrow H^+} \phi_{\text{III}}(r) = \lim_{z \rightarrow H^-} \phi_{\text{I}}(r)$, which leads to

$$\lim_{z \rightarrow H^+} \frac{\partial \phi_{\text{III}}}{\partial r} = \lim_{z \rightarrow H^-} \frac{\partial \phi_{\text{I}}}{\partial r}, \text{ i.e.,}$$

$$\lim_{z \rightarrow H^+} E_{r, \text{III}} = \lim_{z \rightarrow H^-} E_{r, \text{I}}. \quad (4.20)$$

Meanwhile, the normal component of the electric displacement is also continuous across the interface:

$$\lim_{z \rightarrow H^+} \epsilon_3 E_{z, \text{III}} = \lim_{z \rightarrow H^-} \epsilon_1 E_{z, \text{I}}. \quad (4.21)$$

Applying Eqs. (4.20) and (4.21) in Eqn. (4.14) yields $f_{r, \text{I,III}} = 0$. Therefore, only the z -component, $f_{z, \text{I,III}}$ contributes to the surface force density in Eqn. (4.13). Using the same equations, Eqn. (4.15) can be expressed in terms of the electric field components of the upper region as

$$f_{z, \text{I,III}} = \frac{\epsilon_0}{2} (\epsilon_1 - \epsilon_3) \left[\frac{\epsilon_3}{\epsilon_1} E_{z, \text{III}}^2 + E_{r, \text{III}}^2 \right]_{z=H}. \quad (4.22)$$

Having determined the surface force density, the total force acting on the upper interface is

therefore $\mathbf{F}_{\text{I,III}} = \int_0^\infty \int_0^{2\pi} \mathbf{f}_{\text{I,III}} r dr d\theta = F_{\text{I,III}} \mathbf{e}_z$, the last step due to the fact that $\mathbf{f}_{\text{I,III}}$ only has z -component.

The magnitude of the force, $F_{\text{I,III}}$, is given by

$$F_{\text{I,III}} = 2\pi \int_0^\infty f_{z, \text{I,III}} r dr. \quad (4.23)$$

The procedure above can also be applied to obtain the surface force density and the total force on the lower interface. Specifically, the surface force density on the lower interface is given by

$$\mathbf{f}_{1,II}(r,0) = f_{z,1,II} \mathbf{e}_z \quad (4.24)$$

where the r -component of the surface force density is again zero everywhere similar to what was shown earlier for the upper interface. Following the similar methods of calculating $f_{z,1,III}$, Eqs. (4.2) and (4.12) are again used to determine $f_{z,1,II}$ as:

$$f_{z,1,II} = \frac{\epsilon_0}{2} \left[(E_{zI}^2 - E_{rI}^2) \epsilon_1 - (E_{zII}^2 - E_{rII}^2) \epsilon_2 \right]_{z=0}. \quad (4.25)$$

Similar to Eqn. (4.22), $f_{z,1,II}$ can be also expressed in terms of the electric field components of the lower region as

$$f_{z,1,II} = \frac{\epsilon_0}{2} (\epsilon_2 - \epsilon_1) \left[\frac{\epsilon_2}{\epsilon_1} E_{zII}^2 + E_{rII}^2 \right]_{z=0}. \quad (4.26)$$

The quantities E_{rII} and E_{zII} in Eqn. (4.26) can be found by using $z=0$ in Eqs. (4.5) and (4.6) respectively. Thus,

$$E_{rII}|_{z=0} = \frac{q}{2\pi\epsilon_0} \int_0^\infty \left[\frac{\sinh(\rho d) + \sinh[\rho(H-d)] \left[\cosh(\rho H) + \frac{\epsilon_3}{\epsilon_1} \sinh(\rho H) \right]}{\sinh^2(\rho H) \left[(\epsilon_2 + \epsilon_3) \coth(\rho H) + \left(\frac{\epsilon_2 \epsilon_3}{\epsilon_1} + \epsilon_1 \right) \right]} \right] J_1(\rho r) \rho d \rho \quad (4.27)$$

and

$$E_{z,II}|_{z=0} = -\frac{q}{2\pi\epsilon_0} \times \int_0^\infty \left[\frac{\sinh(\rho d) + \sinh[\rho(H-d)] \left[\cosh(\rho H) + \frac{\epsilon_3}{\epsilon_1} \sinh(\rho H) \right]}{\sinh^2(\rho H) \left[(\epsilon_2 + \epsilon_3) \coth(\rho H) + \left(\frac{\epsilon_2 \epsilon_3}{\epsilon_1} + \epsilon_1 \right) \right]} \right] J_0(\rho r) \rho d \rho. \quad (4.28)$$

Finally, the total force on the lower interface is only in the z -direction, $\mathbf{F}_{I,II} = F_{I,II} \mathbf{e}_z$, and its magnitude is calculated by

$$F_{I,II} = 2\pi \int_0^\infty f_{z,I,II} r dr. \quad (4.29)$$

4.4 Normalization of electric field

Before implementing the numerical calculation, the electric field components in the upper and lower interfaces are normalized using following non-dimensionalized parameters:

$$\bar{E}_r = \frac{4\pi\epsilon_0\epsilon_1 E_r H^2}{q}, \bar{E}_z = \frac{4\pi\epsilon_0\epsilon_1 E_z H^2}{q}, \bar{\rho} = \rho H, \bar{d} = \frac{d}{H}, \bar{r} = \frac{r}{H}, \bar{z} = \frac{z}{H}, \epsilon_{21} = \frac{\epsilon_2}{\epsilon_1}, \epsilon_{31} = \frac{\epsilon_3}{\epsilon_1}. \quad (4.30)$$

The normalized r - and z - components which involve in calculation of the electric field for the upper and lower interfaces respectively are given by

$$\bar{E}_{r,III}|_{\bar{z}=1} = \int_0^\infty \left[\frac{\sinh[\bar{\rho}(1-\bar{d})] + \sinh(\bar{\rho}\bar{d}) \left[\cosh(\bar{\rho}) + \epsilon_{21} \sinh(\bar{\rho}) \right]}{\sinh^2(\bar{\rho}) \left[(\epsilon_{21} + \epsilon_{31}) \coth(\bar{\rho}) + (\epsilon_{21}\epsilon_{31} + 1) \right]} \right] J_1(\bar{\rho}\bar{r}) \bar{\rho} d \bar{\rho}, \quad (4.31)$$

$$\bar{E}_{z,III}|_{\bar{z}=1} = \int_0^\infty \left[\frac{\sinh[\bar{\rho}(1-\bar{d})] + \sinh(\bar{\rho}\bar{d}) \left[\cosh(\bar{\rho}) + \epsilon_{21} \sinh(\bar{\rho}) \right]}{\sinh^2(\bar{\rho}) \left[(\epsilon_{21} + \epsilon_{31}) \coth(\bar{\rho}) + (\epsilon_{21}\epsilon_{31} + 1) \right]} \right] J_0(\bar{\rho}\bar{r}) \bar{\rho} d \bar{\rho} \quad (4.32)$$

and

$$\bar{E}_{r \text{ II}} \Big|_{z=0} = \int_0^\infty \left[\frac{\sinh(\bar{\rho}\bar{d}) + \sinh[\bar{\rho}(1-\bar{d})] [\cosh(\bar{\rho}) + \varepsilon_{31} \sinh(\bar{\rho})]}{\sinh^2(\bar{\rho}) [(\varepsilon_{21} + \varepsilon_{31}) \coth(\bar{\rho}) + (\varepsilon_{21}\varepsilon_{31} + 1)]} \right] J_1(\bar{\rho}\bar{r}) \bar{\rho} d\bar{\rho}, \quad (4.33)$$

$$\bar{E}_{z \text{ II}} \Big|_{z=0} = - \int_0^\infty \left[\frac{\sinh(\bar{\rho}\bar{d}) + \sinh[\bar{\rho}(1-\bar{d})] [\cosh(\bar{\rho}) + \varepsilon_{31} \sinh(\bar{\rho})]}{\sinh^2(\bar{\rho}) [(\varepsilon_{21} + \varepsilon_{31}) \coth(\bar{\rho}) + (\varepsilon_{21}\varepsilon_{31} + 1)]} \right] J_0(\bar{\rho}\bar{r}) \bar{\rho} d\bar{\rho}. \quad (4.34)$$

4.5 Normalization of total surface force

To reduce the number of parameters and widen the applicability of the results presented here for the total surface force, the following normalized quantities will be used:

$$\bar{F} = \frac{16\pi\varepsilon_0\varepsilon_1 FH^2}{q^2}, \bar{f}_z = \frac{32\pi^2\varepsilon_0\varepsilon_1 f_z H^4}{q^2}, \bar{\rho} = \rho H, \bar{d} = \frac{d}{H}, \bar{r} = \frac{r}{H}, \bar{z} = \frac{z}{H}, \varepsilon_{21} = \frac{\varepsilon_2}{\varepsilon_1}, \varepsilon_{31} = \frac{\varepsilon_3}{\varepsilon_1}. \quad (4.35)$$

Subscripts I, II and I, III will be added to \bar{f}_z and \bar{F} to indicate the quantities on the lower and upper interfaces, respectively. Because r -component of the surface force density is zero, in the discussions below \bar{f}_z will be referred to simply as the normalized surface force density. With the introduced normalization, it can be easily shown that \bar{f}_z depends on the normalized radial position \bar{r} as well as the following parameters: \bar{d} , ε_{21} and ε_{31} , whereas \bar{F} only depends on \bar{d} , ε_{21} and ε_{31} .

Chapter 5

RESULTS AND DISCUSSIONS

5.1 Parametric analysis for the electric potential

The electric potential of the point charge depends on three parameters that include the location of the charge and two dielectric constant ratios (\bar{d} , ε_{21} and ε_{31}). In this section, these important factors, which influence the electric potential tremendously, will be fully analyzed from the numerical results to examine more general situations in detail.

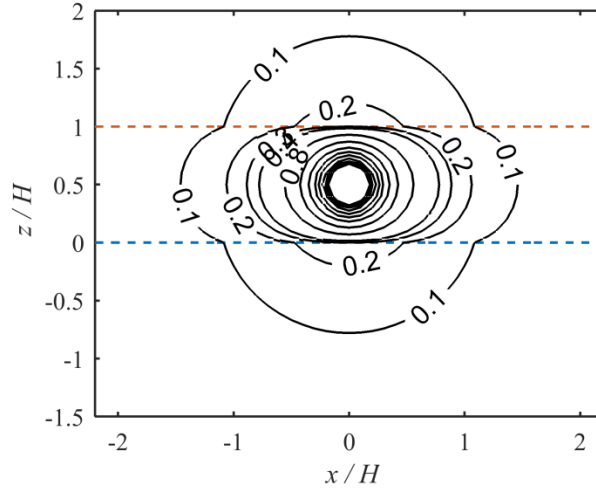
5.1.1 Variation of the electric potential with dielectric constant ratios

Fig. 5.1 shows the contour plots of electric potential due to a charge located at $\bar{d} = 0.5$. For Fig. 5.1(a), the dielectric constants of the materials in the upper and lower regions are considered equal and much higher than that of the middle layer ($\varepsilon_{21} = \varepsilon_{31} \gg 1$). It can be seen that the electric potential retains spherical symmetry near the point charge while it becomes distorted gradually at larger distance from the point charge where the effect of the different dielectrics becomes significant. For the configuration of the system considered in this figure, the electric potential is symmetric in both vertical and horizontal directions. The potential also decays at equal rate in upward and downward directions. But the decay is faster in the vertical direction than in the horizontal direction, which is due to the higher dielectric constant in the upper and lower regions. The electric field of the point charge induces polarization in all dielectric regions where the dipoles are rearranged in such a way that the induced field opposes and reduces the magnitude

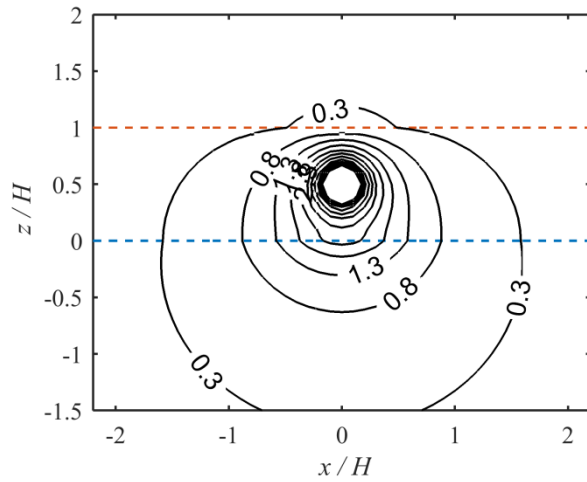
of the external field. The higher dielectric constants of the isotropic dielectric materials in the upper and lower regions cause higher magnitude of polarization which leads to higher reduction of the external field. When the dielectric constant of a medium approaches infinity, the external field of the point charge is exactly cancelled by the induced field of the dipoles and the medium behaves like a conductor where the total electric field is constrained to zero. Therefore, if ϵ_{21} and ϵ_{31} are further increased for the configuration considered in Fig. 5.1(a), it can be expected that the system will approach the case where a uniform dielectric is sandwiched between two identical conductors. The electric field of charges in dielectric between capacitors and other semiconductors has been commonly studied in literatures. In the work of Pumpllin [39], the results of induced potential were presented for a system with two grounded parallel plates and a point charge located midway between the plates. The equipotential surfaces were shown for this configuration, which resemble the shape of the contours in Fig. 5.1(a) although they did not extend into the upper and lower regions due to the presence of conducting materials.

Fig. 5.1(b) represents a system with a very high dielectric constant in the upper region ($\epsilon_{31} \gg 1$) and a much lower dielectric constant in the lower region ($\epsilon_{21} \ll 1$) compared to that of the middle layer. Similar to Fig. 5.1(a), the spherical symmetry of the electric potential only retains very close to the point charge. Though the electric potential is symmetric about a vertical plane, unlike in Fig. 5.1(a) its rate of decay is different in the upward and downward directions, with much faster decay towards the upper interface due to the higher value of ϵ_{31} . It is interesting to observe that, though the value of ϵ_{31} is the same in both figures, the values of $\bar{\phi}$ near the upper interface in Fig. 5.1(b) is drastically different from those in Fig. 5.1(a). The smaller dielectric constant in the lower region has caused slower decay in both upward and downward directions in

Fig. 5.1(b) compared to Fig. 5.1(a), which demonstrates the strong interactions among the dielectric materials in the three regions.



(a)



(b)

FIGURE 5.1: Normalized electric potential of a single point charge in the middle layer of a three-layered dielectric system. The upper and lower interfaces are at the positions of $z/H=1$ and $z/H=0$, and marked by orange and blue lines respectively. (a) $\epsilon_{21}=10$ and $\epsilon_{31}=10$, (b) $\epsilon_{21}=0.1$ and $\epsilon_{31}=10$. For all cases, $\bar{d}=0.5$.

To more systematically study the effect of dielectric constant ratios, the normalized potential is plotted as a function of ϵ_{21} in Fig. 5.2 while fixing the other dielectric constant ratio ϵ_{31} , as well as the charge location \bar{d} . Due to the symmetry, varying ϵ_{31} with fixed ϵ_{21} would correspond to the same result if regions II and III were swapped. The electric potential is evaluated at three spatial points: $P_1(1,0.5)$, $P_2(0,-0.5)$ and $P_3(0,0.5)$ in the middle, lower and upper regions respectively. All three points are at equal distance from the point charge. It is clear that the electric potentials at all three points decrease with the increase of ϵ_{21} , indicating that the increase of dielectric constant of a single region reduces the potential in all three regions, consistent with what was found in Fig. 5.1. But the rate of decay is quite different at the three points. As the dielectric is being varied in the region where P_2 is located, the change of ϵ_{21} has more direct impact on the potential at this point than at P_1 and P_3 , leading to the highest rate of decay at P_2 . The slowest decay is found at P_3 as this point is located at the furthest distance from the region in which the dielectric constant is being changed. The curves for P_2 and P_3 intersect at $\epsilon_{21} = 10$, where the materials in the upper and lower regions become identical. Although the materials in the middle and lower regions become identical at $\epsilon_{21} = 1$, the potential at P_1 is still lower than that at P_2 when $\epsilon_{21} = 1$, because P_1 is closer to the upper region with a higher dielectric constant. These two curves intersect at a ϵ_{21} value greater than one.

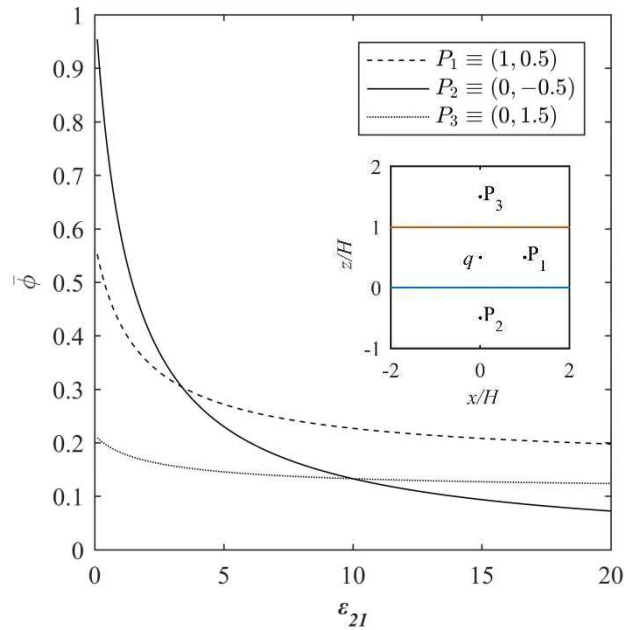


FIGURE 5.2: Normalized electric potential, plotted against the dielectric constant ratio between the lower and middle regions, at three points $P_1(1,0.5)$, $P_2(0,-0.5)$ and $P_3(0,1.5)$, located in the middle, lower and upper layers respectively. For all cases, $\bar{d} = 0.5$ and $\varepsilon_{31} = 10$.

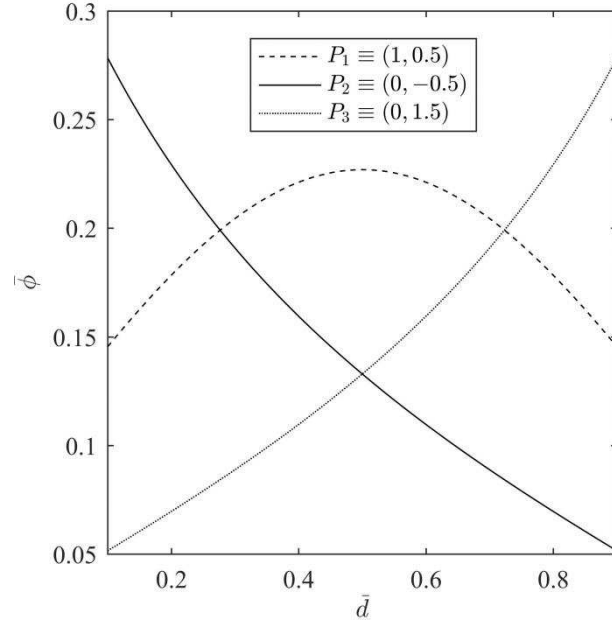
5.1.2 Variation of the electric potential with charge location

The distance of the point charge from the interfaces also affects the potential distribution in the system. In Fig. 5.3, plots of $\bar{\phi}$ are shown as a function of \bar{d} where the location of point charge varies from 0.1 to 0.9 along the z -axis. At $\bar{d} = 0.1$, the point charge is just above the lower interface and at $\bar{d} = 0.9$ it is close to the upper interface. The same three locations P_1 , P_2 and P_3 are chosen as before and the electric potential is presented for these points. Fig. 5.3(a) represents the system that has two identical materials in the upper and lower regions with higher dielectric constant ($\varepsilon_{21} = \varepsilon_{31} = 10$) than the middle one. The potential at P_3 monotonically increases as the

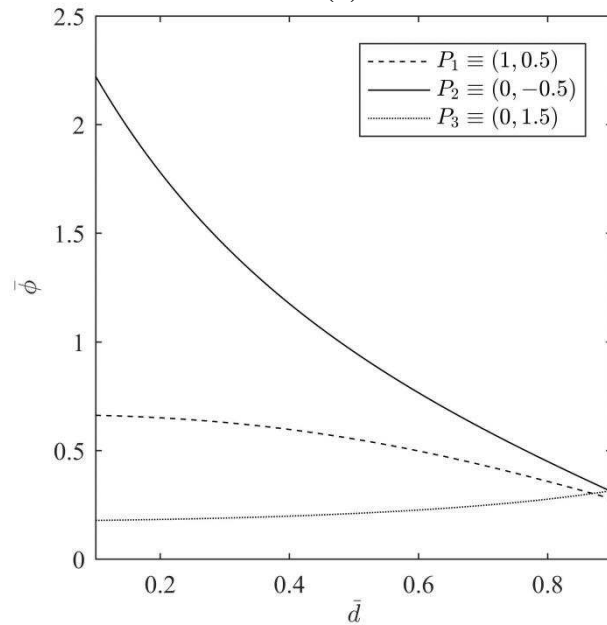
point charge approaches from the lower to the upper interface, because the distance between the point charge and P_3 decreases. Similarly, at P_2 , the potential decreases monotonically as the point charge moves away from it. The magnitudes for the rate of change of potential at P_2 and P_3 are equal, and the two curves intersect at $\bar{d} = 0.5$, in which case the dielectrics are identical in the upper and lower regions and these two points are located at equal distance from the point charge. The potential at P_1 first increases as its distance from the point charge decreases, reaches maximum when the point charge is located midway between the two interfaces ($\bar{d} = 0.5$), and then starts decreasing due to the increase in distance from the point charge.

In Fig. 5.3(b), different dielectric is considered in each layer: the highest dielectric constant material is in the upper region and the lowest one is in the lower region. As the point charge approaches the upper interface, it comes closer to P_3 and hence the potential increases at this point. For the same reason, the potential at P_2 decreases as the point charge moves away from it. The most interesting phenomena are found at P_1 . As the charge moves from the lower to the upper interface, the distance between the point charge and P_1 first decreases and as it passes the midpoint ($\bar{d} = 0.5$), the distance increases. However, the potential at P_1 is found to monotonically decrease for the entire range of \bar{d} . To explain, as the charge moves towards the midway between the two interfaces, without considering the influence of the dielectrics in the upper and lower regions, the potential at P_1 should increase as the distance between the point charge and P_1 decreases. But at the same time, the charge is approaching a region with higher dielectric constant, which tends to decrease the potential at P_1 . These two competing effects can cause a complex relation between the location of the point charge and the potential at P_1 . For $\epsilon_{21} = 0.1$ and $\epsilon_{31} = 10$, the influence from the high dielectric constant in the upper region appears to be dominant, which results in net decrease in the potential at P_1 . However, the rate of decay is quite small, as a consequence of the

two competing factors. After $\bar{d} = 0.5$, the distance between the point charge and P_1 starts to increase and the point charge continues to approach the higher dielectric constant region. Both tend to introduce decay in the potential at P_1 , hence a faster decrease is observed from Fig. 5.3(b).



(a)



(b)

FIGURE 5.3: Normalized electric potential, plotted against the normalized location \bar{d} , at three points $P_1(1,0.5)$, $P_2(0,-0.5)$ and $P_3(0,1.5)$ located in the upper, lower and middle layers respectively (see inset in Fig. 5.2). (a) $\epsilon_{21} = 10$ and $\epsilon_{31} = 10$, (b) $\epsilon_{21} = 0.1$ and $\epsilon_{31} = 10$.

To further investigate this interesting phenomenon, normalized potential $\bar{\phi}$ at P_1 is plotted as a function of \bar{d} in Fig. 5.4 for several different ε_{21} . The other dielectric constant ratio ε_{31} remains at 10. The maximum for each curve, either as a local maximum in the interior of the domain or as a global maximum at the boundaries, is marked with *. As the charge approaches the upper interface, the change of $\bar{\phi}$ at P_1 is found to be quite different for different values of ε_{21} . For small ε_{21} (<0.4), $\bar{\phi}$ monotonically decreases for the entire range of \bar{d} although the distance between the point charge and P_1 decreases till $\bar{d} = 0.5$. As discussed earlier, the effect of the high dielectric constant in the upper region is dominant in this case, which reduces the net potential at P_1 as the point charge moves upwards. For $\varepsilon_{21} > 0.4$, $\bar{\phi}$ shows non-monotonic behavior with the change in charge location and the maximum for each curve is found at a distance from the boundaries. In addition, as ε_{21} increases, the local maximum shifts towards the upper interface due to the increased screening from the lower region. Finally, for large values of ε_{21} (>10), the curves exhibit the trend of converging together as the lower region approaches a conductor-like material.

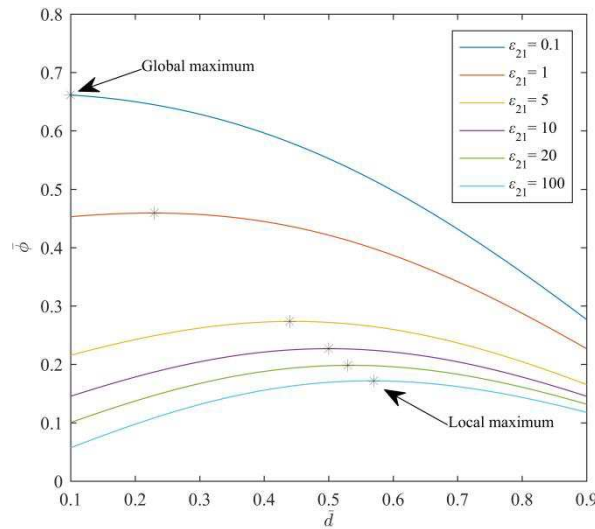


FIGURE 5.4: Normalized electric potential at $P_1(1,0.5)$, located in the middle layer, as a function of the normalized location \bar{d} of the point charge. For all cases, $\varepsilon_{31} = 10$.

5.2 Implications of the electric potential

The results above have demonstrated that the electric potential due to the point charge is strongly influenced by the dielectric materials used in the different layers, which can provide means of modulating the electric potential in the multi-layered system by adjusting the properties of materials. Due to the linear nature of the electrostatic problem, the current work can be extended to study the electric potential due to a line of charges, for example, present in multilayered microstrips (used in microwave technologies) [51]. The expression for the electric potential can also be used directly to calculate other physical quantities such as the polarization surface charge density in Barrera *et al.* [43] or the surface force on the interfaces evaluated in Chapter 4 of this thesis.

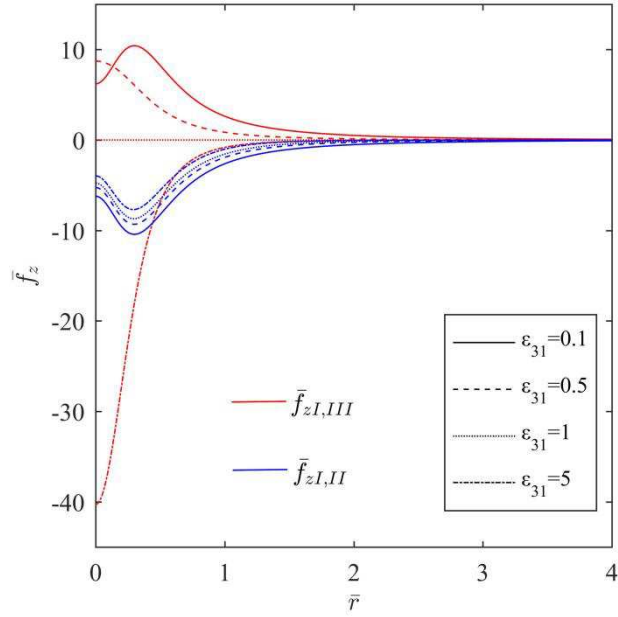
5.3 Parametric analysis of the surface force density

The distribution of the surface force density along the radial direction is affected by several factors. The surface force density derived in Chapter 4 will be evaluated numerically in this part to study its dependence on three dimensionless physical parameters (\bar{d} , ε_{21} and ε_{31}).

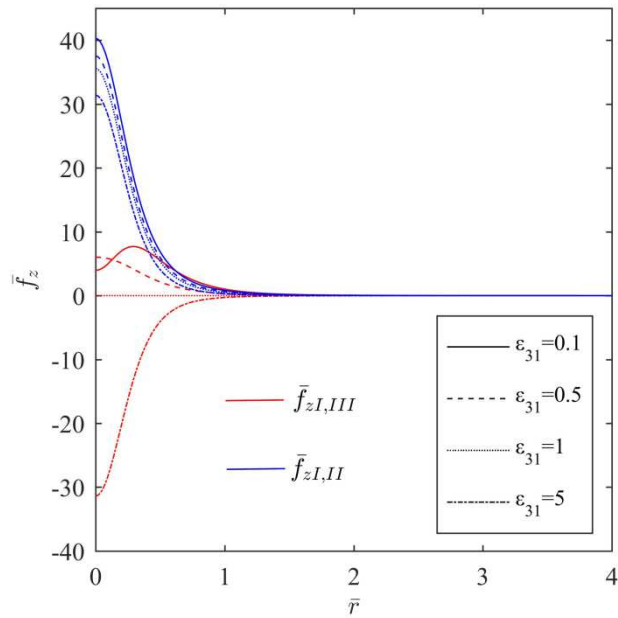
5.3.1 Variation of the surface force density with dielectric constant ratios

In Fig. 5.5, \bar{f}_z is plotted as a function of \bar{r} for a number of different combinations of ε_{21} and ε_{31} , while fixing the charge location at $\bar{d} = 0.5$. The red and blue lines correspond to the surface force density on the upper and lower interfaces respectively. Positive values of \bar{f}_z indicate upward direction and negative values indicate downward direction.

Fig. 5.5(a) shows the results for $\varepsilon_{21} = 0.1$, i.e., the lower region has a much smaller dielectric constant than the middle layer. Let us first look at the situation where $\varepsilon_{31} = 0.1 = \varepsilon_{21}$. In this case, the upper and lower regions have identical materials, and the distributions of the surface force density, as expected, exhibit symmetric patterns where \bar{f}_z on the two interfaces are equal and opposite at any given \bar{r} . In addition, \bar{f}_z on the upper interface is positive while it is negative on the lower interface. This corresponds to repulsive interactions between the two interfaces, induced by the presence of the charge. On both interfaces, the magnitude of \bar{f}_z decays to zero at large \bar{r} . This is expected, and is observed for all the other parameter values since the surface force density is a local quantity and the influence of the point charge should effectively vanish at locations sufficiently far from it.



(a)



(b)

FIGURE 5.5: Normalized surface force density on the interfaces, with red and blue lines corresponding to the upper and lower interfaces respectively. (a) $\epsilon_{21} = 0.1$, (b) $\epsilon_{21} = 5$. For each subfigure, $\bar{d} = 0.5$ and ϵ_{31} varies from 0.1 to 5 (see legend for different line styles used for different ϵ_{31}).

As ε_{31} is increased from 0.1 to larger values (0.5, 1 and 5) in Fig. 5.5(a), it only introduces minor reduction in the magnitude of $\bar{f}_{z1,II}$, while the sign and overall trend of $\bar{f}_{z1,II}$ remain the same. This is because although ε_{31} affects the electric potential in all three regions, its direct impact is on the upper region, and the impact on the lower and middle regions is more indirect (see Sec. 5.1 for details). For the same reason, $\bar{f}_{z1,III}$ undergoes significant changes as ε_{31} is increased. At $\varepsilon_{31} = 0.5$, $\bar{f}_{z1,III}$ has already differed substantially from the curve at $\varepsilon_{31} = 0.1$. When $\varepsilon_{31} = 1$, $\bar{f}_{z1,III}$ is zero everywhere. This is because the upper and middle regions are identical, and there is no real physical interface between them. What is most interesting is that when ε_{31} is increased to 5, $\bar{f}_{z1,III}$ becomes negative with a large magnitude. Physically, the point charge in this case has induced downward forces on both interfaces. The change of sign in $\bar{f}_{z1,III}$ can be understood from the expression in Eqn. (4.22) where it is clear that the factor $(\varepsilon_1 - \varepsilon_3)$ determines the sign of $\bar{f}_{z1,III}$. When the dielectric constant in the upper region is lower than that in the middle region ($\varepsilon_3 < \varepsilon_1$), $\bar{f}_{z1,III} > 0$ (upward), and when the dielectric constant in the upper region is higher ($\varepsilon_3 > \varepsilon_1$), $\bar{f}_{z1,III} < 0$ (downward). That is, \bar{f}_z always points from the region with higher dielectric constant towards the region with lower dielectric constant. This also explains why $\bar{f}_{z1,II}$ in Fig. 5.5(a) is always negative, pointing from the middle region towards the lower region which has a smaller dielectric constant ($\varepsilon_{21} = 0.1$).

Another interesting observation from Fig. 5.5(a) is how the surface force density varies with location. For all combinations of ε_{21} and ε_{31} , $\bar{f}_{z1,II}$ is found to be non-monotonic along \bar{r} , its magnitude first increasing with \bar{r} , reaching a maximum and then decreasing to zero far away

from the center of the interface. The trend in $\bar{f}_{z, \text{I,III}}$ is more complex: its magnitude decreases monotonically with \bar{r} for $\varepsilon_{31} = 0.5$ and 5 but is non-monotonic for $\varepsilon_{31} = 0.1$. To explain this phenomenon, we examine Eqn. (4.22) again: while the factor $(\varepsilon_1 - \varepsilon_3)$ governs the sign of $f_{z, \text{I,III}}$, its variation with r is controlled by the two terms $(\varepsilon_3 / \varepsilon_1)E_{z, \text{III}}^2$ and $E_{r, \text{III}}^2$. As r increases (moving away from the charge), $|E_{z, \text{III}}|$ and hence $E_{z, \text{III}}^2$ monotonically decrease. On the other hand, due to the symmetry, $E_{r, \text{III}}$ is zero at $r = 0$. With r increasing, $E_{r, \text{III}}^2$ first increases to non-zero values, and then decays at sufficiently large distance from the point charge. That is, the change of $E_{r, \text{III}}^2$ with r is non-monotonic. In addition, $E_{z, \text{III}}^2$ is accompanied by a factor $\varepsilon_3 / \varepsilon_1 = \varepsilon_{31}$. Since $E_{z, \text{III}}^2$ and $E_{r, \text{III}}^2$ vary differently with r , depending on the magnitude of ε_{31} , the overall trend of $f_{z, \text{I,III}}$ can be governed by the r - or z -component of the electric field. When $\varepsilon_3 / \varepsilon_1$ is sufficiently small (e.g. $\varepsilon_{31} = 0.1$), the trend of $f_{z, \text{I,III}}$ is governed by $E_{r, \text{III}}^2$ and hence is non-monotonic with r . As ε_{31} is increased to 0.5 and 5 , $\varepsilon_{31}E_{z, \text{III}}^2$ dominates in the evaluation of $f_{z, \text{I,III}}$, which leads to the monotonic changes of $f_{z, \text{I,III}}$ with r . Similarly, the non-monotonic changes of $f_{z, \text{I,II}}$ seen in Fig. 5.5(a) can be also explained from Eqn. (4.26). Since $\varepsilon_2 / \varepsilon_1 = 0.1$ is small in all cases, the trend of $f_{z, \text{I,II}}$ is determined by $E_{r, \text{II}}^2$, which is non-monotonic.

In Fig. 5.5(b), we consider a system with a very high dielectric constant in the lower region ($\varepsilon_{21} = 5$) compared to that of the middle layer while ε_{31} takes the same values as in Fig. 5.5(a). Since \bar{f}_z always points from the region with higher dielectric constant towards the region with lower dielectric constant, $\bar{f}_{z, \text{I,II}}$ is positive (upwards) for all combination of ε_{21} and ε_{31} , while the sign and trend of $\bar{f}_{z, \text{I,III}}$ is exactly the same as in Fig. 5.5(a). The trend of $\bar{f}_{z, \text{I,II}}$ is completely

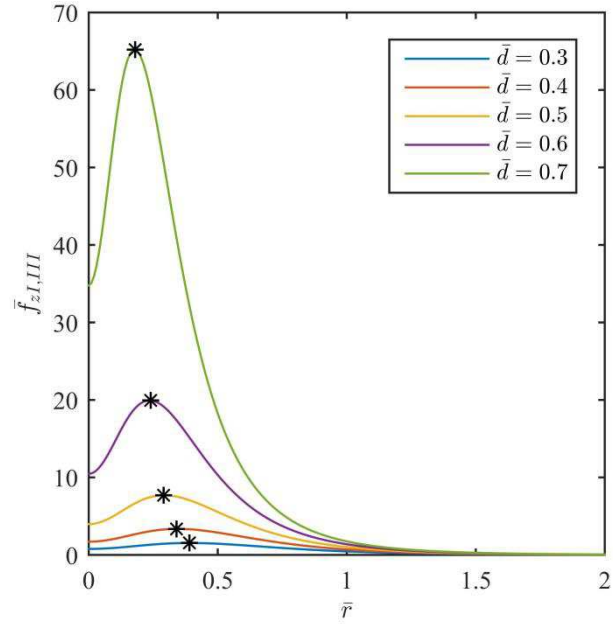
different from Fig. 5.5(a) as it decreases monotonically with \bar{r} in this case, due to the dominance of the $\varepsilon_{21}E_{z\text{II}}^2$ term in Eqn. (4.26). As ε_{31} is increased from 0.1 to 5, it causes only minor quantitative changes in $\bar{f}_{z\text{I,II}}$ while the change is significant for $\bar{f}_{z\text{I,III}}$, which manifests more direct impact of ε_{31} on $\bar{f}_{z\text{I,III}}$ similar to what is seen in Fig. 5.5(a). While comparing the magnitude of $\bar{f}_{z\text{I,III}}$ with that in Fig. 5.5(a), slightly reduced values are observed in Fig. 5.5(b). Although ε_{21} does not explicitly appear in the evaluation of $\bar{f}_{z\text{I,III}}$ in Eqn. (4.22), it does influence the electric fields in all regions. Specifically, higher value of ε_{21} causes larger screening of the induced electric field in the upper region, hence $E_{z\text{III}}^2$ and $E_{r\text{III}}^2$ are reduced, resulting in smaller $\bar{f}_{z\text{I,III}}$ in Fig. 5.5(b) than in Fig. 5.5(a).

5.3.2 Variation of the surface force density with charge location

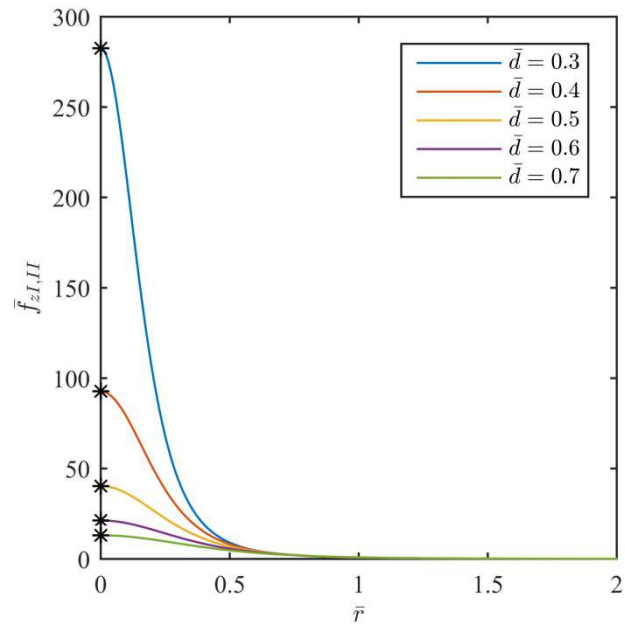
The location of the point charge also affects the surface force density. Fig. 5.6 plots \bar{f}_z vs. \bar{r} on both interfaces for different charge locations (\bar{d} varying from 0.3 to 0.7). The materials considered in this figure ($\varepsilon_{21} = 5$, $\varepsilon_{31} = 0.1$) are identical to those of a system studied earlier, represented by the solid curves in Fig. 5.5(b). Fig. 5.6(a) shows $\bar{f}_{z\text{I,III}}$, on the upper interface. Due to the non-monotonic change of $\bar{f}_{z\text{I,III}}$ in Fig. 5.5(b), a local maximum is found for each \bar{d} which is marked with *. As the point charge approaches the upper interface (\bar{d} increases), the location of the maximum shifts towards the center of the upper interface; as well, the maximum value of $\bar{f}_{z\text{I,III}}$ increases, corresponding to a more non-uniform distribution of the surface force density. Unlike in Fig. 5.6(a), for each \bar{d} , $\bar{f}_{z\text{I,II}}$ on the lower interface decreases monotonically along \bar{r} in

Fig. 5.6(b) with the maximum attained at the center ($\bar{r}=0$), which is consistent with the observation found in Fig. 5.5(b). As the point charge approaches the upper interface (\bar{d} increases), its influence on the lower interface becomes smaller and $\bar{f}_{z, \text{II}}$ decreases.

The above results have demonstrated the essential role of the two ratios between dielectric constants of the three layers. They determine not only the direction of \bar{f}_z (always from the region with higher dielectric constant to the region with lower dielectric constant) but also its distribution (monotonic or non-monotonic with the radial position). The position of the point charge, on the other hand, only affects the magnitude of the surface force, hence having a secondary influence.



(a)



(b)

FIGURE 5.6: Normalized surface force density on the interfaces for different normalized charge location. (a) Upper interface (b) Lower interface. For all cases, $\varepsilon_{21} = 5$, $\varepsilon_{31} = 0.1$ and \bar{d} varies from 0.3 to 0.7 (see legend).

5.4 Parametric analysis of the total surface force

The normalized total surface force \bar{F} is calculated by performing surface integration of \bar{f}_z (Eqs. (4.22) and (4.26)). Due to the fast decay of \bar{f}_z with \bar{r} (see for example Figs. 5.5 and 5.6), the integration was found to converge quickly and a cut-off distance of $\bar{r} = 4$ was sufficient for the evaluation of \bar{F} (with a small numerical tolerance). Similar to \bar{f}_z , \bar{F} is affected by the material properties (dielectric constants) of the three regions and the location of the point charge.

Fig. 5.7 plots \bar{F} against ε_{31} for two different ε_{21} (0.1 in Fig. 5.7(a) and 5 in Fig. 5.7(b)) and four different \bar{d} (from 0.3 to 0.7, different line styles in each figure). The red and blue lines in each figure correspond to the total surface force on the upper ($\bar{F}_{1,III}$) and lower ($\bar{F}_{1,II}$) interfaces respectively. Similar to \bar{f}_z , positive values of \bar{F} correspond to upward direction while negative \bar{F} is downward.

In Fig. 5.7(a), where the dielectric constant is smaller in the lower region than in the middle layer ($\varepsilon_2 < \varepsilon_1$), $\bar{F}_{1,II}$ is negative (pointing downward) for the entire range of ε_{31} . Regardless of the \bar{d} values, as ε_{31} increases the magnitude of $\bar{F}_{1,II}$ reduces and it approaches a plateau value when $\varepsilon_{31} \rightarrow \infty$. This plateau value is essentially the normalized total surface force on the lower interface when region III is occupied by a conductor. As the point charge is moved towards the upper region (\bar{d} increases), the surface force on the lower interface becomes smaller in magnitude; correspondingly the $\bar{F}_{1,II}$ curve shifts upward and the plateau value for $\varepsilon_{31} \rightarrow \infty$ is reduced accordingly.

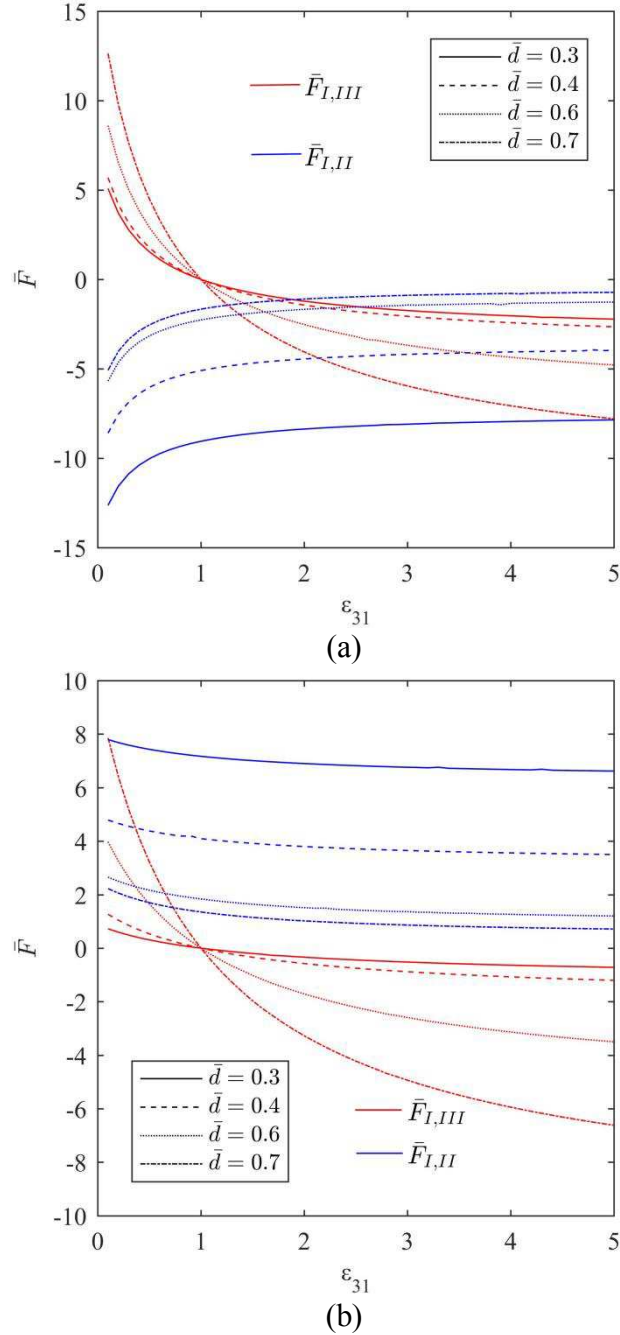


FIGURE 5.7: Normalized total surface force on the interfaces, with red and blue lines corresponding to the upper and lower interfaces respectively. (a) $\varepsilon_{21} = 0.1$, (b) $\varepsilon_{21} = 5$. For each subfigure, ε_{31} varies from 0.1 to 5 on the horizontal axis and \bar{d} takes four different values from 0.3 to 0.7 (see legend for different line styles used for different \bar{d}).

Compared with $\bar{F}_{1,II}$, the variation of $\bar{F}_{1,III}$ with ε_{31} is more complex: for $\varepsilon_{31} < 1$ it is positive (pointing upward) and its magnitude decreases with ε_{31} ; at $\varepsilon_{31} = 1$ the upper interfaces no longer exist and $\bar{F}_{1,III}$ becomes zero; with further increase in ε_{31} , $\bar{F}_{1,III}$ becomes negative (pointing downward) and starts increasing in the opposite direction. Increasing \bar{d} causes the magnitude of $\bar{F}_{1,III}$ to be larger for all ε_{31} , however, this does not correspond to a simple shift of the $\bar{F}_{1,III}$ curves, because of the direction change of $\bar{F}_{1,III}$ at $\varepsilon_{31} = 1$. In fact, for larger \bar{d} , the $\bar{F}_{1,III}$ curve is steeper, indicating the greater influence of ε_{31} on $\bar{F}_{1,III}$ when the charge is closer to the upper interface. This coupled influence was not observed for $\bar{F}_{1,II}$, where the curves for different \bar{d} are more or less parallel.

Behaviors observed in Fig. 5.7(b) for $\varepsilon_{21} = 5$ are qualitatively similar to those in Fig. 5.7(a), with a few notable differences. First of all, due to the higher dielectric constant in region II than in region I, $\bar{F}_{1,II}$ is now pointing upwards. Secondly, while the magnitude of $\bar{F}_{1,II}$ decreases with ε_{31} in both Figs. 5.7(a) and 5.7(b), the rate of decay is slower in Fig. 5.7(b). The higher ε_{21} value in Fig. 5.7(b) has caused the impact of ε_{31} to be less significant on $\bar{F}_{1,II}$. Finally, compared with Fig. 5.7(a), a small reduction in the magnitude of $\bar{F}_{1,III}$ can be seen as ε_{21} is increased in Fig. 5.7(b), due to the greater screening provided by the lower region.

5.5 Implications of the total surface force

The results from the parametric study above have useful implications in applications where layered dielectrics are involved. First of all, the direction of surface forces on each interface can be modulated individually by adjusting the dielectric constants of the materials on the two sides of the interface. One can introduce attractive or repulsive interactions between the two surfaces (forces on the two interfaces having opposite directions), as well as forces in the same direction. This is useful in applications where a certain nature of the interaction (e.g., attractive or repulsive) is desired, for instance in the development of electrostatic chuck design for holding electrical devices [18], or in the design of wall climbing robot technologies [19], [20]. Secondly, the distribution of the surface force density can be fine tuned with the dielectric properties of the materials, to generate the desired range of interaction (nonzero surface force) and strength of interaction (magnitude of surface force).

Chapter 6

EXTENSION OF THE PROBLEM

In this chapter, the methodology of extending the work to a distribution of charges is presented. To demonstrate the extension, a new problem is examined where a pair of equal and opposite point charges are present in the middle layer. Following the basic formulation for this problem, the electric field, and the interfacial forces are calculated and results are described in details with comparison to those in Chapter 5 for a single point charge.

6.1 Extended problem with a distribution of charges

Many problems that involve multilayered semiconductors or dielectrics often have the need to deal with a distribution of charges near the interfaces. Therefore, the calculation of induced electric potential as well as interfacial forces are found to be of common interest. The formulations for the model with a single point charge in this work can also be extended to establish a theoretical framework for modeling multilayered devices where interfacial forces arise from a distribution of charges. Because the equations governing the electric potential in the system are linear, the electric field due to a distribution of charges can be calculated by using linear superposition of the electric field obtained in the present work for a point charge (differentiations of Eqs. (3.53), (3.54) and (3.55)). The MST can then be calculated, from which the surface forces due to the distributed charges can be evaluated.

The distribution of charges has also significant implications in contact adhesion which is the result of electrostatic contact charging. Most of the available experimental evidence suggest that the charged surfaces after contact hold complementary mosaic patches where each charged patch on one surface is matched to one on the other surface with opposite charge. Motivated from this phenomenon, an example for extending the current problem is presented where an equal and opposite point charge is introduced in the same multilayered model. The method of calculating interfacial forces in this problem can be applied in determining the induced surface forces due to a distribution of correlated charge mosaics on the two surfaces.

6.2 Multilayered dielectrics with a pair of point charges

The schematic is shown in Fig. 6.1, where two point charges (one is positive and the other is negative) of the same magnitude q are embedded in region II which has a dielectric with the dielectric constant ϵ_1 . The two charges are located symmetrically in the middle layer, namely that the $+q$ charge is located at a distance d above the lower interface, same as Fig. 2.1, while a new charge $-q$ is introduced in the same layer at a distance d from the upper interface. The dielectric properties of other regions as well as all other physical description of the system remain the same as in Fig. 2.1. The same cylindrical coordinate system is used for the analysis.

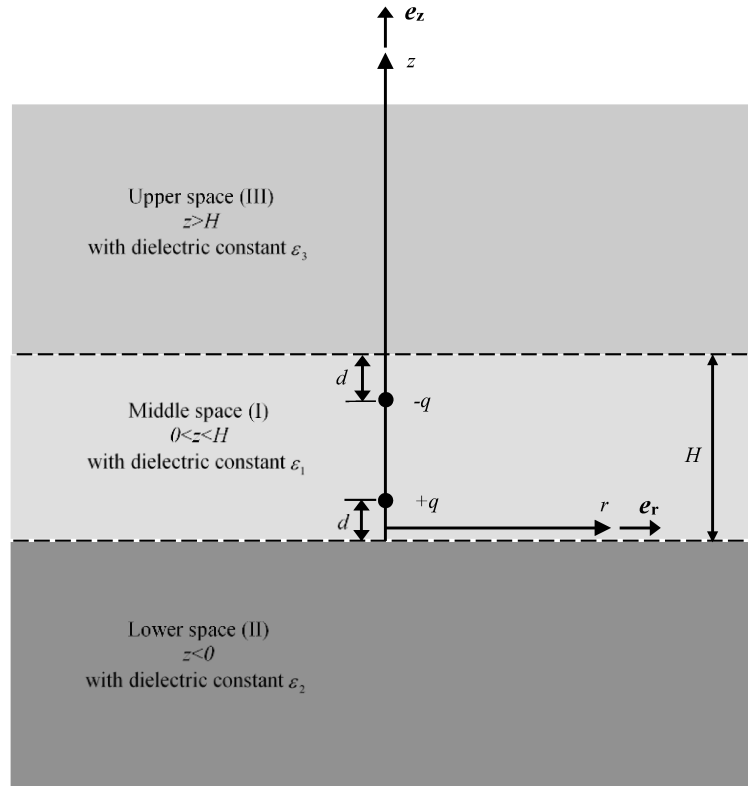


FIGURE 6.1: Schematic of the electrostatic problem with a pair of equal and opposite point charges in the middle layer.

6.3 Calculation of surface forces

For the model in Fig. 6.1, the electric potential of the single point charge is used to first calculate the total ϕ induced by the pair of point charges. As the point charge $+q$ is embedded at a distance d from the lower interface, the electric potentials $\phi(r, z)$ in all regions are same as what is found in Eqs. (3.49)-(3.51). Because the location of $-q$ is at a distance $(H - d)$ from the lower interface, it is sufficient to replace $+q$ and d in Eqs. (3.49)-(3.51) by $-q$ and $(H - d)$

respectively to calculate the electric potential of $-q$ in all three regions. This results the following expressions:

Region I:

$$\begin{aligned}
\phi_I|_{-q}(r, 0 < z < H) = & -\frac{q}{4\pi\epsilon_0\epsilon_1\sqrt{r^2 + (z - H + d)^2}} \\
& -\frac{q}{4\pi\epsilon_0} \int_0^\infty \left[\frac{2 \sinh(\rho d) + 2 \sinh[\rho(H-d)] \left[\cosh(\rho H) + \frac{\epsilon_2}{\epsilon_1} \sinh(\rho H) \right]}{\sinh^3(\rho H) \left[(\epsilon_2 + \epsilon_3) \coth(\rho H) + \left(\frac{\epsilon_2 \epsilon_3}{\epsilon_1} + \epsilon_1 \right) \right]} \right] \\
& \quad \times \sinh(\rho z) J_0(\rho r) d\rho \\
& -\frac{q}{4\pi\epsilon_0} \int_0^\infty \left[\frac{2 \sinh[\rho(H-d)] + 2 \sinh(\rho d) \left[\cosh(\rho H) + \frac{\epsilon_3}{\epsilon_1} \sinh(\rho H) \right]}{\sinh^3(\rho H) \left[(\epsilon_2 + \epsilon_3) \coth(\rho H) + \left(\frac{\epsilon_2 \epsilon_3}{\epsilon_1} + \epsilon_1 \right) \right]} \right] \\
& \quad \times \sinh[\rho(H-z)] J_0(\rho r) d\rho \\
& + \frac{q}{4\pi\epsilon_0\epsilon_1} \int_0^\infty \frac{e^{-\rho d} \sinh(\rho z) + e^{-\rho(H-d)} \sinh[\rho(H-z)]}{\sinh(\rho H)} J_0(\rho r) d\rho, \tag{6.1}
\end{aligned}$$

Region II:

$$\begin{aligned}
\phi_{II}|_{-q}(r, z < 0) = & -\frac{q}{4\pi\epsilon_0} \\
& \times \int_0^\infty \left[\frac{2 \sinh[\rho(H-d)] + 2 \sinh(\rho d) \left[\cosh(\rho H) + \frac{\epsilon_3}{\epsilon_1} \sinh(\rho H) \right]}{\sinh^2(\rho H) \left[(\epsilon_2 + \epsilon_3) \coth(\rho H) + \left(\frac{\epsilon_2 \epsilon_3}{\epsilon_1} + \epsilon_1 \right) \right]} \right] e^{\rho z} J_0(\rho r) d\rho, \tag{6.2}
\end{aligned}$$

Region III:

$$\phi_{III}|_{-q}(r, z > H) = -\frac{q}{4\pi\epsilon_0} \times \int_0^\infty \left[\frac{2 \sinh(\rho d) + 2 \sinh[\rho(H-d)] \left[\cosh(\rho H) + \frac{\epsilon_2}{\epsilon_1} \sinh(\rho H) \right] e^{-\rho d}}{\sinh^2(\rho H) \left[(\epsilon_2 + \epsilon_3) \coth(\rho H) + \left(\frac{\epsilon_2 \epsilon_3}{\epsilon_1} + \epsilon_1 \right) \right]} \right] e^{\rho(H-z)} J_0(\rho r) d\rho. \quad (6.3)$$

As the Laplace equation in all layers of the system is linear, the total potential ϕ_{total} produced by a pair of point charges is calculable by linear superposition. Therefore,

$$\phi_{\text{total}} = \phi_q + \phi_{-q} \quad (6.4)$$

where, ϕ_q and ϕ_{-q} correspond to the electric potential due to $+q$ and $-q$ charges respectively in the space.

Similarly, the total electric field $\mathbf{E}_{\text{total}}$ induced by the pair of point charges can be determined from the individual contributions from $+q$ and $-q$, which yields,

$$\mathbf{E}_{\text{total}} = \mathbf{E}_q + \mathbf{E}_{-q} = -\nabla\phi_q - \nabla\phi_{-q}. \quad (6.5)$$

In component form, the total electric field can be expressed as,

$$\mathbf{E}_{\text{total}} = E_{r \text{ total}} \mathbf{e}_r + E_{z \text{ total}} \mathbf{e}_z \quad (6.6)$$

where, $E_{r \text{ total}}$ and $E_{z \text{ total}}$ are the r - and z -components of the total electric field. Following the results of the total electric field, the surface force densities in the upper and lower interfaces are obtained. Specifically, similar to the single point charge problem, the continuity of electric potential and normal electric displacement require that the r -component of the surface force

density vanishes everywhere. The surface force densities on the upper and lower interfaces therefore only have the z -component, denoted by $f_{z \text{ I,III total}}$ and $f_{z \text{ I,II total}}$ respectively.

$$f_{z \text{ I,III total}} = \frac{\epsilon_0}{2} \left[\left(E_{z\text{III total}}^2 - E_{r\text{III total}}^2 \right) \epsilon_3 - \left(E_{z\text{I total}}^2 - E_{r\text{I total}}^2 \right) \epsilon_1 \right]_{z=H} \quad (6.7)$$

and

$$f_{z \text{ I,II total}} = \frac{\epsilon_0}{2} \left[\left(E_{z\text{II total}}^2 - E_{r\text{II total}}^2 \right) \epsilon_1 - \left(E_{z\text{I total}}^2 - E_{r\text{I total}}^2 \right) \epsilon_2 \right]_{z=0}. \quad (6.8)$$

Here, $E_{ri \text{ total}}$ and $E_{zi \text{ total}}$ correspond to the components of the total electric field in i -th layer ($i=I, II, III$). Using the continuity conditions of the electric field and the normal electric displacement across the interface again, Eqs. (6.7) and (6.8) can be expressed in terms of the electric field in the upper and lower regions respectively. Similar to the final expressions of \bar{f}_z for the single charge in Eqs. (4.22) and (4.26), \bar{f}_z for the pair of charges can be written as

$$f_{z \text{ I,III total}} = \frac{\epsilon_0}{2} (\epsilon_1 - \epsilon_3) \left[\frac{\epsilon_3}{\epsilon_1} E_{z\text{III total}}^2 + E_{r\text{III total}}^2 \right]_{z=H} \quad (6.9)$$

and

$$f_{z \text{ I,II total}} = \frac{\epsilon_0}{2} (\epsilon_2 - \epsilon_1) \left[\frac{\epsilon_2}{\epsilon_1} E_{z\text{II total}}^2 + E_{r\text{II total}}^2 \right]_{z=0}. \quad (6.10)$$

Finally, the total surface force is calculated knowing the surface force density on the interfaces. Due to the fact that the surface force density only has z -component, the magnitude of the total force acting on the upper interface is given by

$$F_{I,III \text{ total}} = 2\pi \int_0^{\infty} f_{z \text{ I,III total}} r dr . \quad (6.11)$$

Similarly, the magnitude of the total surface force on the lower interface is determined by

$$F_{I,II \text{ total}} = 2\pi \int_0^{\infty} f_{z \text{ I,II total}} r dr . \quad (6.12)$$

Numerical implementation of the above procedure is very straight forward. First, the electric fields on the upper and lower interfaces for $+q$ and $-q$ are calculated. As the normalized solution of the electric field is used in the numerical calculations and the magnitude of both charges is same, the electric field components of \mathbf{E}_{-q} in all layers are obtained by only changing the sign (from $+$ to $-$) and the charge location (from d to $H-d$) in those of \mathbf{E}_q (Eqs. (4.16)-(4.19), (4.27) and (4.28)). By adding \mathbf{E}_q and \mathbf{E}_{-q} numerically, the total electric field $\mathbf{E}_{\text{total}}$ due to the pair of charges is calculated. Having determined the total electric field, the surface force density is obtained following the same integrals (Eqs. (4.22) and (4.26)). Finally, a surface integration of the force density is implemented to evaluate the total surface forces. For further implementation with more charges in the system, the same numerical scheme can be applied by repeating the calculation of the electric field for each charge, thus providing a convenient approach to determine the interfacial forces due to a distribution of charges.

The above procedure explained for a pair of charges can be extended further to situations involving a distribution of charges (along a line, over a surface, or through a volume). To calculate the electric field at any point in the system, the value of point charge in the expressions of the electric field need to be replaced with $\rho_L dL$, $\rho_S dS$ and $\rho_V dV$ for line, surface and volume distributions, respectively. Here ρ_L , ρ_S and ρ_V are respectively line, surface and volumetric

charge densities, and dL , dS and dV are respectively a line, surface and volume element. The total electric field can then be determined by performing a line, surface or volume integration to account for contribution from all the charged elements. Following this calculation, the MST can be determined from where the surface forces due to the distribution of charges can be obtained.

6.4 Results and comparison

Below the results for the surface force density \bar{f}_z and the total surface force \bar{F} on the upper and lower interfaces induced by the pair of charges are presented. To compare with the case of a single point charge, the same normalized quantities as in Eqn. (4.35) are used. \bar{f}_z and \bar{F} on the lower and upper interfaces are denoted with subscripts I, II and I, III respectively for both the single charge and pair of charges.

6.4.1 Comparison of the surface force density (effect of dielectric constant ratios)

In this section, surface force densities due to a single charge and due to a pair of charges are compared for different combinations of the dielectric constant ratios (ϵ_{21} and ϵ_{31}). In Fig. 6.2, \bar{f}_z is plotted as a function of \bar{r} . ϵ_{31} is varied from 0.1 to 5 with the other dielectric constant ratio fixed at $\epsilon_{21} = 0.1$. In the case of a single charge (Fig. 6.2(a)), it is located at $\bar{d} = 0.4$. This charge is also placed at the same location in the case of a pair of charges, but with the addition of an equal and opposite charge located at $\bar{d} = 0.6$ (Fig. 6.2(b)). The red and blue lines correspond to the surface force density on the upper and lower interfaces respectively. The normalized surface force

density for the lower and upper interfaces due to the pair of charges are denoted by $\bar{f}_{z, I, II \text{ total}}$ and $\bar{f}_{z, I, III \text{ total}}$ while the corresponding quantities for the single point charge are denoted by the subscripts without the term “total”. Positive values of \bar{f}_z indicate upward direction and negative values indicate downward direction.

As can be seen, the sign and trend of $\bar{f}_{z, I, II \text{ total}}$ and $\bar{f}_{z, I, III \text{ total}}$ remain same as those of the single charge indicating that the inclusion of $-q$ has no qualitative impact on the surface force density. Specifically, in both sub-figures $\bar{f}_{z, I, II}$ and $\bar{f}_{z, I, II \text{ total}}$ for the lower interface is negative (as $\varepsilon_{21} < 1$) and non-monotonic (due to the small ε_{21} , 0.1). Similarly, in both sub-figures, $\bar{f}_{z, I, III}$ and $\bar{f}_{z, I, III \text{ total}}$ change from non-monotonic to monotonic as ε_{31} increases, and from positive to negative as ε_{31} passes one.

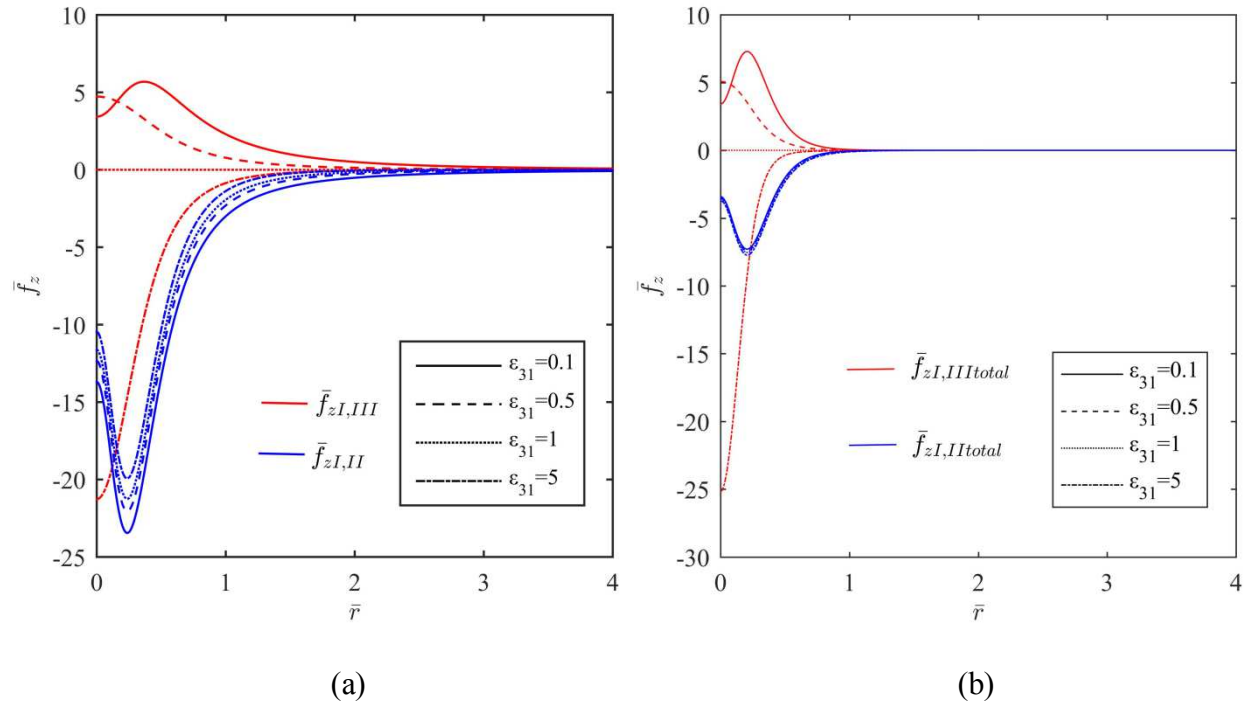


FIGURE 6.2: Normalized surface force density on the interfaces, with red and blue lines corresponding to the upper and lower interfaces respectively. (a) a single charge, (b) a pair of charges. For each subfigure, $\bar{d} = 0.4$, $\epsilon_{21} = 0.1$ and ϵ_{31} varies from 0.1 to 5 (see legend for different line styles used for different ϵ_{31}).

On the other hand, the quantitative influence of $-q$ on \bar{f}_z is clear from the sub-figures. The magnitude of $\bar{f}_{zI,IItotal}$ decreases significantly in Fig. 6.2(b); as well, the effect of ϵ_{31} on $\bar{f}_{zI,IItotal}$ is reduced, evidenced by the fact that the four curves with different ϵ_{31} almost coincide with one another in Fig. 6.2(b). The presence of the additional charge also leads to interesting results for $\bar{f}_{zI,IIItotal}$ in Fig. 6.2(b): for small \bar{r} i.e. locations near the center of the upper interface,

the magnitude of $\bar{f}_{z \text{ I,III total}}$ is larger than that of the single point charge, while for large \bar{r} , $\bar{f}_{z \text{ I,III total}}$ decays faster with the extra charge.

To investigate these phenomena, Eqs. (6.9) and (6.10) are taken into consideration where the variation of $f_{z \text{ I,III total}}$ is governed by the two terms $(\varepsilon_3 / \varepsilon_1) E_{z\text{III total}}^2$ and $E_{r\text{III total}}^2$ while $f_{z \text{ I,II total}}$ is controlled by $(\varepsilon_2 / \varepsilon_1) E_{z\text{II total}}^2$ and $E_{r\text{II total}}^2$. The electric field components along the upper and lower interfaces, in the normalized form (see Eqn. (4.30) for the normalization), are plotted in Fig. 6.3 as functions of \bar{r} for $\varepsilon_{31} = 0.1, 0.5$ and 5 . Subscripts II and III are used to denote the electric field components on the lower and upper interfaces, respectively. In addition, the electric field components for the single charge from Eqn. (4.22) are added in the same figure, denoted by symbols without the subscript of “total”. For example, in Fig. 6.3(a), $\bar{E}_{z \text{ II}}$ is the normalized z -component of the electric field on the lower interface in the case of a single point charge, and $\bar{E}_{z\text{II total}}$ is the normalized z -component of the electric field on the lower interface caused by a pair of charges.

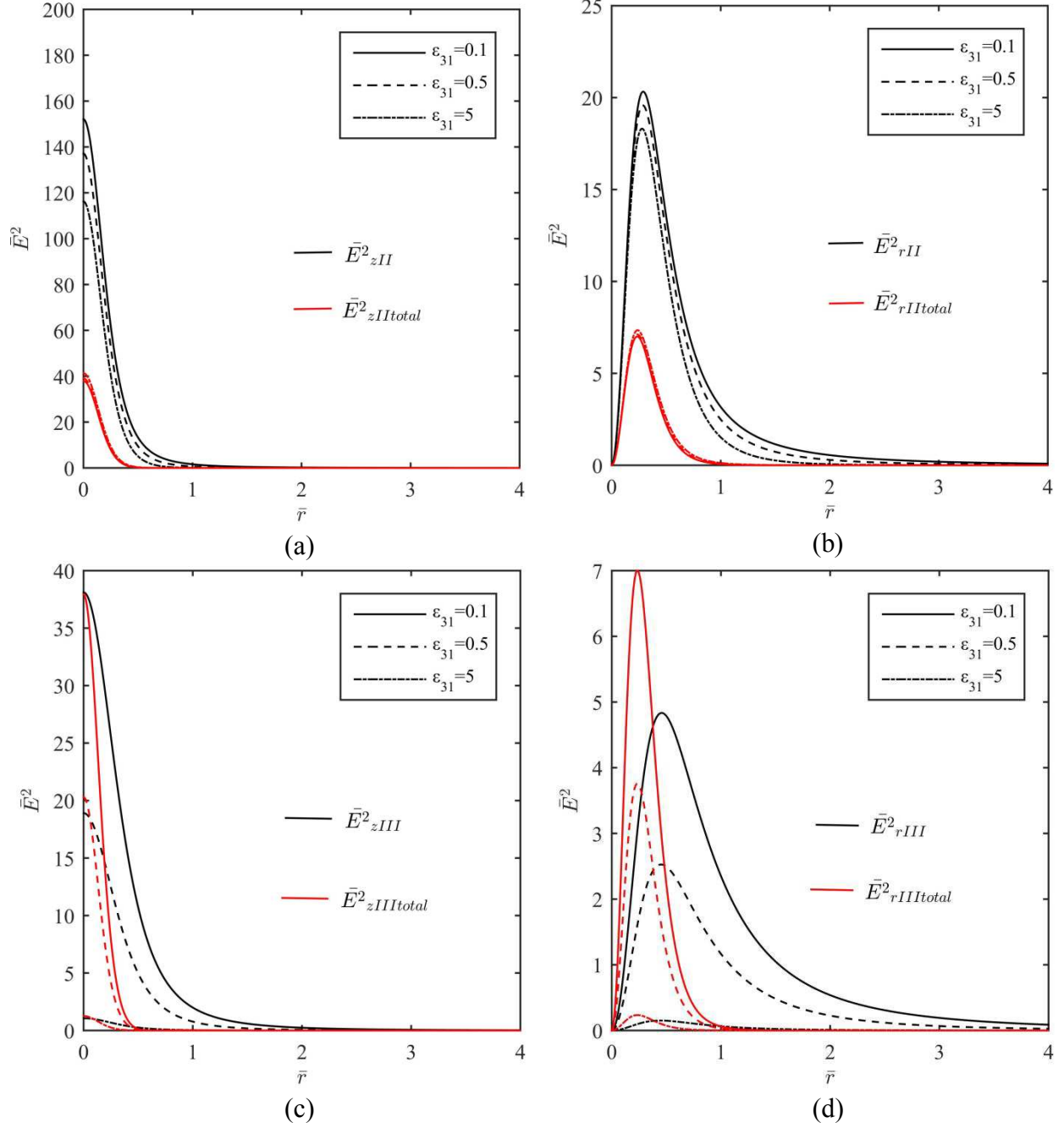


FIGURE 6.3: Normalized electric field components on the interfaces with black and red lines correspond to the single and pair of charges respectively. (a) z -component on the lower interface, (b) r -component on the lower interface, (c) z -component on the upper interface, (d) r -component on the upper interface. For each subfigure, $\bar{d} = 0.4$, $\epsilon_{21} = 0.1$ and ϵ_{31} varies from 0.1 to 5 (see legend for different line styles used for different ϵ_{31}).

Let us first examine the squared electric field components on the lower interface, given by Fig. 6.3(a) and (b). It can be seen clearly that $\bar{E}_{z\text{ II total}}^2$ and $\bar{E}_{r\text{ II total}}^2$ are much lower than those of the single charge regardless of the values of ε_{31} . Also the red curves in Fig. 6.3(a) and (b) are much closer to each other which suggests that the variation of \bar{E} with ε_{31} on the lower interface for the pair of charges is less significant. Physically, the electric field on the lower interface is still primarily governed by the $+q$ charge since that two charges have the same magnitude and the $+q$ charge is closer. The addition of the $-q$ charge creates a compensating effect and partially screens the electric field induced by the $+q$ charge. This leads to a reduction in the magnitude of the net electric field and consequently reduces $f_{z\text{ I,II total}}$ according to Eqn. (6.10).

For the upper interface, in Fig. 6.3(c), $\bar{E}_{z\text{ III total}}^2$ is found always smaller than $\bar{E}_{z\text{ III}}^2$ for $\varepsilon_{31} = 0.1$. For other values of ε_{31} (0.5 and 5), $\bar{E}_{z\text{ III total}}^2$ is also smaller except for the locations near the center of the upper interface. On the other hand, $\bar{E}_{r\text{ III total}}^2$ is found much larger than $\bar{E}_{r\text{ III}}^2$ at small \bar{r} in Fig. 6.3(d) for all ε_{31} . Also, in both Fig. 6.3(c) and (d), \bar{E}^2 for the pair of charges decays much faster at large \bar{r} . The overall enhanced electric field at small \bar{r} and faster decay at large \bar{r} , observed for the pair of charges, are consistent with the observations from Fig. 6.2 for the surface force density on the upper interface. The enhanced electric field may be counter-intuitive as the $-q$ charge is expected to partially screen the electric field of the $+q$ charge. However, since now the $-q$ charge is the one closer to the upper interface, it mainly determines the net electric field on the upper interface. The increased electric field at small \bar{r} arises from the over-compensation of $-q$ to the electric field of the $+q$ charge, that is, the magnitude of the net

electric field (due to both the $+q$ and $-q$) has exceeded the original electric field (due to $+q$ only).

To further study the influence of dielectric constant ratios on \bar{f}_z , ε_{21} is increased to 5 in Fig. 6.4 while the charge location and other dielectric constant ratio remain same as in Fig. 6.2. Similar to the comparison seen in Fig. 6.2, the trend and sign of \bar{f}_z are not altered by the addition of the $-q$ charge. The magnitude of $\bar{f}_{zI,II\text{total}}$ on the lower interface is reduced due to the screening from the $-q$ charge, whereas the magnitude of $\bar{f}_{zI,III\text{total}}$ on the upper interface is increased at small \bar{r} due to the over-compensation.

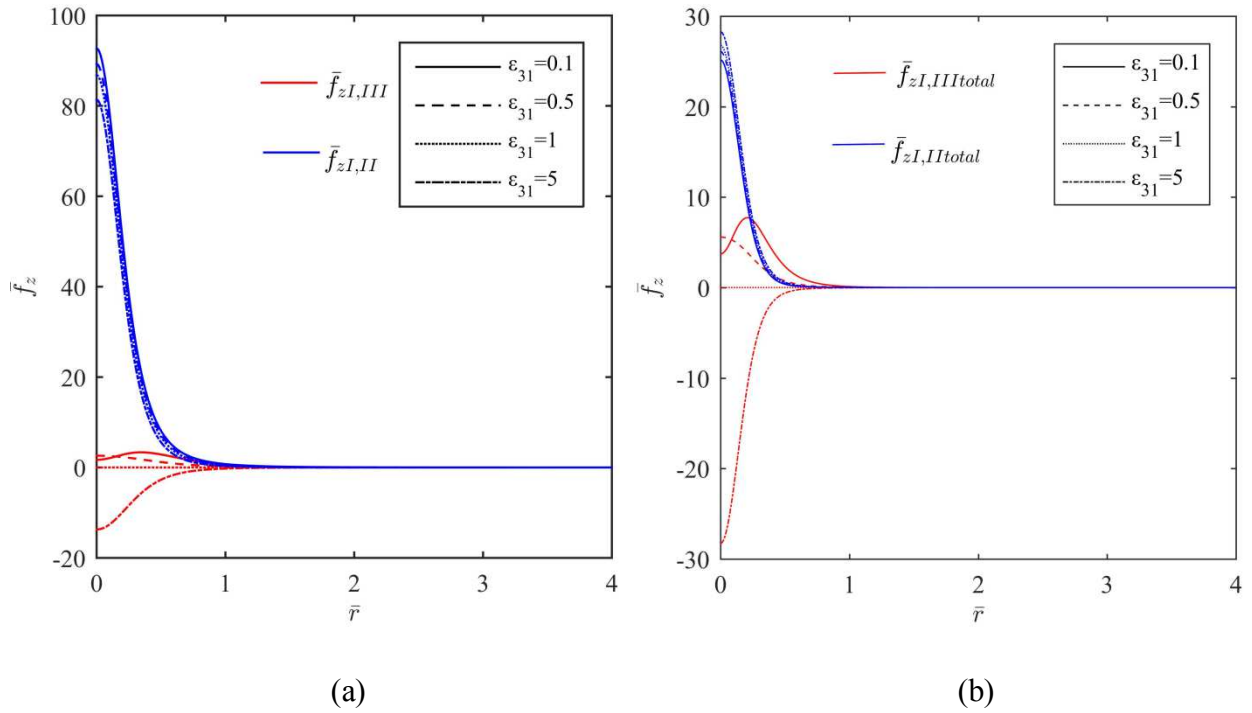


FIGURE 6.4: Normalized surface force density on the interfaces, with red and blue lines corresponding to the upper and lower interfaces respectively. (a) a single charge, (b) a pair of charges. For each subfigure, $\bar{d} = 0.4$, $\varepsilon_{21} = 5$ and ε_{31} varies from 0.1 to 5 (see legend for different line styles used for different ε_{31}).

6.4.2 Comparison of the surface force density (effect of charge location)

The location of point charge was shown in Chapter 5 to influence the magnitude of the surface force density without changing its sign or trend for a single charge. To compare the results with a pair of charges, \bar{f}_z is plotted as a function of \bar{r} in Fig. 6.5 for both single charge and a pair of charges. In both cases, $\bar{d} = 0.3$, and thus the location of $-q$ is at 0.7 in Fig. 6.4(b). Physically, $+q$ and $-q$ shifts closer to the lower and upper interfaces respectively than that in Fig. 6.2. The other parameters are considered same as in Fig. 6.2.

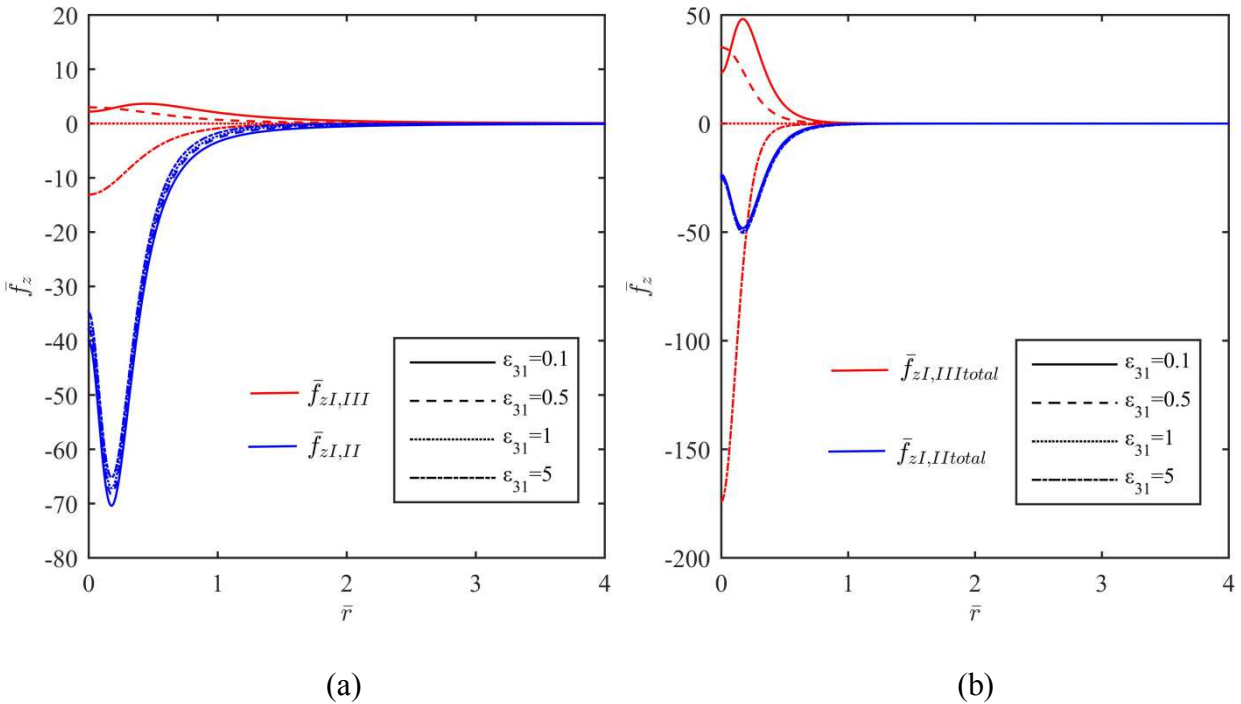


FIGURE 6.5: Normalized surface force density on the interfaces, with red and blue lines corresponding to the upper and lower interfaces respectively. (a) a single charge, (b) a pair of charges. For each subfigure, $\bar{d} = 0.3$, $\epsilon_{21} = 0.1$ and ϵ_{31} varies from 0.1 to 5 (see legend for different line styles used for different ϵ_{31}).

The trend and sign of \bar{f}_z in Fig. 6.5 are found similar to those in Fig. 6.2 as all the parametric conditions are the same except the charge location. Compared with Fig. 6.2(b), the magnitude of \bar{f}_z on both interfaces is much larger in Fig. 6.5(b) for each ε_{31} . As the $+q$ charge mainly influences the electric field on the lower interface, its reduced distance in Fig. 6.5(b) causes an enhanced net electric field and consequently higher magnitude of $\bar{f}_{z\text{ I,II total}}$. Similarly, the magnitude of $\bar{f}_{z\text{ I,III total}}$ increases significantly as the $-q$ charge shifts closer to the upper interface. The influence of the extra charge on the magnitude of \bar{f}_z for $\bar{d} = 0.3$, observed by comparing Fig. 6.5(b) with Fig. 6.5(a), is similar to the influence seen in Fig. 6.2: the extra charge caused increase in the magnitude of $\bar{f}_{z\text{ I,III total}}$ (over-compensation) at small \bar{r} but decrease at large \bar{r} as well as decrease in the magnitude of $\bar{f}_{z\text{ I,II total}}$ (partial compensation) for the entire range of \bar{r} . With the charges closer to the interfaces, the increase in $\bar{f}_{z\text{ I,III total}}$ (near the center of upper interface) is more significant due to the greater over-compensation from $-q$. For instance, the magnitude of $\bar{f}_{z\text{ I,III total}}(\bar{r} = 0, \varepsilon_{31} = 5)$ in Fig. 6.2(b) was observed about 1.2 times than that of $\bar{f}_{z\text{ I,III}}$ in Fig. 6.2(a), while the magnitude of $\bar{f}_{z\text{ I,III total}}(\bar{r} = 0, \varepsilon_{31} = 5)$ in Fig. 6.5(b) was observed about 13.2 times than that of $\bar{f}_{z\text{ I,III}}$ in Fig. 6.5(a). Because $-q$ is further from the lower interface, its partial compensation for the electric field on the lower interface is weaker, and hence the reduction in the magnitude of $\bar{f}_{z\text{ I,II total}}$ is less in Fig. 6.5. In particular, the magnitude of $\bar{f}_{z\text{ I,II}}(\bar{r} = 0.24, \varepsilon_{31} = 0.1)$ in Fig. 6.2(a) was observed about 4 times than that of $\bar{f}_{z\text{ I,II}}$ in Fig. 6.2(b), while the magnitude of $\bar{f}_{z\text{ I,II}}(\bar{r} = 0.24, \varepsilon_{31} = 0.1)$ in Fig. 6.5(a) was observed 1.5 times than that of $\bar{f}_{z\text{ I,II}}$ in Fig. 6.5(b).

6.4.3. Comparison of the total surface force

The total surface force \bar{F} for a pair of charges is calculated from Eqs. (6.11) and (6.12) following the same method as applied to the single charge. \bar{f}_z for the pair of charges decays much faster with \bar{r} (see for example Fig. 6.2) than that of the single charge which leads to a quicker convergence of the integration for the evaluation of \bar{F} . Still, the same cut-off distance ($\bar{r}=0.4$) was maintained during the numerical calculations. In this section, the influences of the material properties (dielectric constants) of the three regions as well as the charge location on \bar{F} are described. First, \bar{F} on both interfaces is plotted as a function of ε_{31} in Fig. 6.6 for $\bar{d}=0.4$ ($\varepsilon_{21}=0.1$ in Fig. 6.6(a) and $\varepsilon_{21}=5$ in Fig. 6.6(b)). The results for the pair of charges are denoted by $\bar{F}_{\text{I,III total}}$ (upper interface) and $\bar{F}_{\text{I,II total}}$ (lower interface), while their counterparts for a single point charge are included in the same figure and denoted by symbols without the subscript of “total”. Similar to \bar{f}_z , positive values of \bar{F} correspond to upward direction while negative \bar{F} is downward.

In both subfigures, the direction of \bar{F} induced by a pair of charges is the same as that caused by a single charge. In particular, the direction of $\bar{F}_{\text{I,II}}$ and $\bar{F}_{\text{I,II total}}$ on the lower interface is completely determined by the value of ε_{21} , positive for $\varepsilon_{21} > 1$ and negative for $\varepsilon_{21} < 1$. While the direction of $\bar{F}_{\text{I,III}}$ and $\bar{F}_{\text{I,III total}}$ are governed by the value of ε_{31} , positive for $\varepsilon_{31} < 1$ and negative for $\varepsilon_{31} > 1$. That is, \bar{F} always points from the region with higher dielectric constant to the region with lower dielectric constant.

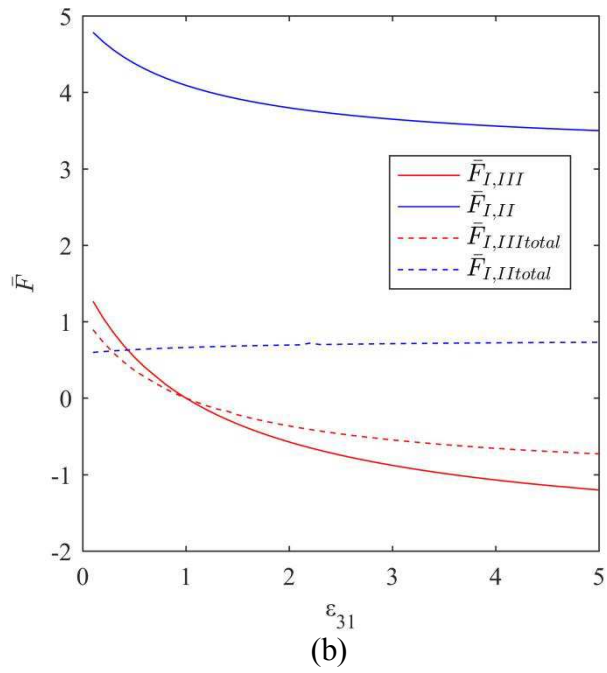
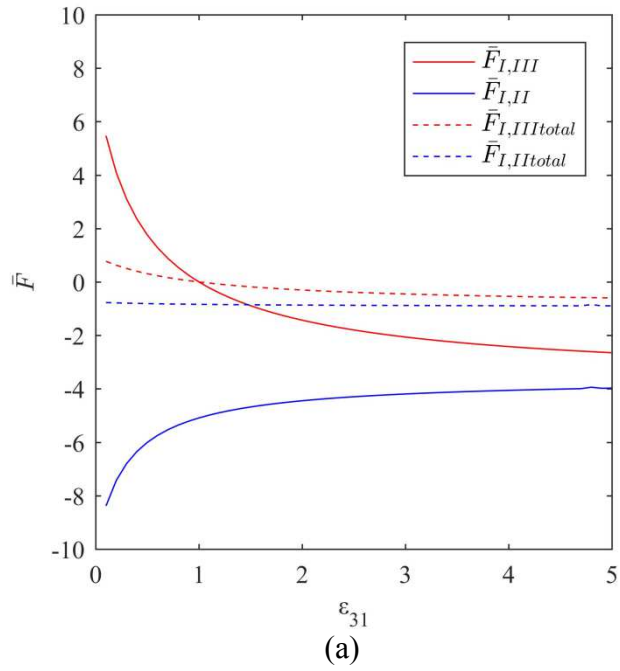


FIGURE 6.6: Normalized total surface force due to a single charge and a pair of charges, with red and blue lines corresponding to the upper and lower interfaces respectively. For all cases, $\bar{d} = 0.4$.

(a) $\varepsilon_{21} = 0.1$, (b) $\varepsilon_{21} = 5$.

Despite the similarity, the pair of charges does introduce significant quantitative differences. Let us first consider the upper interface. While the trend of $\bar{F}_{I,III}$ and $\bar{F}_{I,III \text{ total}}$ with increasing ε_{31} is monotonically decreasing in both subfigures, the magnitude of $\bar{F}_{I,III \text{ total}}$ is always smaller than $\bar{F}_{I,III}$. Because of this, the change in $\bar{F}_{I,III \text{ total}}$ with ε_{31} is more gradual than $\bar{F}_{I,III}$. To further study this phenomenon as well as to analyze the effect of charge location, $\bar{F}_{I,III}$ and $\bar{F}_{I,III \text{ total}}$ are also determined for other values of \bar{d} . In Fig. 6.7, both $\bar{F}_{I,III}$ and $\bar{F}_{I,III \text{ total}}$ are plotted as functions of ε_{31} for $\bar{d} = 0.1, 0.2$ and 0.3 while the other dielectric constant remains the same as that of Fig. 6.6(a). It is interesting to observe from the subfigures that due to the different charge locations, the relative magnitudes of $\bar{F}_{I,III}$ and $\bar{F}_{I,III \text{ total}}$ change significantly from what is found in Fig. 6.6(a). Specifically, unlike in Fig. 6.6(a), the magnitude of $\bar{F}_{I,III \text{ total}}$ in Fig. 6.7(a) and (b) where $\bar{d} = 0.1$ and 0.2 respectively, is always higher than $\bar{F}_{I,III}$ for the entire range of ε_{31} . These are the situations where the two charges are very close to the interfaces. The addition of an opposite charge near the upper interface introduces strong over-compensation for the electric field on the upper interface induced by the original charge near the lower interface. As the charges are located further from the interfaces, the compensation from the additional charge becomes smaller, which can be seen from the behavior of $\bar{F}_{I,III \text{ total}}$ in Fig. 6.7(c) ($\bar{d} = 0.3$) where its magnitude is smaller (partial compensation) than $\bar{F}_{I,III}$ for small ε_{31} while it remains higher (over-compensation) for large ε_{31} . Therefore, both the charge location and ε_{31} have significant influence on the effect of the additional charge on $\bar{F}_{I,III \text{ total}}$, and their influences are not independent of each other.

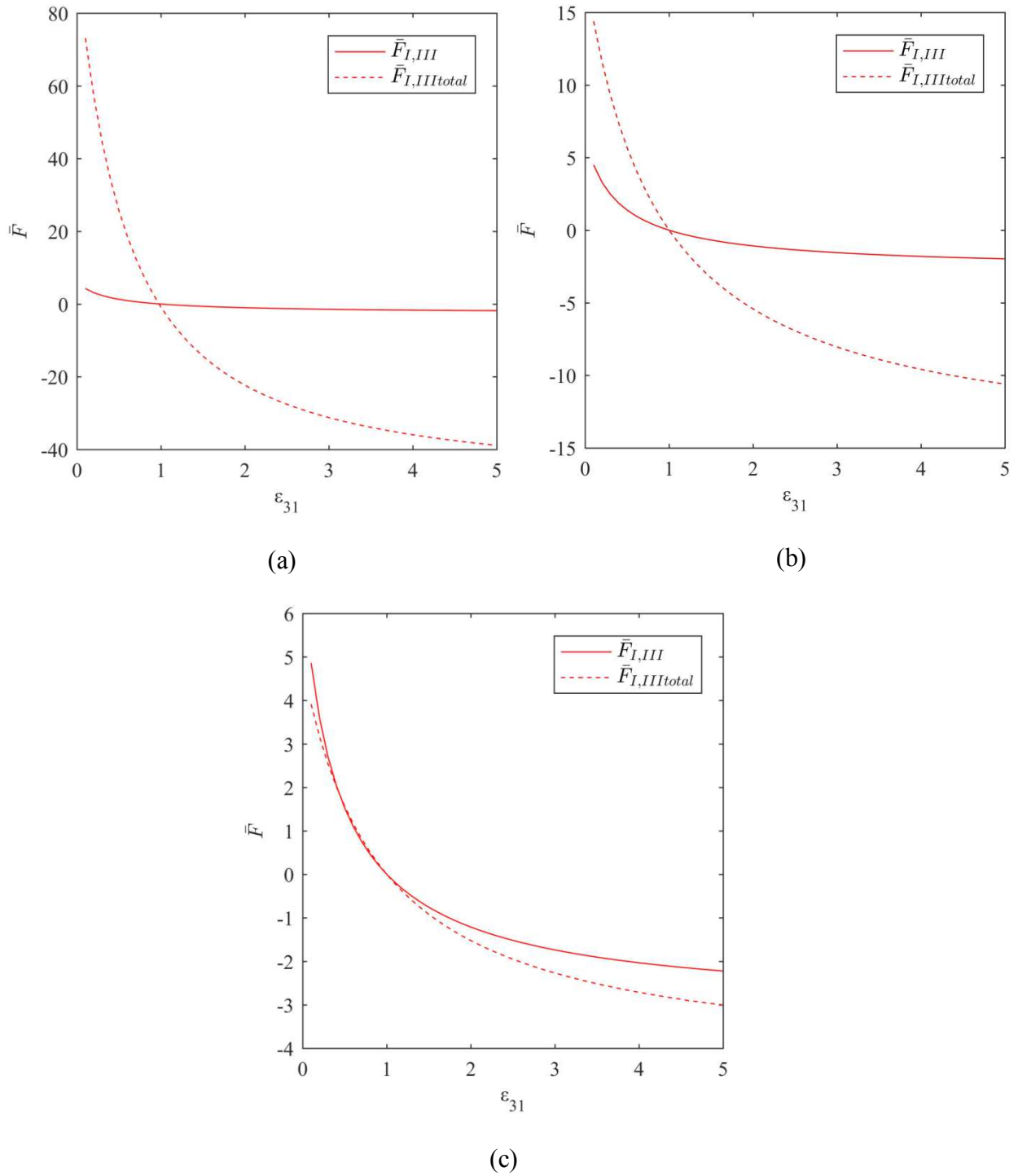


FIGURE 6.7: Normalized total surface force on the upper interface due to a single charge (solid line) and a pair of charges (dashed line). (a) $\bar{d} = 0.1$, (b) $\bar{d} = 0.2$, (c) $\bar{d} = 0.3$. For all cases, $\varepsilon_{21} = 0.1$.

To discuss the total surface force on the lower interface, the trend of $\bar{F}_{I,II\text{ total}}$ in Fig. 6.6 is found more interesting. While similar to $\bar{F}_{I,III\text{ total}}$ for $\bar{d} = 0.4$, the change of $\bar{F}_{I,II\text{ total}}$ with ε_{31} is more gradual in the case of a pair of charges (supported by the results of $\bar{f}_{z,I,II\text{ total}}$ in Fig. 6.2(b) where the curves for different ε_{31} almost coincide with one another), the trend of $\bar{F}_{I,II}$ vs. ε_{31} can be reversed (from decreasing with ε_{31} to increasing with ε_{31} , or vice versa) when an extra charge is introduced. This interesting phenomenon is investigated by examining more closely the results of $\bar{f}_{z,I,II\text{ total}}$ in Fig. 6.2. For better comparison, $\bar{f}_{z,I,II}$ and $\bar{f}_{z,I,II\text{ total}}$ are re-produced in Fig. 6.8 with a shorter range of \bar{r} .

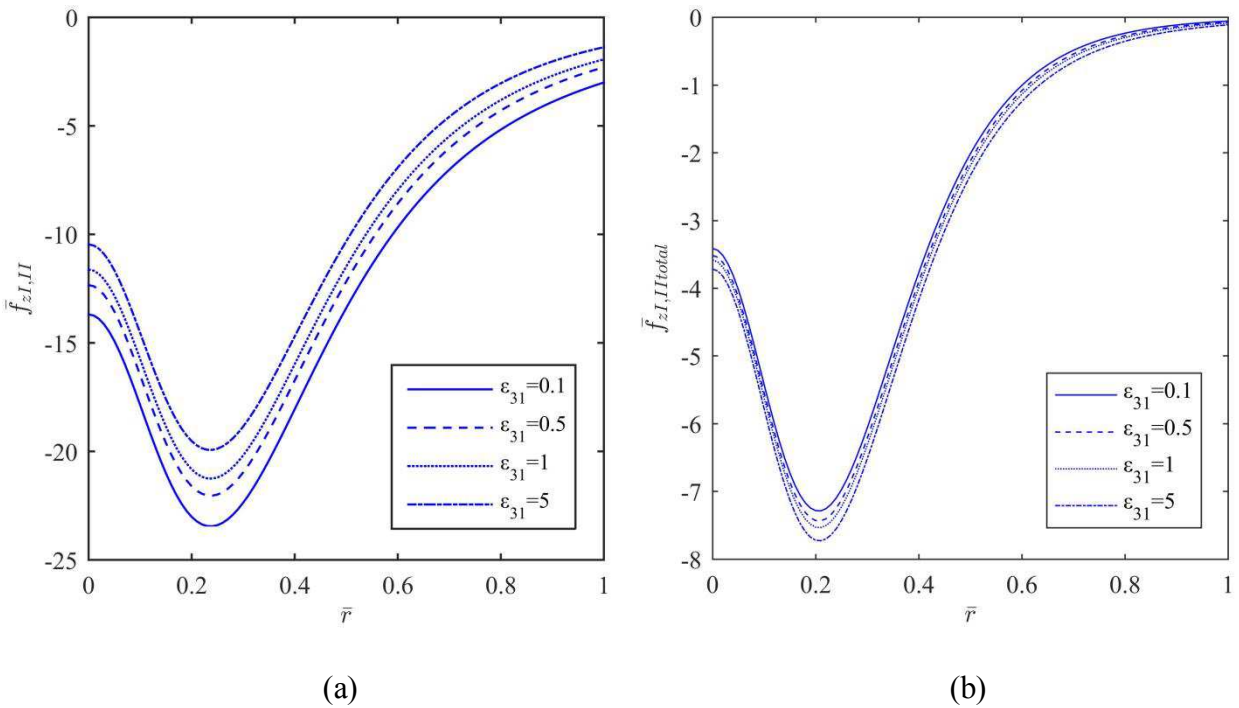


FIGURE 6.8: Normalized surface force density on the lower interface. (a) a single charge, (b) a pair of charges. For each subfigure, $\bar{d} = 0.4$, $\varepsilon_{21} = 0.1$ and ε_{31} varies from 0.1 to 5 (see legend for different line styles used for different ε_{31}).

$\bar{f}_{z\ I,II}$ and $\bar{f}_{z\ I,II\ total}$ are plotted as a function of \bar{r} in Fig. 6.8(a) and in Fig. 6.8(b), respectively, where $\bar{d} = 0.4$, $\varepsilon_{21} = 0.1$ and ε_{31} varies from 0.1 to 5. It is clear that at any given \bar{r} as ε_{31} increases the magnitude of $\bar{f}_{z\ I,II}$ reduces while the corresponding $\bar{f}_{z\ I,II\ total}$ increases. Physically, the increase of ε_{31} introduces a screening effect on the electric field of both $+q$ and $-q$ charges. However, because the $-q$ charge is closer to the upper interface, the increase of ε_{31} (ratio of dielectric constants between upper and middle regions) has more impact on the electric field of $-q$. Therefore, as ε_{31} increases the partial compensation by the $-q$ charge for the electric field on the lower interface is reduced and hence $\bar{f}_{z\ I,II\ total}$ increases. This is why $\bar{F}_{I,II\ total}$ also increases with ε_{31} in Fig. 6.6. To further justify this phenomenon and to study the influence of charge location on $\bar{F}_{I,II\ total}$, $\bar{F}_{I,II}$ and $\bar{F}_{I,II\ total}$ are plotted as functions of ε_{31} in Fig. 6.9 where \bar{d} varies from 0.1 to 0.3. The other dielectric constant ratio remains the same as in Fig. 6.6(a) i.e. $\varepsilon_{21} = 0.1$. Therefore, in Fig. 6.9, the charges are considered closer to the interfaces than in Fig. 6.6(a). The solid blue line corresponds to the total surface force on the lower interface due to a single charge while the dashed line represents the force induced by a pair of charges.

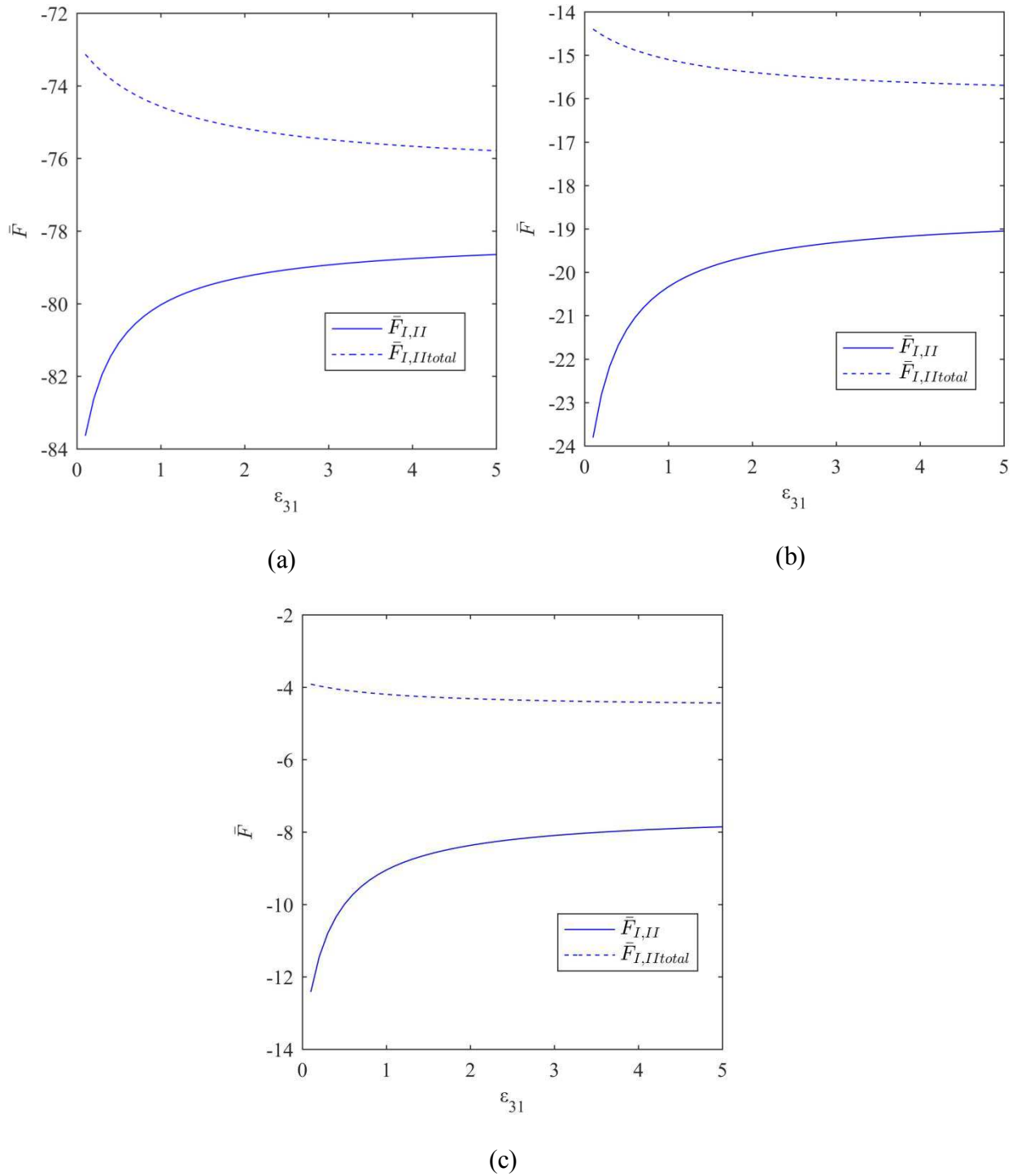


FIGURE 6.9: Normalized total surface force on the lower interface due to a single charge (solid line) and a pair of charges (dashed line). (a) $\bar{d} = 0.1$, (b) $\bar{d} = 0.2$, (c) $\bar{d} = 0.3$. For all cases, $\epsilon_{21} = 0.1$.

It is clear from the subfigures that the magnitude of $\bar{F}_{I,II \text{ total}}$ increases with ϵ_{31} while that of $\bar{F}_{I,II}$ decreases for all values of \bar{d} , similar to Fig. 6.6. Moreover, the magnitude of $\bar{F}_{I,II \text{ total}}$ is always smaller than that of $\bar{F}_{I,II}$. Unlike the upper interface, the additional charge causes only partial compensation of the electric field on the lower interface induced by the $+q$ charge, regardless of the charge positions and hence it results in smaller $\bar{F}_{I,II \text{ total}}$ for the entire range of ϵ_{31} .

Chapter 7

CONCLUSIONS AND FUTURE WORK

An analytical model to calculate the local surface force density and total surface force between two dielectric half-spaces with a dielectric gap has been established in this work. The surface forces are due to the electric field induced by a point charge in the dielectric gap. To calculate these forces, first the electric potential due to the single point charge in that multilayered dielectric system is obtained in closed form from which the electric field in all regions is derived. The electric potential is determined by solving the linear Laplace equation where the technique of Hankel transformation is used. It is found that the mathematical convenience of using Hankel transformation, as compared to the more commonly used image charge method, to solve the axisymmetric electrostatic problem is evident: it easily converts the boundary value problem into a set of initial value problems, which can be readily solved. Nondimensionalization of the solution reveals three dimensionless parameters that govern the normalized electric potential: \bar{d} , ε_{21} and ε_{31} . A parametric study was performed to demonstrate the influence of these parameters. The results show that the electric potential, and hence the electric field, in the system can be modulated, both quantitatively and qualitatively, by adjusting the governing parameters.

Based on the solution of the electric potential, the normalized surface force density, \bar{f}_z and the normalized total surface force, \bar{F} are calculated using the Maxwell Stress Tensor. Furthermore, the three dimensionless parameters: \bar{d} , ε_{21} and ε_{31} which influence the surface force density and the total surface force are analyzed and discussed in detail. It reveals from the solution

of \bar{f}_z that it always points towards the lower dielectric constant region irrespective of the charge location between the two interfaces. More interestingly, the trend of \bar{f}_z can be monotonic or non-monotonic with the radial position, depending on the dielectric constant ratios. Specifically, for high values of ε_{21} and ε_{31} , the trend of \bar{f}_z is governed by the z -component of the electric field, and hence it shows monotonic changes, whereas for smaller dielectric constant ratios the r -component of the electric field has significant impact on \bar{f}_z and causes \bar{f}_z to be non-monotonic. The overall influence of the dielectric constant ratios on the magnitude and sign are found similar for both \bar{f}_z and \bar{F} . Like \bar{f}_z , \bar{F} always act in the direction from the higher dielectric constant region towards the lower dielectric constant region. On the other hand, the parametric analysis of \bar{d} shows that it only plays the role of changing the magnitudes of \bar{F} and not direction. Finally, these analyses support that the surface force density and the total surface force can be manipulated, quantitatively and qualitatively, by adjusting the dielectric materials as well as the location of the point charge embedded in the dielectric gap of the multilayered system.

Lastly, the problem is extended by introducing an extra charge with opposite sign and equal magnitude to demonstrate the formulation for a distribution of charges. The comparative study with the single charge problem reveals interesting influence of the pair charges. While the surface force density on the lower interface $\bar{f}_{z \text{ I,II total}}$ is found smaller for all \bar{r} due to the partial compensation of the electric field introduced by the new charge, $\bar{f}_{z \text{ I,III total}}$ on the upper interface is found higher (over-compensation) for small \bar{r} and smaller for large \bar{r} (partial compensation). The charge location is again observed to only alter the magnitude of $\bar{f}_{z \text{ I,II total}}$ and $\bar{f}_{z \text{ I,III total}}$. The total surface force $\bar{F}_{\text{I,II total}}$ and $\bar{F}_{\text{I,III total}}$ due to the pair of charges maintain the same trend and

direction as that of the single charge regardless of the charge location. However, the effect of charge location on the magnitude of $\bar{F}_{I,III \text{ total}}$ is significant as $\bar{F}_{I,III \text{ total}}$ can be higher than that of the single charge when the charges are near the interfaces and smaller when they shift further from the interfaces. On the other hand, the magnitude of $\bar{F}_{I,II \text{ total}}$ is always smaller than the single charge values for all charge locations. Different combinations of the dielectric constant ratios show that the trend of $\bar{F}_{I,III \text{ total}}$ vs. ϵ_{31} does not change from that of the single point charge where the trend of $\bar{F}_{I,II \text{ total}}$ is reversed due to the extra charge. These comparisons give the idea about the impact of an opposite and equal charge in the multilayered dielectric model as it may increase or decrease the surface force density and total surface force depending on three non-dimensional parameters: the charge location and two dielectric constant ratios.

The established formulation of the surface forces due to a pair of charges can be applied to solve problems that involve adhesive forces between two surfaces with a mosaic distribution of charges. For example, using the solution of the electric potential for the pair of charges model, the interaction force can be calculated between two mosaics of charge where positively charged patches on one side are accompanied by their complementary negatively charged patches on the other side. Future work could also include determining the physical deformation of the materials on the interfaces by solving the deformation field with appropriate boundary conditions caused by the interfacial forces. Finally, experimental work could be done using different dielectric materials in a multilayered system to verify the influence of the dielectric constants on the surface forces as well as use the analytical model to measure the adhesion energies.

BIBLIOGRAPHY

- [1] M.-J. Pan and C. A. Randall, "A brief introduction to ceramic capacitors," *Electr. Insul. Mag. IEEE*, vol. 26, no. 3, pp. 44–50, 2010.
- [2] P. Jain and E. J. Rymaszewski, "Embedded thin film capacitors-theoretical limits," *IEEE Trans. Adv. Packag.*, vol. 25, no. 3, pp. 454–458, 2002.
- [3] G. Ribes, J. Mitard, M. Denais, S. Bruyere, F. Monsieur, C. Parthasarathy, E. Vincent, and G. Ghibaudo, "Review on high- k dielectrics reliability issues," *IEEE Trans. Device Mater. Reliab.*, vol. 5, no. 1, pp. 5–19, 2005.
- [4] W.-C. Shih, C.-H. Cheng, J. Y.-M. Lee, and F.-C. Chiu, "Charge-trapping devices using multilayered dielectrics for nonvolatile memory applications," *Adv. Mater. Sci. Eng.*, vol. 2013, pp. 2–7, 2013.
- [5] E. Tuncer, "Layered binary-dielectrics for energy applications: Limitations and potentials," *Curr. Appl. Phys.*, vol. 12, no. 1, pp. 337–340, 2012.
- [6] H. A. Wheeler, "Transmission-line properties of parallel strips separated by a dielectric sheet," *IEEE Trans. Microw. Theory Tech.*, vol. 13, no. 2, pp. 172–185, 1965.
- [7] H. R. Kaupp, "Characteristics of microstrip transmission lines," *IEEE Transactions on Electronic Computers*, vol. EC-16, no. 2, pp. 185-193, 1967.
- [8] T. G. Bryant and J. A. Weiss, "Parameters of microstrip transmission lines and of coupled pairs of microstrip lines," *IEEE Trans. Microw. Theory Tech.*, vol. 16, no. 12, pp. 1021–1027, 1968.

- [9] C. Wei, R. F. Harrington, J. R. Mautz, and T. K. Sarkar, "Multiconductor transmission lines in multilayered dielectric media," *IEEE Trans. Microw. Theory Tech.*, vol. 32, no. 4, pp. 439–449, 1984.
- [10] R. Crampagne, M. Ahmadpanah, and J. L. Guiraud, "A simple method for determining the Green's function for a large class of MIC lines having multilayered dielectric structures," *IEEE Trans. Microw. Theory Tech.*, vol. 26, no. 2, pp. 82–87, 1978.
- [11] P. Silvester, "TEM wave properties of microstrip transmission lines," *Electr. Eng. Proc. Inst.*, vol. 115, no. 1, pp. 43–48, 1968.
- [12] E. Smith and R.-S. Chang, "Microstrip transmission line with finite-width dielectric," *IEEE Trans. Microw. Theory Tech.*, vol. 28, no. 2, pp. 90–94, 1980.
- [13] S. J. Woo and T. Higuchi, "Electric field and force modeling for electrostatic levitation of lossy dielectric plates," *J. Appl. Phys.*, vol. 108, no. 10, p. 104906, 2010.
- [14] T. Watanabe and T. Kitabayashi, "Effect of additives on the electrostatic force of Alumina electrostatic chucks," *J. Ceramic Soc. Jpn.*, vol. 100, no. 1, pp. 1-6, 1992.
- [15] D. R. Wright, L. Chen, P. Federlin, and K. Forbes, "Manufacturing issues of electrostatic chucks," *J. Vac. Sci. Technol. B*, vol. 13, no. 4, pp. 1910–1916, 1995.
- [16] J. F. Daviet, L. Peccoud, and F. Mondon, "Electrostatic clamping applied to semiconductor plasma processing I. Theoretical modeling," *J. Electrochem. Soc.*, vol. 140, no. 11, pp. 3245–3256, 1993.
- [17] K. Asano, F. Hatakeyama, and K. Yatsuzuka, "Fundamental study of an electrostatic chuck for silicon wafer handling," *IEEE Trans. Ind. Appl.*, vol. 38, no. 3, pp. 840–845,

- 2002.
- [18] G. Kalkowski, S. Risse, G. Harnisch, and V. Guyenot “Electrostatic chucks for lithography applications,” *Microelectron. Eng.*, vol. 57–58, pp. 219–222, 2001.
- [19] A. Yamamoto, T. Nakashima, and T. Higuchi, “Wall climbing mechanisms using electrostatic attraction generated by flexible electrodes,” *Micro-NanoMechatronics and Human Science, 2007. MHS '07. International Symposium on*, Nagoya, 2007, pp. 389-394.
- [20] H. Prahlad, R. Pelrine, S. Stanford, J. Marlow, and R. Kornbluh, “Electroadhesive robots - Wall climbing robots enabled by a novel, robust, and electrically controllable adhesion technology,” *2008 IEEE Int. Conf. Robot. Autom.*, pp. 3028–3033, 2008.
- [21] S. Wu, M. Li, S. Xiao, and Y. Li, “A wireless distributed wall climbing robotic system for reconnaissance purpose,” *2006 IEEE Int. Conf. Mechatronics Autom.*, pp. 1308-1312, 2006.
- [22] H. Zhang, J. Zhang, W. Wang, R. Liu, and G. Zong, “A series of pneumatic glass-wall cleaning robots for high-rise buildings,” *Ind. Robot An Int. J.*, vol. 34, no. 2, pp. 150–160, 2007.
- [23] D. Santos, S. Kim, M. Spenko, A. Parness, and M. Cutkosky, “Directional adhesive structures for controlled climbing on smooth vertical surfaces,” *2007 IEEE Int. Conf. Robot. Autom.*, pp. 1262–1267, 2007.
- [24] A. T. Asbeck, S. Kim, A. McClung, A. Parness, and M. R. Cutkosky, “Climbing walls with microspines,” *2006 IEEE Int. Conf. Robot. Autom.*, pp. 4315–4317, 2006.
- [25] L. P. Kalra and J. Gu, “An autonomous self contained wall climbing robot for non-

- destructive inspection of above-ground storage tanks,” *Ind. Robot An Int. J.*, vol. 34, no. 2, pp. 122–127, 2007.
- [26] R. Liu, R. Chen, H. Shen, and R. Zhang, “Wall climbing robot using electrostatic adhesion force generated by flexible interdigital electrodes,” *Int. J. Adv. Robot. Syst.*, vol. 10, no. 36, pp. 1-9, 2013.
- [27] J. Mao, L. Qin, and W. Zhang, “Modelling and simulation of electrostatic adhesion force in concentric-ring electrode structures of multilayer dielectrics,” *J. Adhes.*, vol. 92, no. 4, pp. 319-340, 2016.
- [28] K.-T. Wan, D. T. Smith, and B. R. Lawn, “Fracture and contact adhesion energies of Mica-Mica, Silica-Silica, and Mica-Silica interfaces in dry and moist atmospheres,” *J. Am. Ceram. Soc.*, vol. 75, no. 3, pp. 667–676, 1992.
- [29] K. Brörmann, K. Burger, A. Jagota, and R. Bennewitz, “Discharge during detachment of micro-structured PDMS sheds light on the role of electrostatics in adhesion,” *J. Adhes.*, vol. 88, no. 7, pp. 589–607, 2012.
- [30] J. Lowell and A. C. Rose-Innes, “Contact electrification,” *Adv. Phys.*, vol. 29, no. 6, pp. 947–1023, 1980.
- [31] H. T. Baytekin, A. Z. Patashinski, M. Branicki, B. Baytekin, S. Soh, and B. A. Grzybowski, “The mosaic of surface charge in contact electrification,” *Science*, vol. 333, no. 6040, pp. 308–312, 2011.
- [32] J. Lowell and W. S. Truscott, “Triboelectrification of identical insulators: I. An experimental investigation,” *J. Phys. D: Appl. Phys.*, vol. 19, no. 7, pp. 1273–1280, 1986.

- [33] B. V. Derjaguin, Ju. P. Toporov, I. N. Aleinikova, and L. N. Burta-Gapanovitch, "Investigation on the adhesion of polymer particles to the surface of a semiconductor," *J. Adhes.*, vol. 4, no. 1, pp. 65-71, 1972.
- [34] R. Pham, R. C. Virnelson, R. M. Sankaran, and D. J. Lacks, "Contact charging between surfaces of identical insulating materials in asymmetric geometries," *J. Electrostat.*, vol. 69, no. 5, pp. 456–460, 2011.
- [35] D. J. Lacks and A. Levandovsky, "Effect of particle size distribution on the polarity of triboelectric charging in granular insulator systems," *J. Electrostat.*, vol. 65, no. 2, pp. 107–112, 2007.
- [36] Z. Xu, "Electrostatic interaction in the presence of dielectric interfaces and polarization-induced like-charge attraction," *Phys. Rev. E*, vol. 87, no. 1, 2013.
- [37] A. Farrar and A. T. Adams, "Characteristic impedance of microstrip by the method of moments," *IEEE Trans. Microw. Theory Tech.*, vol. 18, no. 1, pp. 65–66, 1970.
- [38] E. Yamashita and K. Atsuki, "Strip line with rectangular outer conductor and three dielectric layers," *IEEE Trans. Microw. Theory Tech.*, vol. 18, no. 5, pp. 238–244, 1970.
- [39] J. Pumplin, "Application of Sommerfeld-Watson transformation to an electrostatics problem," *Am. J. Phys.*, vol. 37, no. 7, pp. 737-739, 1969.
- [40] O. Pronic, V. Markovic, and B. Milovanovic, "Numerically efficient Green's function for planar structures on multilayered dielectric in cylindrical enclosure," *COMPEL Int. J. Comput. Math. Electr. Electron. Eng.*, vol. 20, no. 4, pp. 1055–1070, 2001.
- [41] J. C.-E. Sten and R. Ilmoniemi, "Image theory for a point charge inside a layered

- dielectric sphere,” *Arch. für Elektrotechnik*, vol. 77, no. 5, pp. 327–335, 1994.
- [42] T. Heubrandtner, B. Schnizer, C. Lippmann, and W. Riegler, “Static electric fields in an infinite plane condenser with one or three homogeneous layers,” *Nucl. Instruments Methods Phys. Res. Sect. A: Accel., Spectrometers, Detect. Assoc. Equi.*, vol. 489, no. 1–3, pp. 439–443, 2002.
- [43] R. G. Barrera, O. Guzman, and B. Balaguer, “Point charge in a three-dielectric medium with planar interfaces,” *Am. J. Phys.*, vol. 46, no. 11, pp. 1172–1179, 1978.
- [44] F. M. Pont and P. Serra, “Comment on: ‘Point charge in a three-dielectric medium with planar interfaces’ [Am. J. Phys. 46, 1172–1179 (1978)],” *Am. J. Phys.*, vol. 83, no. 5, pp. 475–476, 2015.
- [45] W. K. H. Panofsky and M. Phillips, *Classical electricity and magnetism*, 2nd ed. Massachusetts: Addison-Wesley Pub. Co., 1962.
- [46] L. D. Landau and E. M. Lifshitz, *Electrodynamics of continuous media (Course of Theoretical Physics Vol.8)*, 1st ed. New York: Pergamon Press, 1960.
- [47] R. Piessens, “The Hankel Transform,” in *The Transforms and Applications Handbook*, A. D. Poularikas, Ed., 2nd ed. Boca Raton: CRC Press LLC, 2000.
- [48] A. Erdelyi (Ed.), *Tables of Integral Transforms*, Bateman Manuscript Project, vol. II, McGraw-Hill, New York, 1954.
- [49] J. D. Jackson, *Classical Electrodynamics*, 3rd ed. New York: John Wiley & Sons, 1999.
- [50] H. H. Woodson *et al.*, “Field Description of Magnetic and Electric Forces,” in *Electromechanical Dynamics*, Massachusetts Institute of Technology: MIT

OpenCourseWare.

- [51] A. Farrar and A. T. Adams, “Multilayer microstrip transmission lines (Short Papers),” *IEEE Trans. Microw. Theory Tech.*, vol. 22, no. 10, pp. 889–891, 1974.

APPENDIX

MATLAB codes

1. Main Functions

- a. The following codes calculate $\bar{\phi}_I$, $\bar{\phi}_{II}$ and $\bar{\phi}_{III}$ given a particular set of parameters: \bar{d} , ϵ_{21} , ϵ_{31} . Varying one of the parameters generates the dependence of electric potential on this parameter, as shown in the plots in Chapter 5.

Solve the Electric Potential due to a single charge

```
% A single point charge in a three-layered dielectric system;  
% The charge is located at (0, d);  
% The coordinates are r and z normalized by H, i.e., the charge is now  
% located at (r=0, z=(d/H));  
% Potential is normalized by q/(4*pi*eps0*eps1*H);  
% rho is normalized by 1/H;  
  
clear;  
clc;
```

Parameters

```
H=1.0;    % gap between two interfaces  
d=0.5;    % distance between the point charge and the lower interface  
e21=10;   % dielectric constant ratio between the lower and middle regions  
e31=10;   % dielectric constant ratio between the upper and middle regions  
N=50;    % number of steps for integration  
lbd=0;    % lower limit of integration
```

Mesh generation (Upper region)

```
[x1,z1] = meshgrid(-2.2:0.1:2.2, H:0.1:2);  
r1 = abs(x1);  
s1 = size(r1);
```

Calculate electric potential in the upper region

```
for i = 1 : s1(1)  
    for j = 1 : s1(2)
```

```

        phi_1(i,j) = 2 * quad1(@fundcupH, lbd, N, [], [], r1(i,j), z1(i,j), d, e21, e31);
    end
end

```

Mesh generation (Lower region)

```

[x2,z2] = meshgrid(-2.2:0.1:2.2, -1.5:0.1:0);
r2 = abs(x2);
s2 = size(r2);

```

Calculate electric potential in the lower region

```

for i = 1 : s2(1)
    for j = 1 : s2(2)
        phi_2(i,j) = 2 * quad1(@fundc1rH, lbd, N, [], [], r2(i,j), z2(i,j), d, e21, e31);
    end
end

```

Mesh generation (Middle region)

```

[x3,z3] = meshgrid(-2.2:0.1:2.2, 0:0.1:H);
r3 = abs(x3);
s3 = size(r3);

```

Calculate electric potential in the middle region

```

for i = 1 : s3(1)
    for j = 1 : s3(2)
        phi_0(i,j) = 1/(sqrt((r3(i,j)).^2+(z3(i,j)-d).^2));
        sum = 2 * quad1(@fundcmid1H, lbd, N, [], [], r3(i,j), z3(i,j), d, e21, e31) + 2 *
quad1(@fundcmid2H, lbd, N, [], [], r3(i,j), z3(i,j), d, e21, e31) - quad1(@fundcmid3H, lbd, N,
[], [], r3(i,j), z3(i,j), d);
        phi_3(i,j) = phi_0(i,j) + sum;
    end
end

```

Contour plot of the electric potential distribution

```

figure;
a = [-2.2 2.2];
b = [0 0];
f = [1 1];
plot(a,b,'--');
set(gca, 'FontSize',16, 'FontName', 'Times New Roman');
hold on
plot(a,f,'--');

```

```

% plot of electric potential in the upper region

[c,m] = contour(x1, z1, phi_1, 'k');
set(m, 'LevelList', [0.1 0.3 0.8 1.3 1.8 2.3 2.8 3.3 3.8 4.3 4.8]);
clabel(c, m, 'FontSize',8, 'LabelSpacing', 400);
xlabel('\it x / H','FontName', 'Times New Roman'); ylabel('\it z / H','FontName','Times New Roman');
axis equal tight;
hold on

% plot of electric potential in the lower region

[c,m] = contour(x2, z2, phi_2, 'k');
set(m, 'LevelList', [0.1 0.3 0.8 1.3 1.8 2.3 2.8 3.3 3.8 4.3 4.8]);
clabel(c, m, 'FontSize',8, 'LabelSpacing', 400);
axis equal tight;

% plot of electric potential in the middle region

[c,m] = contour(x3, z3, phi_3, 'k');
set(m, 'LevelList', [0.1 0.3 0.8 1.3 1.8 2.3 2.8 3.3 3.8 4.3 4.8],
'TextList', [0.3 0.8 1.3 1.8 2.3]);
clabel(c, m, 'FontSize',8, 'LabelSpacing', 200);
axis equal tight;

```

b. The following codes generate $\bar{\phi}$ at three spatial points: $P_1(1, 0.5)$, $P_2(0, -0.5)$ and $P_3(0, 1.5)$

for varying ε_{21} given a particular set of parameters: \bar{d} , ε_{31} .

Solve the Electric Potential at three spatial points

```

clear;
clc;

```

Parameters

```

H=1.0; % gap between two interfaces
d=0.5; % distance between the point charge and the lower interface
e21=0.1:0.1:20; % varying dielectric constant ratio between the lower and middle regions
e31=10; % dielectric constant ratio between the upper and middle regions
N=50; % number of steps for integration
lbd=0; % lower limit of integration

```

Locations of spatial points

```
% P_3
x1=0;
z1=1.5;

% P_2
x2=0;
z2=-0.5;

% P_1
x3=1;
z3=0.5;
```

Calculate electric potential

```
s=length(e21);

for i = 1 : s
    phi_up(i) = 2 * quadl(@fundcupH, lbd, N, [], [], x1, z1, d, e21(i), e31);
    phi_low(i) = 2 * quadl(@fundc1rH, lbd, N, [], [], x2, z2, d, e21(i), e31);
    phi_0(i) = 1/(sqrt(x3.^2+(z3-d).^2));
    sum = 2 * quadl(@fundcmid1H, lbd, N, [], [], x3, z3, d, e21(i), e31) + 2 * quadl(@fundcmid2H,
lbd, N, [], [], x3, z3, d, e21(i), e31) - quadl(@fundcmid3H, lbd, N, [], [], x3, z3, d);
    phi_mid(i) = phi_0(i) + sum;
end
```

Plot of electric potentials at P₁, P₂ and P₃

```
fig1=figure(1);
plot(e21,phi_mid,'k--',e21,phi_low,'k-',e21,phi_up,'k:');

set(gca,'FontSize',16,'FontName','Times New Roman');
xlabel(['\it',char(949),'_{21}'],'FontWeight','bold','interpreter','tex','FontSize',
16,'FontName','Times New Roman');
ylabel(['\it $\bar{\phi}$'],'FontWeight','bold','interpreter','latex','FontSize',
16,'FontName','Times New Roman');
legend({'$P_{1}$equiv(1,0.5)$','$P_{2}$equiv(0,-
0.5)$','$P_{3}$equiv(0,1.5)$'],'Interpreter','latex');
```

- c. The following codes calculate $\bar{f}_{z,II}$ and $\bar{f}_{z,III}$ for a single point charge given a particular set of parameters: \bar{d} , ϵ_{21} , ϵ_{31} . Varying one of the parameters generates the dependence of surface force density on this parameter, as shown in the plots in Chapter 5.

Solve the Surface force density due to a single charge

```
% A single point charge in a three-layered dielectric system;
% The charge is located at (0, d);
% The coordinates are r and z normalized by H, i.e., the charge is now
% located at (r=0, z=(d/H));
% Surface force density is normalized by  $q^2/(32*\pi^2*\epsilon_0*\epsilon_1*H^4)$ ;
% rho is normalized by 1/H;

clear;
clc;
```

Parameters

```
d=0.5; % distance between the point charge and the lower interface
e21=0.1; % dielectric constant ratio between the lower and middle regions
e31=[0.1;0.5;1;5]; % varying dielectric constant ratio between the upper and middle regions
n=50; % number of steps for integration
del_r=0.01; % discretization of radius
r = 0:del_r:4; % range of radius
s = length(r);
t = length(e31);
```

Calculate surface force density

```
for i = 1 : t
    for j = 1 : s

        ez_up(i,j) = (1-d)/((r(j).^2+(1-d).^2).^(3/2));
        er_up(i,j) = r(j)/((r(j).^2+(1-d).^2).^(3/2));

        ez_3(i,j) = 2.*quadl(@funefupH1, 0, n, [], [], r(j), d, e21, e31(i));
        er_3(i,j) = 2.*quadl(@funefupH2, 0, n, [], [], r(j), d, e21, e31(i));

        ez_1(i,j) = ez_up(i,j) - 2.*quadl(@funefmidH11, 0, n, [], [], r(j), d, e21, e31(i)) +
        2.*quadl(@funefmidH12, 0, n, [], [], r(j), d, e21, e31(i)) + quadl(@funefmidH13, 0, n, [], [],
        r(j), d);
        er_1(i,j) = er_up(i,j) + 2.*quadl(@funefmidH21, 0, n, [], [], r(j), d, e21, e31(i)) -
        quadl(@funefmidH22, 0, n, [], [], r(j), d);

        f_up(i,j) = (ez_3(i,j).^2 - er_3(i,j).^2).*e31(i) - (ez_1(i,j).^2 - er_1(i,j).^2); %
        surface force density on the upper interface

        ez_lr(i,j) = -d./((r(j).^2+d.^2).^(3/2));
        er_lr(i,j) = r(j)/((r(j).^2+d.^2).^(3/2));

        ez_2(i,j) = -2 * quadl(@funeflr1_H, 0, n, [], [], r(j), d, e21, e31(i));
        er_2(i,j) = 2 * quadl(@funeflr2_H, 0, n, [], [], r(j), d, e21, e31(i));

        ez_1(i,j) = ez_lr(i,j) - 2.*quadl(@funefmid21_H, 0, n, [], [], r(j), d, e21, e31(i)) +
```

```

2.*quadl(@funefmid22_H, 0, n, [], [], r(j), d, e21, e31(i)) + quadl(@funefmid23_H, 0, n, [], [],
r(j), d);
    er_1(i,j) = er_lr(i,j) + 2.*quadl(@funefmid11_H, 0, n, [], [], r(j), d, e21, e31(i)) -
quadl(@funefmid12_H, 0, n, [], [], r(j), d);

    f_lr(i,j) = (ez_1(i,j).^2 - er_1(i,j).^2) - (ez_2(i,j).^2 - er_2(i,j).^2).*e21; % surface
force density on the lower interface
end
end

```

Plot of surface force density

```

figure;

x=6:10;
y1=x+1;y2=x+2;y3=x+3;y4=x+4;
plot(x,y1,'-k',x,y2,'--k',x,y3,':k',x,y4,'-.k')
hold on
plot(r,f_up(1,:), '-r', r, f_up(2,:), '--r', r, f_up(3,:), ':r', r, f_up(4,:), '-.r')
plot(r,f_lr(1,:), '-b', r, f_lr(2,:), '--b', r, f_lr(3,:), ':b', r, f_lr(4,:), '-.b')
xlim([0 4]);
set(gca(), 'FontSize', 16, 'FontName', 'Times New Roman')
xlabel('\it $\bar{r}$', 'FontWeight', 'bold', 'interpreter', 'latex', 'FontSize',
16, 'FontName', 'Times New Roman');
ylabel('\it $\bar{f}_z$', 'FontWeight', 'bold', 'interpreter', 'latex', 'FontSize',
16, 'FontName', 'Times New Roman');
legend([char(949) '_{31}=0.1'], [char(949) '_{31}=0.5'], [char(949) '_{31}=1'], [char(949)
'_{31}=5']);
gtext('\it $\bar{f}_{zI,III}$', 'FontWeight', 'bold', 'interpreter', 'latex', 'FontSize',
16, 'FontName', 'Times New Roman')
gtext('\it $\bar{f}_{zI,II}$', 'FontWeight', 'bold', 'interpreter', 'latex', 'FontSize',
16, 'FontName', 'Times New Roman')

```

- d. The following codes calculate $\bar{F}_{I,II}$ and $\bar{F}_{I,III}$ for a single point charge given a particular set of parameters: \bar{d} , ϵ_{21} , ϵ_{31} . Varying one of the parameters generates the dependence of total surface force on this parameter, as shown in the plots in Chapter 5.

Solve the Total surface force due to a single charge

```

% A single point charge in a three-layered dielectric system;
% The charge is located at (0, d);
% The coordinates are r and z normalized by H, i.e., the charge is now
% located at (r=0, z=(d/H));
% Total force is normalized by q^2/(16*pi*eps0*eps1*H^2);

```

```
% rho is normalized by 1/H;
```

```
clear;  
clc;
```

Parameters

```
d=0.3;           % distance between the point charge and the lower interface  
e21=0.1;        % dielectric constant ratio between the lower and middle regions  
e31=0.1:0.1:5;  % varying dielectric constant ratio between the upper and middle regions  
n=50;          % number of steps for integration  
del_r=0.01;    % discretization of radius  
r1 = 0:del_r:10; % range of radius  
s1 = length(r1);  
t1 = length(e31);
```

Calculate total surface forces

```
for i = 1 : t1  
    for j = 1 : s1  
  
        ez_0_up(i,j) = (1-d)/((r1(j).^2+(1-d).^2).^3/2);  
        er_0_up(i,j) = r1(j)/((r1(j).^2+(1-d).^2).^3/2);  
  
        ez_3_up(i,j) = (2 * quadl(@funefupH1, 0, n, [], [], r1(j), d, e21, e31(i))).^2;  
        er_3_up(i,j) = (2 * quadl(@funefupH2, 0, n, [], [], r1(j), d, e21, e31(i))).^2;  
  
        ez_1_up(i,j) = (ez_0_up(i,j) - 2 * quadl(@funefmidH11, 0, n, [], [], r1(j), d, e21,  
e31(i)) + 2 * quadl(@funefmidH12, 0, n, [], [], r1(j), d, e21, e31(i)) + quadl(@funefmidH13, 0,  
n, [], [], r1(j), d)).^2;  
        er_1_up(i,j) = (er_0_up(i,j) + 2 * quadl(@funefmidH21, 0, n, [], [], r1(j), d, e21,  
e31(i)) - quadl(@funefmidH22, 0, n, [], [], r1(j), d)).^2;  
  
        fun_r_up(i,j) = ((ez_3_up(i,j) - er_3_up(i,j)).*e31(i) - (ez_1_up(i,j) -  
er_1_up(i,j))).*r1(j); % function for the upper interface  
  
        ez_0_lr(i,j) = -d/((r1(j).^2+d.^2).^3/2);  
        er_0_lr(i,j) = r1(j)/((r1(j).^2+d.^2).^3/2);  
  
        ez_2_lr(i,j) = (-2 * quadl(@funeflr1_H, 0, n, [], [], r1(j), d, e21, e31(i))).^2;  
        er_2_lr(i,j) = (2 * quadl(@funeflr2_H, 0, n, [], [], r1(j), d, e21, e31(i))).^2;  
  
        ez_1_lr(i,j) = (ez_0_lr(i,j) - 2 * quadl(@funefmid21_H, 0, n, [], [], r1(j), d, e21,  
e31(i)) + 2 * quadl(@funefmid22_H, 0, n, [], [], r1(j), d, e21, e31(i)) + quadl(@funefmid23_H, 0,  
n, [], [], r1(j), d)).^2;  
        er_1_lr(i,j) = (er_0_lr(i,j) + 2 * quadl(@funefmid11_H, 0, n, [], [], r1(j), d, e21,  
e31(i)) - quadl(@funefmid12_H, 0, n, [], [], r1(j),d)).^2;  
  
        fun_r_lr(i,j) = ((ez_1_lr(i,j) - er_1_lr(i,j)) - (ez_2_lr(i,j) -  
er_2_lr(i,j))).*e21).*r1(j); % function for the lower interface
```

```

end
end

for k=1:t1

    e_force1_up(k) = trapz(r1,fun_r_up(k,:)); % total surface force on the upper interface

    e_force1_lr(k) = trapz(r1,fun_r_lr(k,:)); % total surface force on the lower interface
end

```

Plot of total surface forces

```

set(gca(),'FontSize',16,'FontName','Times New Roman')
plot(e31,e_force1_up,e31,e_force1_lr)
xlabel([char(949) '_{31}'], 'FontSize', 16,'FontName','Times New Roman');
ylabel('\it $\bar{F}$', 'interpreter','latex','FontSize', 16,'FontName','Times New Roman');
legend({'\it $\bar{F}_{I,III}$', '\it
$\bar{F}_{I,II}$'}, 'FontWeight','bold','interpreter','latex','FontSize', 16,'FontName','Times New
Roman')

```

- e. The following codes calculate $\bar{f}_{z,I,II\text{ total}}$ and $\bar{f}_{z,I,III\text{ total}}$ for a pair of charges given a particular set of parameters: \bar{d} , ϵ_{21} , ϵ_{31} . Varying one of the parameters generates the dependence of surface force density on this parameter, as shown in the plots in Chapter 6.

Solve the Surface force density due to a pair of charges

```

% A pair of charges in the middle layer of a three-layered dielectric system;
% The positive charge is located at (0, d);
% The negative charge is located at (0, H-d);
% The coordinates are r and z normalized by H, i.e., the charges are now
% located at (r=0, z=(d/H)) and (r=0, z=(1-d/H)) respectively;
% Surface force density is normalized by q^2/(32*pi^2*eps0*eps1*H^4);
% rho is normalized by 1/H;

clear;
clc;

```

Parameters

```

dcharge=0.4;           % distance between the positive charge and the lower interface
e21=0.1;              % dielectric constant ratio between the lower and middle regions
e31=[0.1;0.5;1;5];   % varying dielectric constant ratio between the upper and middle regions
n=50;                % number of steps for integration
del_r=0.01;          % discretization of radius
r = 0:del_r:4;       % range of radius
s = length(r);
t = length(e31);

```

Calculate surface force density

```

for i = 1 : t
    for j = 1 : s

        % calculate electric fields on the upper interface
        % for positive charge

        d=dcharge; % location of the positive charge

        ez_up(i,j) = (1-d)/((r(j).^2+(1-d).^2).^(3/2));
        er_up(i,j) = r(j)/((r(j).^2+(1-d).^2).^(3/2));

        ez_3(i,j) = 2.*quadl(@funefupH1, 0, n, [], [], r(j), d, e21, e31(i));
        er_3(i,j) = 2.*quadl(@funefupH2, 0, n, [], [], r(j), d, e21, e31(i));

        ez_1_up(i,j) = ez_up(i,j) - 2.*quadl(@funefmidH11, 0, n, [], [], r(j), d, e21, e31(i)) +
        2.*quadl(@funefmidH12, 0, n, [], [], r(j), d, e21, e31(i)) + quadl(@funefmidH13, 0, n, [], [],
        r(j), d);
        er_1_up(i,j) = er_up(i,j) + 2.*quadl(@funefmidH21, 0, n, [], [], r(j), d, e21, e31(i)) -
        quadl(@funefmidH22, 0, n, [], [], r(j), d);

        ez_3_tot_up(i,j)=ez_3(i,j);
        er_3_tot_up(i,j)=er_3(i,j);
        ez_1_tot_up(i,j)=ez_1_up(i,j);
        er_1_tot_up(i,j)=er_1_up(i,j);

        % calculate electric fields on the upper interface
        % for negative charge

        d=1-dcharge; % location of the negative charge

        ez_up(i,j) = (1-d)/((r(j).^2+(1-d).^2).^(3/2));
        er_up(i,j) = r(j)/((r(j).^2+(1-d).^2).^(3/2));

        ez_3(i,j) = 2.*quadl(@funefupH1, 0, n, [], [], r(j), d, e21, e31(i));
        er_3(i,j) = 2.*quadl(@funefupH2, 0, n, [], [], r(j), d, e21, e31(i));

        ez_1_up(i,j) = ez_up(i,j) - 2.*quadl(@funefmidH11, 0, n, [], [], r(j), d, e21, e31(i)) +
        2.*quadl(@funefmidH12, 0, n, [], [], r(j), d, e21, e31(i)) + quadl(@funefmidH13, 0, n, [], [],
        r(j), d);
        er_1_up(i,j) = er_up(i,j) + 2.*quadl(@funefmidH21, 0, n, [], [], r(j), d, e21, e31(i)) -

```

```

quad1(@funefmidH22, 0, n, [], [], r(j), d);

ez_3_tot_up(i,j)=ez_3_tot_up(i,j)-ez_3(i,j);
er_3_tot_up(i,j)=er_3_tot_up(i,j)-er_3(i,j);
ez_1_tot_up(i,j)=ez_1_tot_up(i,j)-ez_1_up(i,j);
er_1_tot_up(i,j)=er_1_tot_up(i,j)-er_1_up(i,j);

f_up(i,j) = (ez_3_tot_up(i,j).^2 - er_3_tot_up(i,j).^2).*e31(i) - (ez_1_tot_up(i,j).^2 -
er_1_tot_up(i,j).^2); % surface force density on the upper interface

% calculate electric fields on the lower interface
% for positive charge

d=dcharge; % location of the positive charge

ez_lr(i,j) = -d./((r(j).^2+d.^2).^3/2);
er_lr(i,j) = r(j)./((r(j).^2+d.^2).^3/2);

ez_2(i,j) = -2 * quad1(@funeflr1_H, 0, n, [], [], r(j), d, e21, e31(i));
er_2(i,j) = 2 * quad1(@funeflr2_H, 0, n, [], [], r(j), d, e21, e31(i));

ez_1_lr(i,j) = ez_lr(i,j) - 2.*quad1(@funefmid21_H, 0, n, [], [], r(j), d, e21, e31(i)) +
2.*quad1(@funefmid22_H, 0, n, [], [], r(j), d, e21, e31(i)) + quad1(@funefmid23_H, 0, n, [], [],
r(j), d);
er_1_lr(i,j) = er_lr(i,j) + 2.*quad1(@funefmid11_H, 0, n, [], [], r(j), d, e21, e31(i)) -
quad1(@funefmid12_H, 0, n, [], [], r(j), d);

ez_2_tot_lr(i,j)=ez_2(i,j);
er_2_tot_lr(i,j)=er_2(i,j);
ez_1_tot_lr(i,j)=ez_1_lr(i,j);
er_1_tot_lr(i,j)=er_1_lr(i,j);

% calculate electric fields on the upper interface
% for negative charge

d=1-dcharge; % location of the negative charge

ez_lr(i,j) = -d./((r(j).^2+d.^2).^3/2);
er_lr(i,j) = r(j)./((r(j).^2+d.^2).^3/2);

ez_2(i,j) = -2 * quad1(@funeflr1_H, 0, n, [], [], r(j), d, e21, e31(i));
er_2(i,j) = 2 * quad1(@funeflr2_H, 0, n, [], [], r(j), d, e21, e31(i));

ez_1_lr(i,j) = ez_lr(i,j) - 2.*quad1(@funefmid21_H, 0, n, [], [], r(j), d, e21, e31(i)) +
2.*quad1(@funefmid22_H, 0, n, [], [], r(j), d, e21, e31(i)) + quad1(@funefmid23_H, 0, n, [], [],
r(j), d);
er_1_lr(i,j) = er_lr(i,j) + 2.*quad1(@funefmid11_H, 0, n, [], [], r(j), d, e21, e31(i)) -
quad1(@funefmid12_H, 0, n, [], [], r(j), d);

ez_2_tot_lr(i,j)=ez_2_tot_lr(i,j)-ez_2(i,j);
er_2_tot_lr(i,j)=er_2_tot_lr(i,j)-er_2(i,j);
ez_1_tot_lr(i,j)=ez_1_tot_lr(i,j)-ez_1_lr(i,j);
er_1_tot_lr(i,j)=er_1_tot_lr(i,j)-er_1_lr(i,j);

```

```

        f_lr(i,j) = (ez_1_tot_lr(i,j).^2 - er_1_tot_lr(i,j).^2) - (ez_2_tot_lr(i,j).^2 -
er_2_tot_lr(i,j).^2).*e21; % surface force density on the lower interface
    end
end

```

Plot of surface force density due to a pair of charges

```

figure;

x=6:10;
y1=x+1;y2=x+2;y3=x+3;y4=x+4;
plot(x,y1,'-k',x,y2,'--k',x,y3,':k',x,y4,'-.k')
hold on
plot(r,f_up(1,:), '-r', r, f_up(2,:), '--r', r, f_up(3,:), ':r', r, f_up(4,:), '-.r')
plot(r,f_lr(1,:), '-b', r, f_lr(2,:), '--b', r, f_lr(3,:), ':b', r, f_lr(4,:), '-.b')
xlim([0 4])
set(gca(),'FontSize',16,'FontName', 'Times New Roman')
xlabel('\it $\bar{r}$', 'FontWeight','bold','interpreter','latex','FontSize',
16,'FontName','Times New Roman');
ylabel('\it $\bar{f}_z$', 'FontWeight','bold','interpreter','latex','FontSize',
16,'FontName','Times New Roman');
legend([char(949) '_{31}=0.1'],[char(949) '_{31}=0.5'],[char(949) '_{31}=1'],[char(949)
'_{31}=5']);
gtext('\it $\bar{f}_{zI,IIItotal}$', 'FontWeight','bold','interpreter','latex','FontSize',
16,'FontName','Times New Roman')
gtext('\it $\bar{f}_{zI,IItotal}$', 'FontWeight','bold','interpreter','latex','FontSize',
16,'FontName','Times New Roman')

```

- f. The following codes calculate $\bar{F}_{I,II\ total}$ and $\bar{F}_{I,III\ total}$ for a pair of charges given a particular set of parameters: \bar{d} , ϵ_{21} , ϵ_{31} . Varying one of the parameters generates the dependence of surface force density on this parameter, as shown in the plots in Chapter 6.

Solve the Total surface force on the upper interface due to a pair of charges

```

% A pair of charges in the middle layer of a three-layered dielectric system;
% The positive charge is located at (0, d);
% The negative charge is located at (0, H-d);
% The coordinates are r and z normalized by H, i.e., the charges are now
% located at (r=0, z=(d/H)) and (r=0, z=(1-d/H)) respectively;
% Total force is normalized by q^2/(16*pi*eps0*eps1*H^2);
% rho is normalized by 1/H;

```

```
clear;
clc;
```

Parameters

```
dcharge=0.4;           % distance between the positive charge and the lower interface
e21=0.1;              % dielectric constant ratio between the lower and middle regions
e31=0.1:0.1:5;       % varying dielectric constant ratio between the upper and middle regions
n=50;                % number of steps for integration
del_r=0.1;           % discretization of radius
r = 0:del_r:4;       % range of radius
s = length(r);
t = length(e31);
```

Calculate total surface force on the upper interface

```
for i = 1 : t
    for j = 1 : s

        % calculate electric fields on the upper interface
        % for positive charge

        d=dcharge; % location of the positive charge

        ez_up(i,j) = (1-d)./((r(j).^2+(1-d).^2).^3/2);
        er_up(i,j) = r(j)./((r(j).^2+(1-d).^2).^3/2);

        ez_3(i,j) = 2.*quadl(@funefupH1, 0, n, [], [], r(j), d, e21, e31(i));
        er_3(i,j) = 2.*quadl(@funefupH2, 0, n, [], [], r(j), d, e21, e31(i));

        ez_1_up(i,j) = ez_up(i,j) - 2.*quadl(@funefmidH11, 0, n, [], [], r(j), d, e21, e31(i)) +
        2.*quadl(@funefmidH12, 0, n, [], [], r(j), d, e21, e31(i)) + quadl(@funefmidH13, 0, n, [], [],
        r(j), d);
        er_1_up(i,j) = er_up(i,j) + 2.*quadl(@funefmidH21, 0, n, [], [], r(j), d, e21, e31(i)) -
        quadl(@funefmidH22, 0, n, [], [], r(j), d);

        ez_3_tot_up(i,j)=ez_3(i,j);
        er_3_tot_up(i,j)=er_3(i,j);
        ez_1_tot_up(i,j)=ez_1_up(i,j);
        er_1_tot_up(i,j)=er_1_up(i,j);

        % calculate electric fields on the upper interface
        % for negative charge

        d=1-dcharge; % location of the negative charge

        ez_up(i,j) = (1-d)./((r(j).^2+(1-d).^2).^3/2);
        er_up(i,j) = r(j)./((r(j).^2+(1-d).^2).^3/2);

        ez_3(i,j) = 2.*quadl(@funefupH1, 0, n, [], [], r(j), d, e21, e31(i));
        er_3(i,j) = 2.*quadl(@funefupH2, 0, n, [], [], r(j), d, e21, e31(i));
```

```

        ez_1_up(i,j) = ez_up(i,j) - 2.*quadl(@funefmidH11, 0, n, [], [], r(j), d, e21, e31(i)) +
        2.*quadl(@funefmidH12, 0, n, [], [], r(j), d, e21, e31(i)) + quadl(@funefmidH13, 0, n, [], [],
        r(j), d);
        er_1_up(i,j) = er_up(i,j) + 2.*quadl(@funefmidH21, 0, n, [], [], r(j), d, e21, e31(i)) -
        quadl(@funefmidH22, 0, n, [], [], r(j), d);

        ez_3_tot_up(i,j)=ez_3_tot_up(i,j)-ez_3(i,j);
        er_3_tot_up(i,j)=er_3_tot_up(i,j)-er_3(i,j);
        ez_1_tot_up(i,j)=ez_1_tot_up(i,j)-ez_1_up(i,j);
        er_1_tot_up(i,j)=er_1_tot_up(i,j)-er_1_up(i,j);

        f_up(i,j) = ((ez_3_tot_up(i,j).^2 - er_3_tot_up(i,j).^2).*e31(i) - (ez_1_tot_up(i,j).^2 -
        er_1_tot_up(i,j).^2)).*r(j); % function for the upper interface

    end
end

for k=1:t
    e_force1_up(k) = trapz(r,f_up(k,:)); % total surface force on the upper interface
end

```

Plot of total surface force on the upper interface

```

figure;
plot(e31,e_force1_up)

set(gca(),'FontSize',16,'FontName','Times New Roman')
xlabel([char(949) '_{31}'], 'FontSize', 16,'FontName','Times New Roman');
ylabel('\it $\bar{F}$', 'FontWeight','bold','interpreter','latex','FontSize',
16,'FontName','Times New Roman');
legend({'\it $\bar{F}_{I,IIItotal}$'}, 'FontWeight','bold','interpreter','latex','FontSize',
16,'FontName','Times New Roman')

```

Solve the total surface force on the lower interface due to a pair of charges

```

clear;
clc;

```

Parameters

```

dcharge=0.4;           % distance between the positive charge and the lower interface
e21=0.1;               % dielectric constant ratio between the lower and middle regions
e31=0.1:0.1:5;        % varying dielectric constant ratio between the upper and middle regions
n=50;                 % number of steps for integration
del_r=0.1;            % discretization of radius
r = 0:del_r:4;        % range of radius

```

```
s = length(r);
t = length(e31);
```

Calculate total surface force on the upper interface

```
for i = 1 : t
    for j = 1 : s

        % calculate electric fields on the lower interface
        % for positive charge

        d=dcharge; % location of the positive charge

        ez_lr(i,j) = -d./((r(j).^2+d.^2).^3/2);
        er_lr(i,j) = r(j)./((r(j).^2+d.^2).^3/2);

        ez_2(i,j) = -2 * quadl(@funeflr1_H, 0, n, [], [], r(j), d, e21, e31(i));
        er_2(i,j) = 2 * quadl(@funeflr2_H, 0, n, [], [], r(j), d, e21, e31(i));

        ez_1_lr(i,j) = ez_lr(i,j) - 2.*quadl(@funefmid21_H, 0, n, [], [], r(j), d, e21, e31(i)) +
        2.*quadl(@funefmid22_H, 0, n, [], [], r(j), d, e21, e31(i)) + quadl(@funefmid23_H, 0, n, [], [],
        r(j), d);
        er_1_lr(i,j) = er_lr(i,j) + 2.*quadl(@funefmid11_H, 0, n, [], [], r(j), d, e21, e31(i)) -
        quadl(@funefmid12_H, 0, n, [], [], r(j), d);

        ez_2_tot_lr(i,j)=ez_2(i,j);
        er_2_tot_lr(i,j)=er_2(i,j);
        ez_1_tot_lr(i,j)=ez_1_lr(i,j);
        er_1_tot_lr(i,j)=er_1_lr(i,j);

        % calculate electric fields on the lower interface
        % for negetive charge

        d=1-dcharge; % location of the negetive charge

        ez_lr(i,j) = -d./((r(j).^2+d.^2).^3/2);
        er_lr(i,j) = r(j)./((r(j).^2+d.^2).^3/2);

        ez_2(i,j) = -2 * quadl(@funeflr1_H, 0, n, [], [], r(j), d, e21, e31(i));
        er_2(i,j) = 2 * quadl(@funeflr2_H, 0, n, [], [], r(j), d, e21, e31(i));

        ez_1_lr(i,j) = ez_lr(i,j) - 2.*quadl(@funefmid21_H, 0, n, [], [], r(j), d, e21, e31(i)) +
        2.*quadl(@funefmid22_H, 0, n, [], [], r(j), d, e21, e31(i)) + quadl(@funefmid23_H, 0, n, [], [],
        r(j), d);
        er_1_lr(i,j) = er_lr(i,j) + 2.*quadl(@funefmid11_H, 0, n, [], [], r(j), d, e21, e31(i)) -
        quadl(@funefmid12_H, 0, n, [], [], r(j), d);

        ez_2_tot_lr(i,j)=ez_2_tot_lr(i,j)-ez_2(i,j);
        er_2_tot_lr(i,j)=er_2_tot_lr(i,j)-er_2(i,j);
        ez_1_tot_lr(i,j)=ez_1_tot_lr(i,j)-ez_1_lr(i,j);
        er_1_tot_lr(i,j)=er_1_tot_lr(i,j)-er_1_lr(i,j);
```

```

        f_lr(i,j) = ((ez_1_tot_lr(i,j).^2 - er_1_tot_lr(i,j).^2) - (ez_2_tot_lr(i,j).^2 -
er_2_tot_lr(i,j).^2).*e21).*r(j); % function for the lower interface

    end
end

for k=1:t
    e_force1_lr(k) = trapz(r,f_lr(k,:)); % total surface force on the lower interface
end

```

Plot of total surface force on the lower interface

```

figure;
plot(e31,e_force1_lr)

set(gca(),'FontSize',16,'FontName','Times New Roman')
xlabel([char(949) '_{31}'], 'FontSize', 16,'FontName','Times New Roman');
ylabel('\it $\bar{F}$', 'FontWeight','bold','interpreter','latex','FontSize',
16,'FontName','Times New Roman');
legend({'\it $\bar{F}_{I,IItotal}$'}, 'FontWeight','bold','interpreter','latex','FontSize',
16,'FontName','Times New Roman')

```

2. Other Functions

The following functions are called by the above codes and are required for the calculation of electric potentials, electric fields and surface forces.

fundcupH.m

```

function y = fundcupH( rho, r, z, d, e21, e31 )
y1 = sinh((1-d).*rho)+(cosh(rho)+e21.*sinh(rho)).*sinh(rho.*d);
y2 = ((sinh(rho)).^2).*((e21+e31).*coth(rho)+(e21*e31+1));
y3 = exp(rho.*(1-z)).*besselj(0,rho.*r);
y = (y1.*y3)./y2;

```

fundclrH.m

```

function y = fundclrH( rho, r, z, d, e21, e31 )
y1 = sinh(rho.*d)+(cosh(rho)+e31.*sinh(rho)).*sinh((1-d).*rho);
y2 = ((sinh(rho)).^2).*((e21+e31).*coth(rho)+(e21*e31+1));
y3 = exp(rho.*z).*besselj(0,rho.*r);
y = (y1.*y3)./y2;

```

fundcmid1H.m

```
function y = fundcmid1H( rho, r, z, d, e21, e31 )
y1 = sinh((1-d).*rho)+(cosh(rho)+e21.*sinh(rho)).*sinh(rho.*d);
y2 = ((sinh(rho)).^3).*((e21+e31).*coth(rho)+(e21*e31+1));
y3 = sinh(rho.*z).*besselj(0,rho.*r);
y = (y1.*y3)./y2;
```

fundcmid2H.m

```
function y = fundcmid2H( rho, r, z, d, e21, e31 )
y1 = sinh(rho.*d)+(cosh(rho)+e31.*sinh(rho)).*sinh((1-d).*rho);
y2 = ((sinh(rho)).^3).*((e21+e31).*coth(rho)+(e21*e31+1));
y3 = sinh((1-z).*rho).*besselj(0,rho.*r);
y = (y1.*y3)./y2;
```

fundcmid3H.m

```
function y = fundcmid3H( rho, r, z, d )
y1 = exp(-(1-d).*rho).*sinh(rho.*z);
y2 = exp(-rho.*d).*sinh((1-z).*rho);
y3 = sinh(rho);
y = ((y1+y2).*besselj(0,rho.*r))./y3;
```

funefupH1.m

```
function y = funefupH1( rho, r, d, e21, e31 )
y1 = sinh(rho.*(1-d))+cosh(rho)+e21.*sinh(rho)).*sinh(rho.*d);
y2 = ((sinh(rho)).^2).*((e21+e31).*coth(rho)+(1+e21.*e31));
y =(y1.*rho.*besselj(0,rho.*r))./y2;
```

funefupH2.m

```
function y = funefupH2( rho, r, d, e21, e31 )
y1 = sinh(rho.*(1-d))+cosh(rho)+e21.*sinh(rho)).*sinh(rho.*d);
y2 = ((sinh(rho)).^2).*((e21+e31).*coth(rho)+(1+e21.*e31));
y =(y1.*rho.*besselj(1,rho.*r))./y2;
```

funefmidH11.m

```
function y = funefmidH11( rho, r, d, e21, e31 )
y1 = sinh(rho.*(1-d))+cosh(rho)+e21.*sinh(rho)).*sinh(rho.*d);
y2 = ((sinh(rho)).^3).*((e21+e31).*coth(rho)+(1+e21.*e31));
y = (y1.*cosh(rho).*rho.*besselj(0,rho.*r))./y2;
```

funefmidH12.m

```
function y = funefmidH12 (rho, r, d, e21, e31)
y1 = sinh(rho.*d)+(cosh(rho)+e31.*sinh(rho)).*sinh(rho.*(1-d));
y2 = ((sinh(rho)).^3).*((e21+e31).*coth(rho)+(1+e21.*e31));
y = (y1.*rho.*besselj(0,rho.*r))./y2;
```

funefmidH13.m

```
function y = funefmidH13 (rho, r, d)
y1 = (exp(-(1-d).*rho)).*cosh(rho)-exp(-rho.*d);
y2 = sinh(rho);
y = (y1.*rho.*besselj(0,rho.*r))./y2;
```

funefmidH21.m

```
function y = funefmidH21 (rho, r, d, e21, e31)
y1 = sinh(rho.*(1-d))+cosh(rho)+e21.*sinh(rho)).*sinh(rho.*d);
y2 = ((sinh(rho)).^2).*((e21+e31).*coth(rho)+(1+e21.*e31));
y = (y1.*rho.*besselj(1,rho.*r))./y2;
```

funefmidH22.m

```
function y = funefmidH22 (rho, r, d)
y = (exp(-(1-d).*rho)).*rho.*besselj(1,rho.*r);
```

funeflr1_H.m

```
function y = funeflr1_H( rho, r, d, e21, e31 )
y1 = sinh(rho.*d)+(cosh(rho)+e31.*sinh(rho)).*sinh(rho.*(1-d));
y2 = ((sinh(rho)).^2).*((e21+e31).*coth(rho)+(1+e21.*e31));
y = (y1.*rho.*besselj(0,rho.*r))./y2;
```

funeflr2_H.m

```
function y = funeflr2_H( rho, r, d, e21, e31 )
y1 = sinh(rho.*d)+(cosh(rho)+e31.*sinh(rho)).*sinh(rho.*(1-d));
y2 = ((sinh(rho)).^2).*((e21+e31).*coth(rho)+(1+e21.*e31));
y = (y1.*rho.*besselj(1,rho.*r))./y2;
```

funefmid11_H.m

```
function y = funefmid11_H (rho, r, d, e21, e31)
y1 = sinh(rho.*d)+(cosh(rho)+e31.*sinh(rho)).*sinh(rho.*(1-d));
```

```
y2 = ((sinh(rho)).^2).*((e21+e31).*coth(rho)+(1+e21.*e31));  
y = (y1.*rho.*besselj(1,rho.*r))./y2;
```

funefmid12_H.m

```
function y = funefmid12_H (rho, r, d)  
y = (exp(-rho.*d)).*rho.*besselj(1,rho.*r);
```

funefmid21_H.m

```
function y = funefmid21_H (rho, r, d, e21, e31)  
y1 = sinh(rho.*(1-d))+cosh(rho)+e21.*sinh(rho).*sinh(rho.*d);  
y2 = (sinh(rho)).^3.*((e21+e31).*coth(rho)+(e21.*e31+1));  
y = (y1.*rho.*besselj(0,rho.*r))./y2;
```

funefmid22_H.m

```
function y = funefmid22_H (rho, r, d, e21, e31)  
y1 = sinh(rho.*d)+(cosh(rho)+e31.*sinh(rho)).*sinh(rho.*(1-d));  
y2 = ((sinh(rho)).^3).*((e21+e31).*coth(rho)+(1+e21.*e31));  
y = (y1.*cosh(rho)).*rho.*besselj(0,rho.*r))./y2;
```

funefmid23_H.m

```
function y = funefmid23_H (rho, r, d)  
y1 = exp(-(1-d).*rho)-(exp(-rho.*d).*cosh(rho));  
y2 = sinh(rho);  
y = (y1.*rho.*besselj(0,rho.*r))./y2;
```

[Published with MATLAB® R2015a](#)